IN-SITU OPTICAL SPECTROSCOPY OF THE POLYMER ELECTROLYTE/ORGANIC SEMICONDUCTOR INTERFACE

A DISSERTATION
SUBMITTED TO THE FACULTY OF THE GRADUATE SCHOOL
OF THE UNIVERSITY OF MINNESOTA
BY

Loren G. Kaake

IN PARTIAL FULFILLMENT OF THE REQUIREMENTS
FOR THE DEGREE OF
DOCTOR OF PHILOSOPHY

Xiaoyang Zhu, Advisor

August 2009

Acknowledgements

Often when I look at a thesis, my first instinct is to look at the acknowledgments and think about what kind of person authored the work, as well as the people who are important in their lives. What I have gathered is that no accomplishments occur in an interpersonal vacuum, and I am no exception. I am fortunate to have many kind and honest people in my life, enough to make listing all of them and their contributions to my life impossible in just a single page. I am especially thankful for my family; my dad Greg, my mom, my sister, and yes, even my brother have been there for me when I needed them, lending an attentive and generous ear to my tales of anguish and ecstatic inspiration.

My scientific career has been aided immensely by the professors and fellow graduate students I have been able to work with. Xiaoyang, thanks for your enthusiasm, and support; I have never been left wanting in regard to either. Dan, thanks for your help and healthy skepticism, I am better because of it. Thank you Yongseok Jun, Chad Lindstrom, Matthias Muntweiler, Yang Deng, Matt Goertz, Brooke Timp, Travis Mills, Will Tisdale, Kenrick Williams, Matt Panzer, Bryan Bourdouris, Bryan Paulsen, Derek Stevens, Jedi Lee, and anyone else I forgot to mention. Thanks also to all the support staff at the U, and everyone at the physics and chemistry machine shop, where I became a bit of a regular. Lastly, thanks to the inanimate universe, just for being your self.

Abstract

The implementation of organic thin film transistors into microelectronic devices hinges upon the development of organic semiconductors and gate dielectric materials. In a working device, the place where the two materials meet is critical to device performance. This buried interface between the organic semiconductor and the gate dielectric is notoriously difficult to characterize. One way to probe this interface is through the use of attenuated total internal reflection Fourier transform infrared and near infrared spectroscopy (ATR-FTIR). This method allows one to do optical spectroscopy on a working device and gain insight into the physical processes which occur at the semiconductor/dielectric interface during the application of voltage. One example of such a process is the induction of charge in the organic semiconductor layer. Charging of an organic semiconductor gives rise to distinct spectroscopic signatures which can be used to characterize properties intrinsic to the semiconductor.

For example, high charge carrier density can give rise to unique spectroscopic signatures which may be related to the Mott insulator to metal transition. Crystallinity affects the spectral signatures of charge carriers, and these effects can give insight into sources of energetic disorder in the solid. Examining semiconductor charging also gives insight into the operating mechanisms of the dielectric material responsible for inducing charge carriers. Dielectric materials using mobile ions have become attractive for use in organic thin film transistors because they allow low voltage transistor operation. The physical mechanisms for charge induction are distinguishable when in-situ optical spectroscopy is applied. For example, the mobile ions in a dielectric material can

penetrate the bulk of the semiconductor film or stop at the semiconductor/dielectric interface depending on the size of the ion. The rate of charging can be analyzed and used to estimate a material specific maximum operating speed of an electrochemical transistor. Using optical spectroscopy to examine the organic semiconductor/electrolyte dielectric interface gives insight into many aspects of device operation, many of which are critical to making organic thin film transistors a viable technology.

Table of Contents

List of Figures

I. Introduction: brief overview

In order to establish an overall context for this thesis, a brief tour of the document is found on the next few pages. The first section outlines the socio-economic motivation for organic semiconductor research as well as calling attention to some of the more general problems which will be addressed later in detail. The experimental perspective from which problems and open questions will be addressed, is described in the next section. Describing the overall notion of the research sets the stage for a more detailed discussion of the contents of the thesis, hopefully allowing the reader to get a clear picture of the direction taken throughout the remainder of the document.

A) Motivating the thesis research

The field of organic semiconductor research is a broad and multidisciplinary in its character and draws the interest and expertise of a variety of researchers. Interest in the field stems not only from the unique and interesting properties of these materials, but also from their broad applicability as cheap and flexible alternatives to the more traditional inorganic semiconductors employed today. One example where organic semiconductor materials have reached the market is organic light emitting diodes. These devices convert electrical power into light and are found in the displays of computer notebooks, cell phones, mp3 players, and televisions.[1,2] Other applications seem very near on the

horizon. Organic semiconductors are being considered for room lighting applications,[3][i] and offer the possibility of cheap and effective solar cells which could lead towards energy independence from fossil fuels.[4] However, many challenges remain which prevent the large scale implementation of all organic devices most notably, the development of high performance organic thin film transistor.

One, if not the most, critical electrical component in a digital device is the transistor. This device can be switched from an insulating state (off) to a conductive state (on) by the application of an auxiliary voltage, making the basic ones and zeroes (bits) which form the instructions comprising the lowest level programming language.[5] Thus the implementation of an all-organic digital device will require organic transistors.

The realization of organic transistors which can operate at commercial specifications is not simply a technological question; it is also a scientific one. The lessons learned by improving the operation characteristics of organic transistors apply broadly to all organic semiconductor devices; studies on transistors focus on the injection, removal and transport of charges, features shared by nearly all of the most important electrical components. Of those features, charge transport is often the aspect most focused upon for two main reasons: it is not completely understood, and the poor transport properties of organic semiconductors are one of the major hurdles in the commercialization of these materials. For example, the hole mobility of rubrene single crystals[6] was measured to be ~15 $cm^2V^{-1}s^{-1}$, as compared with the hole mobility of crystalline silicon,[7] which is 480 $cm^2V^{-1}s^{-1}$. However, the implementation of organic semiconductors as a low cost alternative to silicon technology will likely involve either vapor deposited or solution cast organic semiconductor films, not organic single crystals.

The benchmark for this type of material is amorphous silicon, which has a typical mobility of 1 $cm^2V^{-1}s^{-1}$, comparing that with the mobility of a typical organic semiconductor thin film (0.1 $cm^2V^{-1}s^{-1}$) shows that while organics are getting close, they are still in need of improvement.

Another hurdle to the commercialization of organic transistors in terms of materials development comes from the fact that a transistor is a single electrical component made up of many different materials. One of the most important parts of a transistor, other than the semiconductor, is the gate dielectric material. Switching a transistor from its insulating (off) to its conductive (on) state requires the ability to modulate the number of charge carriers in the active region of the device. The efficiency of this process is, in large measure, related to the properties of the dielectric only. Thus, research into dielectric materials for organic semiconductor devices is a key component to their eventual commercialization.

One material which is a promising candidate as a dielectric material in organic thin film transistors is a polymer electrolyte. Briefly, a polymer electrolyte is comprised of a polymer matrix which contains mobile ion which can move under the force of an applied electric field. Because the ions are mobile, they can distribute themselves in such a way so as to create a large electric field at the semiconductor interface.[8] Thus, the material has a high capacitance and the possibility of low voltage, high performance transistor operation is opened. However, polymer electrolytes add a degree of complexity to the organic transistor, making their investigation in that context worthwhile.

B) Research description

The research comprising this thesis is aimed towards improving our knowledge of the organic thin film transistor. This means understanding the properties of dielectric materials as well as the electronic properties organic semiconductors. While the construction of better organic thin film transistors is the ultimate goal to which this research is directed, the methods employed are primarily spectroscopic, not electrical.

Spectroscopy uses the interaction of light with matter to understand the properties of matter. As it will be seen, many of these properties are related to the mechanism of charge transport and injection, although they are not directly measurable by electrical means. In other words, spectroscopy can provide a unique prospective into the mechanisms of an operating organic semiconductor device, and most importantly, help to discriminate between competing theories of device operation. In particular, infrared spectroscopy is useful because much of the interesting electronic and vibronic structure within the material absorbs light of those frequencies.

In order to use spectroscopy to gain knowledge into device operation, it is important to simulate the conditions of an operating organic transistor during the experiment. The very least that can be done in this regard is to induce carriers in the organic semiconductor by applying a voltage across a dielectric material. Thus a basic description of the experiments performed during the thesis research emerges; build a device using an organic semiconductor and an electrolyte dielectric material and record spectroscopic observations while applying a voltage between them. This technique is particularly useful and interesting because it probes an interface buried between two

materials. This buried, and subsequently, electrified interface is not well understood, nor is it well characterized.

C) Thesis overview

Prior to detailed discussions concerning the main topic of the thesis, a set of background concepts will be introduced in chapter II. Because charge transport is a central topic in condensed matter physics, some basic concepts from that field will be introduced in section A, including segments on the Drude theory of conduction, the Fermi-Dirac distribution and free electron gas theory, band theory, and finally disordered semiconductor theory.

Further background sections (B,C) will focus on the organic semiconductors themselves, examining some of their basic physical and electronic properties. In the current understanding, the relationship between small molecule organic semiconductors and polymer semiconductors has not been fully elucidated. Thus, the two will be given separate sections, beginning with small molecule semiconductors.

Since the experiments undertaken here are primarily of a spectroscopic nature, the interaction of light with organic semiconductors will be explored in section D. Emphasis will be placed on the absorptions most prevalent in the infrared, taking care to connect theories of charge carrier identity in solid state physics with their spectroscopic observables.

After important spectroscopic concepts are introduced, a brief description of three relevant electrical devices will be given in section E. The purpose of this section is not to

give an authoritative account of the device physics, but rather to provide a simple description introducing device operation, along with the physical observables and the prevailing metrics used to describe device performance.

With the relevant background in place, chapter III will explain the details of experiments done throughout the course of the thesis research. Part of this chapter is devoted to a thorough development of main experimental technique, attenuated total internal reflection Fourier transform infrared spectroscopy (ATR-FTIR). The remainder of the chapter is written as a reference manual describing useful techniques developed and/or consistently employed, largely as a guide to anyone wishing to use some of the same techniques.

The next four chapters cover the experimental results obtained throughout the course of this research. The first question to answer about the system is "What is the mechanism of charge induction in at the organic semiconductor/electrolyte dielectric interface?" After that question is answered in chapter IV, questions relating to the kinetics of the charging process will be addressed in chapter V. Attention will turn once again to the mechanism of charge induction in chapter VI, this time with a material showing qualitatively different behavior. Once the properties of the electrolyte dielectric are reasonably well understood, focus is turned to the organic semiconductor side of the buried interface. In chapter VII, questions about charge transport are addressed in the context of the insulator-metal transition. Throughout the results section, one reoccurring theme emerges. The relationship between charge carrier density, the neutral vibrational modes of the semiconductor molecule, and broad electronic absorptions in the mid and near infrared are investigated and used as a guide repeatedly.

D) References

[1] Sonystyle.com. http://www.sonystyle.com/webapp/wcs/stores/servlet/StoreCatalogDisplay?storeId=10151&catalogId=10551&langId=-1 (Accessed July 28, 2009), Search term OLED returns 7 products.

[2] Samsung United States. http://www.samsung.com/us/index.html (Accessed July 28, 2009), Search term OLED returns 43 results.

[3] Universal Display Corporation. http://www.universaldisplay.com/default.asp?contentID=590 (Accessed July 28, 2009), Page title: OLED lighting.

[4] Konarka Power Plastic. http://www.konarka.com/ (Accessed July 28, 2009).

[5] Patterson, D.A.; Hennessy, J.L. *Computer Organization and Design: The Hardware/Software Interface;* Morgan Kaufmann: San Francisco, CA 2005; pp 11-15.

[6] Vikram, S.C.; Zaumseil, J.; Podzorov, V.; Menard, E.; Willett, R.L.; Takao, S.; Gershenson, M.E.; Rogers, J.A. *Science* **2004**, 303, 1644-1646.

[7] Kittel, C. *Introduction to Solid State Physics*, 8th ed.; John Wiley and Sons: Danvers, MA, 2005; pp 208.

[8] Grahame, D.C. *Chem. Rev.* **1947**, 41, 441-501.

II. Background

This section presents a collection of concepts and results which form some of the broader context for the thesis research. Because the length of this document is finite, a careful balance must be struck between variety and thoroughness. In trying to strike this balance, one must exert some bias in not only the selection of topics, but the level of detail for each of the concepts included. With that said, the background will begin by covering some of solid state physics. More specifically, four of the most common theories of electronic structure and conduction will be outlined. The next two sections will describe the organic semiconductors themselves, pointing out a few key results, materials, and theories. The concepts developed in the first two chapters will then be examined from a spectroscopic perspective, in order to relate the spectroscopic results obtained to their relevant physical theories. Finally, a few of the most relevant electrical systems and devices used and studied in the organic semiconductor field will be discussed in section E.

A) Relevant Concepts from Solid State Physics

Organic semiconductor research draws heavily upon concepts originally developed in condensed matter physics. Although many of these concepts are somewhat elementary from the perspective of a physicist, they are anything but familiar to most chemists. Therefore, a discussion is presented here covering some of the more frequently occurring ideas to provide an overall context for discussions concerning organic

semiconductor properties. The discussion will start with classical Drude model, then move to free electron gas theory, progressing to band theory and finally disordered semiconductor theory.

A.1) Drude theory of electrical conduction

The Drude theory is an attempt to make Ohm's law consistent with Newtonian mechanics and the fact that charge is quantized. It is the simplest mechanistic theory of conductivity, and therefore has no trouble finding use in the context of organic semiconductors. The conflict Drude theory tries to address is the results from considering the fact that an electron moving under the influence of a constant electric force should accelerate continuously according to Newton's laws. However, Ohm's law describes a constant electric force generating a constant electric current. To bring these theories into agreement with it is necessary to postulate the existence of some kind of friction that acts on the moving electrons. This would ensure that upon the application of an electric field, electrons would rapidly reach a maximum velocity, also called the drift velocity (v_d). The measured current would then be the product of the density of conducting electrons (n), their charge ($-e$), and the drift velocity. This allows Ohm's law to be written in a way that considers quantized charge.

(1) $$J = \sigma E = -nev_d$$

The above expression is not entirely satisfying, however, because the drift velocity is both a material property and a function of the applied electric field. A better

expression would factor out the electric field from the drift velocity. The macroscopic material property this describes is called the mobility ($\mu = v_d/E$).

Working out an expression for the mobility in terms of atomic scale events can be done in a straightforward fashion by assuming that an electron accelerates according to Newton's laws, and is scattered after some characteristic time (τ). After each scattering event the electron has a random velocity. The magnitude and direction of that velocity, as predicted by kinetic gas theory, is zero. Thus, the mobility is related to the velocity an electron attains before it is scattered. Setting the Lorentz force equation equal to Newton's equation of motion, and integrating from zero to the characteristic time, (τ), one obtains the following expression for mobility after factoring out the electric field:

$$(2) \qquad \mu = \frac{e\tau}{m_e}$$

where (m_e) is the electron mass. [1-3]

A few points are worth briefly mentioning before concluding this section. Collision times calculated for typical metals are on the order of 10 femtoseconds, [6] which is an amazingly accurate description of the timescales relevant to electron dynamics in metals given the crudeness of the model. However, to arrive at these numbers, one must have some idea that not all electrons in the solid participate in conduction. A reasonable estimate is that only the valence electrons participate. However, the Fermi-Dirac distribution discussed in the next section establishes a more quantitative criterion.

Mobility is an entirely classical concept, but it has found great utility in organic semiconductors research. Ideally, the mobility is independent of charge carrier concentration and represents a more general material property related to conductivity.

The metric of mobility is especially useful in experiments where the charge carrier density can be modulated, such as in organic thin film transistors.

A.2) Free electron gas

Attempts to connect the molecular level details of organic semiconductors to measured mobilities will need a quantum mechanical model of conduction. The free electron gas is the simplest quantum mechanical model of electrons in a solid. The model assumes that potential energy is uniform and constant throughout the solid. Also, the effect of interactions between electrons is neglected. Thus, the energy (ε) of any one electron is entirely determined by its momentum ($\hbar k$) according to free particle solution of the Schrödinger equation. [1,2,4]

(3) $$\varepsilon = \frac{\hbar^2 k^2}{2m_e}$$

A critical aspect of the quantum mechanical picture of electrons is that they are Fermions, and therefore must obey the Pauli exclusion principle. The Pauli exclusion principle requires that no two particles have identical quantum numbers. In this case, the Pauli exclusion principle manifests itself in terms of momentum because momentum is the only well defined quantum number in this problem.[4] Thus in a solid containing a free electron gas of many electrons, no two can have the exact same momentum (neglecting spin degeneracy).

A solid containing many electrons will have electrons with many different values of momentum. Such a problem lends itself to statistics, allowing one to ask questions concerning the probability of finding an electron having some momentum value. The

same sorts of questions are appropriate for most gasses. The evaluation of the Gibbs sum for Fermions can be done with the following model: imagine a single state of energy ε which can either be singly occupied (and have a total energy ε), or completely unoccupied (and have an energy of zero). Because only two possibilities exist, calculating the partition function by summing over all states of the system is simple. The probability of finding a particle with an energy (ε) relative to the Fermi energy (ε_F) is described by the Fermi-Dirac distribution, $f(\varepsilon)$.[5] Figure II-1 shows a plot of $f(\varepsilon)$ for at several temperatures.

(4) $$f(\varepsilon) = \frac{1}{1+\exp\left[\frac{(\varepsilon-\varepsilon_F)}{k_B T}\right]}$$

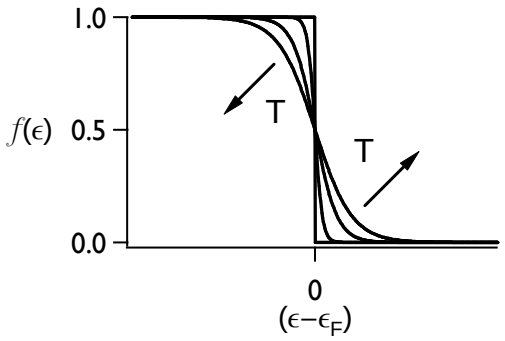

Figure II-1. The Fermi-Dirac distribution function. The occupation probability of an electronic state is given as a function of energy relative to the Fermi level. Arrows indicate the effect of increasing temperature.

The Fermi energy is defined as the chemical potential of electrons in a solid as the temperature goes to zero. The chemical potential is in general, a function of temperature, and is often called the Fermi level. The position of the Fermi level relative to the vacuum level (the energy of an electron in the vacuum with no kinetic energy) can be measured, and the difference between the two is called the work function.[1,2]

The Fermi-Dirac distribution is general: any state containing electrons (or more generally half-integer spin particles) is populated according to Fermi-Dirac statistics. The fact that it was introduced in a discussion of the free electron gas was a matter of convenience and not indicative of a fundamental relationship.

To find out how the electrons of a solid are distributed in energy, one needs know some information concerning the energetic positions of all the states in a solid. For macroscopic solids, the energetic positions are given by a continuous distribution function called the density of states, D_ϵ.

(5) $$D_\varepsilon = \frac{dN}{d\varepsilon}$$

In equation 5, N is the number of states in the solid. To calculate the number of states available at a particular energy, integrate over a volume of momentum space related to the total volume of the solid.

(6) $$N(k') = \int_0^{k'} \frac{V}{(2\pi)^3} 4\pi k^2 dk$$

Equation 3 is used to convert momentum into energy, and allow the calculation of the density of states. The expression relating momentum and energy is called the dispersion relationship and can be used to calculate the density of states. The density of states for the 3D free electron gas is given below.[2]

(7) $$D_\varepsilon = \frac{V}{2\pi^2}\left(\frac{2m_e}{\hbar^2}\right)^{3/2}\sqrt{\varepsilon}$$

To calculate the population of electronic states, one multiplies the Fermi-Dirac distribution by the density of states. The integral of this product is the total number of electrons in the solid.

A few other interesting metrics that describe electron transport emerge from free electron theory. One useful notion is that of Fermi velocity (v_F), that is, the velocity of an electron at the Fermi level. This value can be obtained by placing the Fermi energy in to the dispersion relationship (equation 3) and converting wavevector to velocity. Typical Fermi velocities in elemental metals are on the order of 10^8 *cm* s^{-1}, which is only 1/100 of the speed of light.[7] This makes sense in the context of the very short scattering times found in Drude theory. In fact, combining the two metrics, the Fermi velocity and the scattering time, gives one an estimate of how far an electron travels between scattering events. This distance is called the mean free path ($\ell = \tau v_F$),[2] and for an electron traveling 10^8 *cm* s^{-1} for a time of 10 femtoseconds between collisions, the mean free path is 10 *nm*.

The mean free path computed above is for room temperature metals, and is less than 100 times larger than a single atom. This seems to conflict with the picture of electrons in a metal behaving as free particles. It is found however, that upon cooling high quality metal crystals to liquid helium temperatures, the mean free path approaches macroscopic sizes.[8] The reason is that vibrations of the crystal lattice, called phonons, scatter electrons and create a major source of resistance in metals. Cooling a metal causes the number of phonons to decrease, which in turn decreases the resistance according to a power law.[1,2,5]

The relevance of the free electron model to organic semiconductors is a topic which attracts debate. This is especially true in the context of the insulator-metal transition, as free electron theory does much to explain the behavior of metals. In particular, the temperature dependence of the conductivity is an important aspect of the

conduction mechanism. Also, the Fermi-Dirac distribution described in this section is general and therefore, applies to organic semiconductors.

A.3) Band theory

For all the successes of the free electron theory, it is unable to give an account of why some materials are conductive while others are insulating. Clearly, the ability to make this distinction is important in terms of organic semiconductors because their conductivities can vary over a wide range. In order to address the difference between a conductor and an insulator, the internal potential energy structure of a solid will need to be factored into the theory.

Fortunately, introducing even simple potential energy contributions improve the model considerably. An example of a potential energy contribution would be treating the nuclei in a solid as adding a Coulomb potential to the electron Hamiltonian. Simpler still, would be to include a periodic array of Dirac delta functions to model the potential of the nuclei. Continuing to ignore interactions between the electrons themselves produces a model which can be solved in terms of free electron wavefunctions. This is a variation of the Kronig-Penney model.[2]

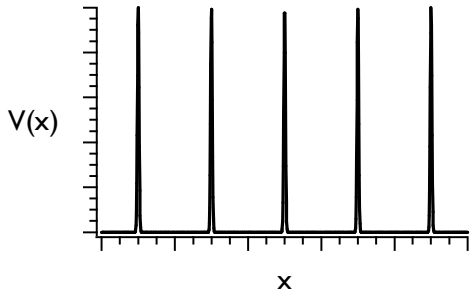

$$V(x) = \sum_{a} \delta(x - a)$$

$$\psi(x) = A\exp[ikx] + B\exp[-ikx]$$

Figure II-2. Kronig Penny model of a solid. Potential energy (V) is represented by a periodic array of Dirac delta functions.

Not all wavevectors are solutions to the Schrodinger equation for the potential energy function described in figure II-2. To explain this, it is important to note that in the presence of any change in the potential energy, a wavefunction is both transmitted and reflected. When the wavefunction has a wavelength similar to that of the periodicity of the lattice, the reflected waves will destructively interfere with one another. Thus, a series of disallowed energies exist as a consequence of the periodicity of the lattice; they do not depend on the shape of the potential energy surface used to approximate the lattice. The energies of the disallowed wavefunctions make up an energy gap within the solid, and the presence of energy gaps explains a host of phenomena, most notably the difference between metals, insulators, and semiconductors.[1-3]

The major experimental difference between a metal and an insulator is that an insulator does not conduct electricity as $T \rightarrow 0\ K$.[9] This can be understood in terms of band theory first by thinking about how a free electron moves under the force of an electric field. The key to obtaining electrical current is to have a situation where more electrons are moving in one direction than are moving in the opposite direction. In more technical language, more electrons have a positive wavevector than have a negative wavevector, requiring the existence of empty states just above the Fermi energy to

accommodate an increased population of electrons with a positive wavevector (see figure II-3). However, if the Fermi energy lies in the middle of the forbidden gap there are no such states, and the material is insulating. To restate, an insulator is a material without a band of states around the Fermi energy.[1,2]

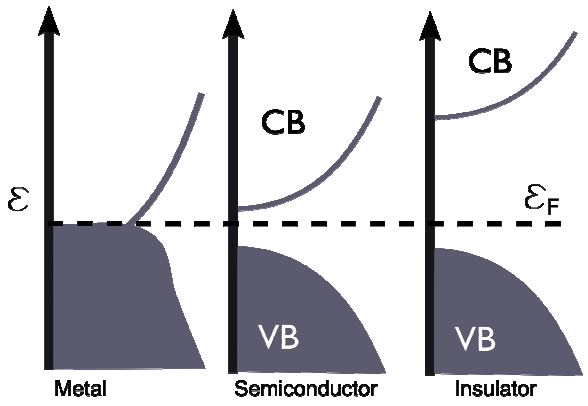

Figure II-3. Schematic band structure. Occupied density of states are shaded while unoccupied states are represented by the area inside a curve. Vertical scale is energy and dashed line marks the Fermi energy. Valence band (VB) and conduction band (CB) are labeled for semiconductor and insulator. The band gap is the energy difference between VB and CB.

The difference between a semiconductor and an insulator is something of a matter of taste. Both insulators and intrinsic semiconductors share the same energy structure, that is, they lack density of states at the Fermi level. However, insulators tend to have larger band gaps and are therefore more resistive at room temperature. The band gap is the difference in energy between the filled band below the Fermi level, called the valence band (VB), and the empty band above the Fermi level, called the conduction band (CB).

Technological applications of semiconductors usually use doped semiconductors, that is, a material where impurities have been intentionally introduced. Often the role of dopants is to introduce a small concentration of electrons into the conduction band; this is

n-type doping. Just as often, however, electron deficient dopants are introduced. They remove an electron from the valence band and create a positively charged electron vacancy, called a hole. The vacant orbital affects the subtle balance of the positive and negative electron momenta, allowing current to flow in the band. The hole appears to move like an electron with a positive charge under the influence of an electric field.[1-3]

Bloch's theorem states that solutions to the Schrödinger equation in a periodic potential consist of a plane wave and a component which has the same periodicity as the underlying lattice. The plane wave component is almost identical to that of a free electron. Thus, concepts developed in free electron theory can often be applied to carriers in a periodic potential. One of the most famous of these applications is the effective mass approximation for semiconductors.

The dispersion relationship in equation 3 is that of a free electron. Most notably it is parabolic in momentum. The steepness of that parabola depends on the mass of the electron. The energies of a Bloch wave near the bottom of a conduction band are very similar to those of a free electron.[2]

(8) $$\varepsilon = \varepsilon_c + \frac{\hbar^2 k^2}{2m^*}$$

The energy of an electron appears from equation 8 to be that of a free electron plus an energy offset (ε_C). The mass (m^*) in equation 8 is called the effective mass and is usually expressed as a multiple of the free electron mass. The magnitude of the effective mass is often between 0.1 m_e and 10 m_e and is related to the magnitude of the periodic potential. This should be expected because one must recover free electron theory as the magnitude of the periodic potential goes to zero.

The effective mass can be thought of as increasing due to a small amount of destructive interference from reflections from the periodic lattice. According to basic quantum mechanics, the magnitude of the reflected wave becomes greater as the magnitude of a change in potential becomes greater, thus the effective mass increases with the size of the periodic potential fluctuations in the lattice.

Effective mass can be calculated from the shape of a band as can be seen from equation 8 and 9. It is only independent of momentum near the bottom of a band, where the band can be approximated as parabolic.[1,2]

(9) $$\frac{1}{m^*} = \frac{1}{\hbar^2}\frac{\partial^2 \varepsilon}{\partial k^2}$$

Effective mass is a concept useful in a variety of contexts and theoretical models. One model where it has a particularly nice interpretation is in tight binding theory. Briefly, tight binding theory describes band formation as the result of wavefunction overlap between adjacent atoms, or more generally, sites.[1] The Hamiltonian of the system includes the energetic position of the individual atoms and magnitude of their wavefunction overlap. In many ways, tight binding theory is reminiscent of molecular orbital bonding theory.

The degree of wavefunction overlap goes by a variety of names including transfer integral, tunneling matrix element, and hopping coefficient. Small values of the transfer integral lead to bands which cover a narrow energy range from top to bottom. In other words, energy depends only weakly upon momentum, and the bands have a very small curvature. When equation 9 is applied, the charge carriers seem to have a very large effective mass. Thus, effective mass is inversely related to the energetic width of a band, which is itself related to the degree of wavefunction overlap between adjacent sites.

The use of tight binding theory in organic semiconductor research cannot be overstated. It is one of the most often used models describing intermolecular electron transfer, including hopping conduction and band formation.[10] Effective mass is another important concept and can also be related to the electronic properties and band structure of organic semiconductors.[11] On a simpler level, the existence of conduction and valence bands and the presence of a band gap serves as an important model for understanding, among other things, elementary optical excitations of an organic semiconductor.

A.4) Disordered semiconductor theory

Of all the theories of electron transport discussed in this section, disordered semiconductor theory is perhaps the one most relevant to the study of organic thin film transistors. Whether vapor or solution deposited, organic thin films are disordered semiconductor materials, and treatments of them as such are successful.[12] Thus, a general discussion of disordered semiconductor theory is warranted, if not imperative in a discussion relating general solid state concepts to organic semiconductor properties.

One of the main aspects of conduction in disordered systems is that carriers are localized, instead of free-electron like. Conduction can be viewed as the hopping of electrons from one localized site to another. A few models of localization exist, but the Anderson model is one of the most frequently discussed, and is depicted in the top panel of figure II-4.

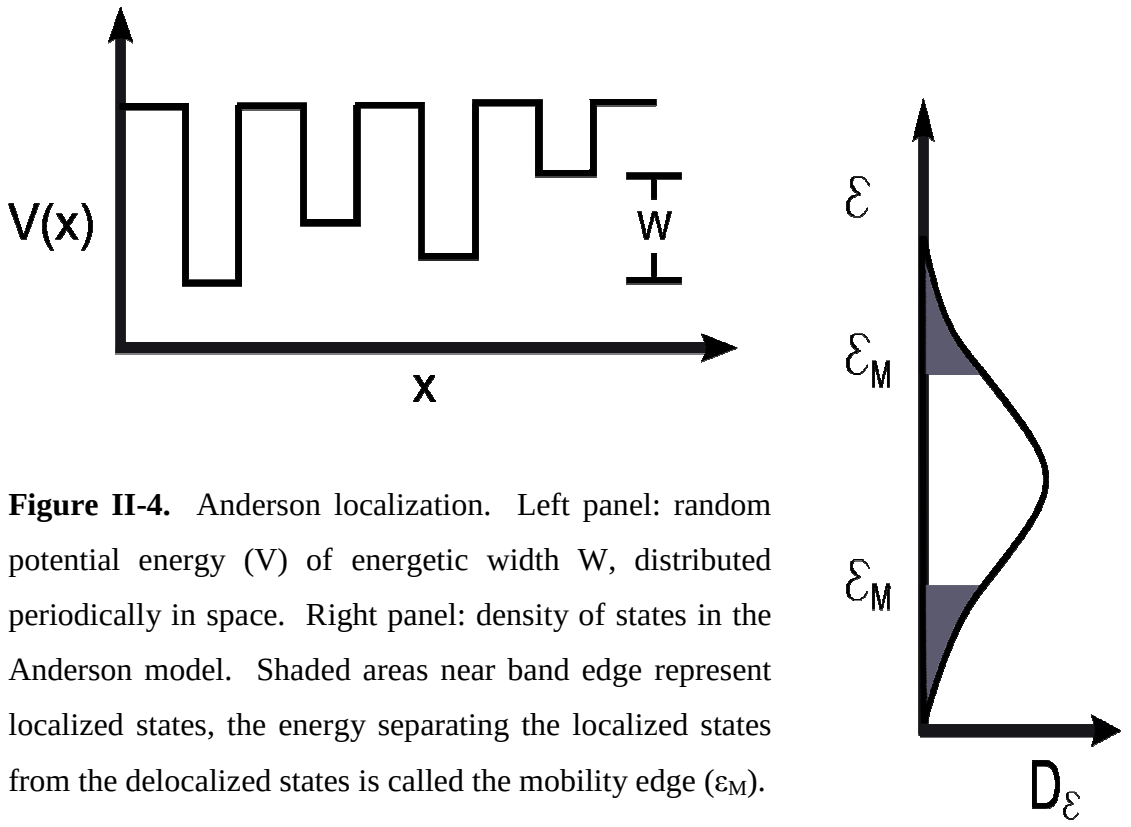

Figure II-4. Anderson localization. Left panel: random potential energy (V) of energetic width W, distributed periodically in space. Right panel: density of states in the Anderson model. Shaded areas near band edge represent localized states, the energy separating the localized states from the delocalized states is called the mobility edge (ε_M).

The Anderson model of electron localization begins with a system which is periodically ordered, but has random site energies. Other models, incorporating random site positions and identical site energies have been constructed, but similar general features arise regardless of the model. In the Anderson model, the distribution of site energies is uniform and has a finite width (*W*). Although no exact solution to the Schrödinger equation exists for this model, numerical solutions show that localization is determined by the ratio *W/I* where *I* is the overlap integral from tight binding theory. As one decreases the value of this ratio past some critical value, some percentage electrons suddenly delocalize. This is the Anderson transition.[9,13]

From a chemistry perspective the problem of localization can be understood by considering the sharing of an electron by two atoms in molecular orbital theory. The more the two orbitals overlap in space and energy the more the electron wavefunction delocalizes over both atoms. In the case when the energies are very different, the electron will be mostly found on one atom, and this effect becomes more pronounced when the orbitals involved have very little spatial overlap. Similarly in a solid, when sites are far away from others with similar energies, the sites will not be able to share electron density effectively and charges will tend to localize.

The concept of mobility edge describes the effect of varying the carrier concentration in disordered semiconductors. In a system where *W/I* is small, some electronic states are localized, and some states are delocalized. Localized states exist at the edges of the band, while around the band center the electrons are delocalized. The energetic boundary between the two is called the mobility edge.[14] Figure II-4 shows a schematic density of states for a disordered material.

In the localized regime, conductivity is a strong function of temperature due to the fact that energetic disorder now requires that conduction be a thermally activated process. There are many models of temperature activated conductivity, but the four that commonly arise are as follows: multiple trap and release,[15] nearest-neighbor hopping[16], Mott variable range hopping[17], and Efros-Shklovskii hopping[18].

Disordered semiconductor theory is important in understanding the conduction mechanism operating in thin film organic semiconductors. Thin films are often either amorphous or polycrystalline, and do not contain the long range order assumed to exist in the free electron and band theories of conduction. Thus carriers are localized to some

degree and temperature activated hopping of the carrier from site to site is an important model for conduction in organic semiconductors.

B) Small Molecule Organic Semiconductors

Part of the driving force for research into organic semiconductors is the ability to harness the variety of organic synthesis to rationally engineer molecules to with specific electronic properties. Thus, one would like to bring about a detailed understanding of the structure property relationship bridging molecular structure and carrier mobility. Two dominant research paradigms address this goal. The first is to synthesize a wide variety of molecules and characterize them with a small number of techniques using the differences between molecules to shed light onto the structure property relationship. The second is to apply a wide variety of characterization techniques to a small number of molecules in order to test theories of transport in a number of unique, but related contexts. This section will employ the latter approach to a large degree and focus on the properties of pentacene and rubrene, two of the most well studied molecules in the field.

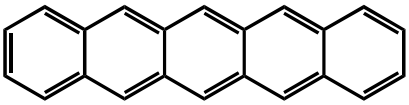

Pentacene

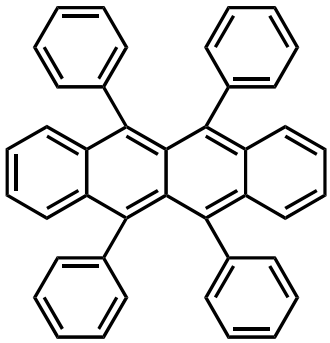

Rubrene

Figure II-5. Pentacene and Rubrene. Two of the most popular small molecule organic semiconductors. Pentacene is noted for is good performance in thin film applications, while rubrene is the highest mobility single crystal material.

Pentacene, like many of small molecule organic semiconductors pictured in figure II-5, is a planar molecule with a system of highly conjugated π bonds. This gives pentacene a delocalized HOMO and LUMO which are generally accepted design characteristics of successful organic semiconductor molecules [19]. Pentacene forms a triclinic crystal structure [20] with a herringbone arrangement of the pentacene molecules[21]. The herringbone structure, although not perfectly suited for it, allows for van der Waals interactions between π orbitals of different molecules in the unit cell. Applying tight binding theory to the van der Waals interactions present between pentacene molecules shows that a band structure can form within the crystal.[10,11] In other words, the van der Waals interactions between molecules provide delocalized pathways for carrier motion. The bands formed in an organic semiconductor crystal are commonly referred to as HOMO and LUMO bands. The HOMO band of a molecular solid and the valence band in an inorganic solid are conceptually almost identical. An important aspect of pentacene band structure is that it is highly anisotropic.[10] That is to say that the van der Waals interactions are significantly stronger within a crystallographic plane, making effects due to inter-plane overlap on transport rather small. This gives the band structure of many organic single crystals a highly two dimensional character.

Rubrene is another heavily studied organic semiconductor, in part because of its ability to form high mobility single crystals. Mobility measurements have been taken as a function of crystallographic directions, and are not only quite high (15 $cm^2V^{-1}s^{-1}$) they are also anisotropic.[22] Band structure calculations combined with spectroscopic measurements show that rubrene has a band gap of 2.2 *eV* and injected holes have an

effective mass between 0.8 m_e and 2 m_e, which is also anisotropic.[23] Temperature dependent mobility measurements of rubrene single crystals display increasing mobility with decreasing temperature over a certain temperature range.[24] This increase follows a power law suggesting that band-like transport is a valid model in that range. However at lower temperatures, mobility decreases with temperature for reasons still being debated.[24,25]

Experiments on single crystal organic semiconductors are highly important to understanding their intrinsic properties. However, the thin film transistor is the more technologically applicable device and much research has gone into their improvement. The pentacene TFT is one of the benchmark devices owing to its fine TFT mobility. Although research has gone into making soluble pentacene derivatives,[26] and solution processable precursors,[27] pentacene itself is insoluble. Thus, vapor deposition is the preparation method of choice. The thin film morphology of vapor deposited pentacene is sensitive to a number of factors including deposition rate, substrate temperature and type of substrate, including effects due to surface modification.[15] However, thin films of pentacene can generally be regarded as microcrystalline, leading towards questions regarding the role of grain boundaries on charge transport. The prevailing wisdom is that grain boundaries limit the field effect mobility, as thin film mobilities are almost always lower than single crystal mobilities. However, the precise role of grain boundaries on charge trapping and transport remains an open question.

C) Polymer Semiconductors

The modern field of conducting and semiconducting polymers began in earnest with the discovery of conducting polyacetylene in 1977.[28] Although much of the initial interest was theoretical, the development of soluble polymer semiconductors provided a substantial technological impetus in their continued research.[29-31] Figure II-6 shows some of the most commonly encountered polymer semiconductors in the literature. The basic motif for polymer semiconductors is not wholly unlike that of small molecule semiconductors; both have extended π conjugation. However, the greater length of the conjugated polymer gives rise to physical properties which impact the nature of charge carriers on the polymer chain.

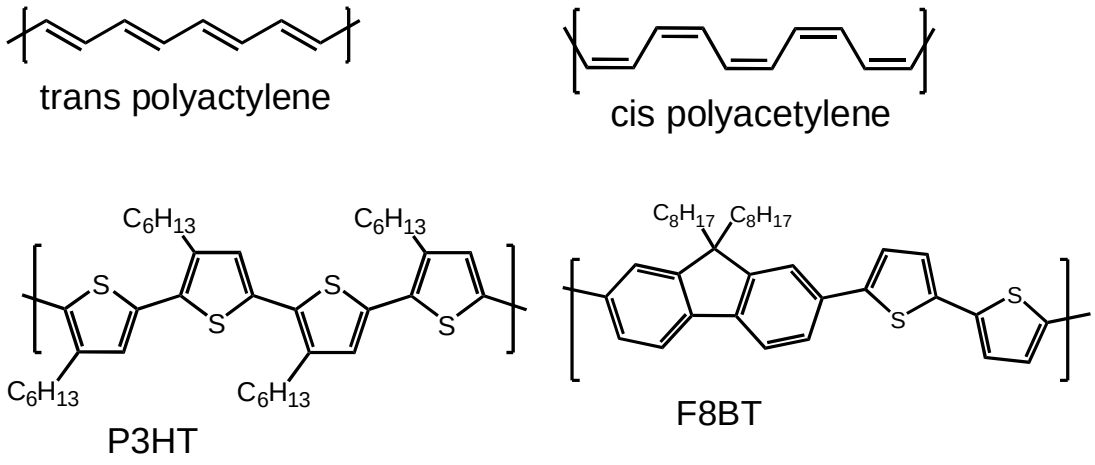

Figure II-6. Several polymer semiconductors.

C.1) SSH Hamiltonian

Theoretical accounts first centered on polyacetylene, which is one of the simplest models for conducting polymers [32,33]. Initially, one might expect that charge conjugation spans the entire polymer chain (see figure II-7 panel a), resulting in one electron per unit cell, one π orbital, and thus a half filled (metallic) band. However, this is found not to be the case, and can be explained through the SSH Hamiltonian.

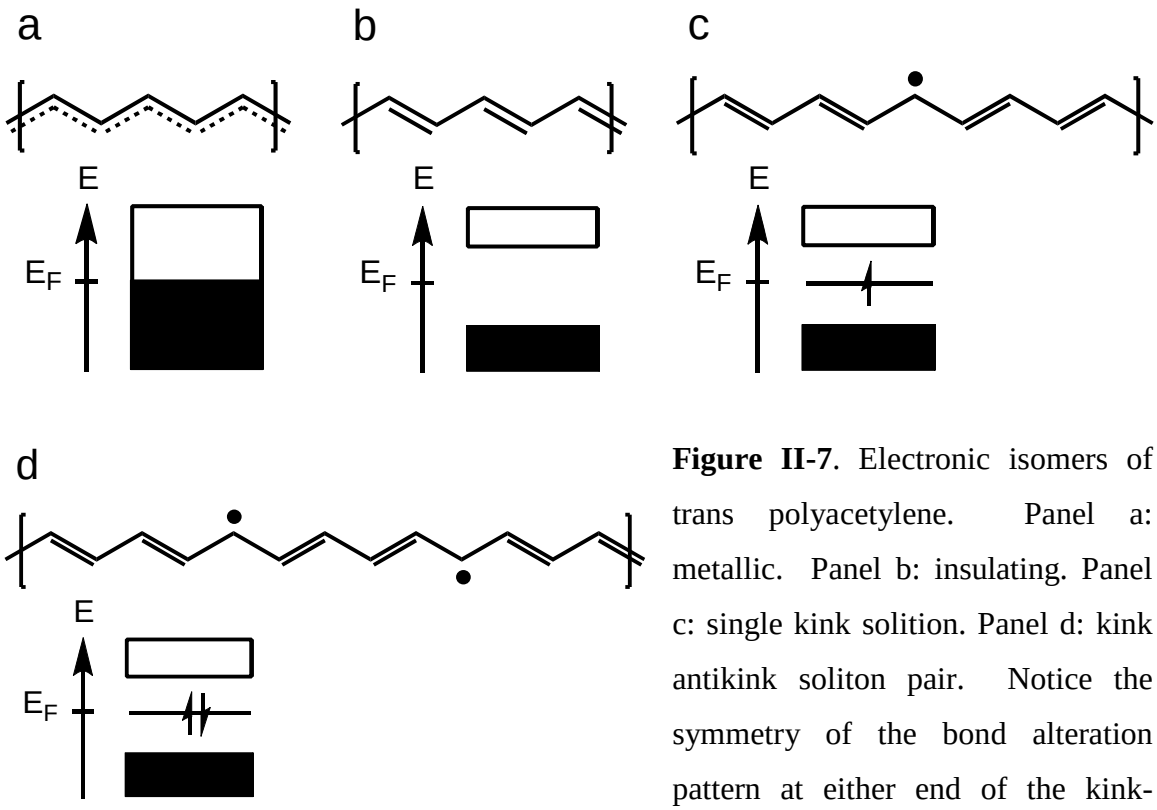

Figure II-7. Electronic isomers of trans polyacetylene. Panel a: metallic. Panel b: insulating. Panel c: single kink solition. Panel d: kink antikink soliton pair. Notice the symmetry of the bond alteration pattern at either end of the kink-antikink pair.

The SSH Hamiltonian describes the basic properties of charge carriers on an isolated 1-D chain. It can be broken up into four components describing π electrons, the

polymer chain, and the interaction between them. More formally, the Hamiltonian consists of a tight binding electron transfer component, (H_e), a harmonic potential of the σ bonds, (H_{ph}), the kinetic energy of the lattice, (H_k), and an electron-phonon coupling term ($H_{e\text{-}ph}$). The spin of the electrons is suppressed here.

(10) $$H = H_e + H_{ph} + H_k + H_{e-ph}$$

$$H_e = -\sum_n t_0 (C^*_{n+1} C_n + C_{n+1} C^*_n)$$

$$H_{ph} = \tfrac{1}{2} K \sum_n (y_{n+1} - y_n)^2$$

$$H_k = \tfrac{1}{2} M \sum_n \dot{y}_n^2$$

$$H_{e-ph} = -\sum_n \alpha (y_n - y_{n+1})(C^*_{n+1} C_n + C_{n+1} C^*_n)$$

In equation 10, the sum over all *n* is a sum over all atoms of the chain. The value of the transfer integral is given as t_0. The creation and annihilation operators, C_n^* and C_n act on the π electrons of the chain, in effect, calculating the decrease in the total energy as a result of adjacent atoms sharing a pair of π electrons. If this was the only term in the Hamiltonian, this decrease in energy would be offset by the loss of π electron sharing by the next nearest neighbors. However, the presence of the electron phonon coupling interaction changes this situation. The term α represents the magnitude the energy is lowered by changing the position (y_n) of the nth atom. This is reminiscent of the decrease in bond length encountered with increasing bond strength. However, bond energy cannot be lowered indefinitely by compressing the double bond and lengthening the single bond; the harmonic potential describing σ bond energy eventually forces the system into equilibrium. A critical observation is that the electron-phonon coupling is first order

while the harmonic term is second order. At very small displacements, the decrease in energy via the electron phonon coupling will always outweigh the harmonic term. Thus the chain is unstable to an infinitesimal lattice distortion. This is also known as a Peierls distortion, and doubles the size of the unit cell. After the dimerization, there are two carbon atoms per unit cell, one π bonding orbital, and two electrons to fill the orbital. Thus, on an infinite chain, the system forms separate HOMO and LUMO bands, representing the bonding and antibonding π orbitals (see figure II-7 panel b).[33]

As shown above, the properties of the system can understood in terms of the dimerization pattern of chain. Following this line of thought further, it can be noticed that there are two degenerate bond alteration patterns in polyacetylene. Thus, one might expect that both could exist on the same chain and that novel phenomena would occur where the bond alteration pattern switches. This turns out to be correct; the change in the bond alteration pattern is characterized by a structural distortion of a finite width. The structural distortion is accompanied by a radical electron and can be considered as a single, neutral particle called a kink soliton (see figure II-7 panel c). The energy of this defect is located at midgap, between the HOMO and LUMO bands of the polymer chain. In other words, the radical electron no longer contributes to the dimerization of the lattice, and is not involved in bonding.[32] For each additional solition created on the chain, symmetry considerations dictate that solitons are always created in pairs. The following argument shows why: imagine an infinite polymer having a single bond alteration pattern. It can be seen that nucleating the flipped bond alteration pattern requires the creation of two solitons, one at either end of the flipped pattern (see figure II-7 panel d).[34]

However, it is important to note that the existence of a single kink soliton depends on the ground state degeneracy of polyacetylene.[34,35] In other words, if the different dimerization patterns are not energetically equivalent, the single kink soliton would not occur, instead, bound kink-antikink soliton pairs would have to be the dominant neutral excitations on the polymer chain. As figure II-8 shows, the different dimerization patterns of cis-polyacetylene are not identical, thus they can be expected to have different energies. The conclusion to be reached is that the ground state of a structural defect must begin and end with the same pattern. It can be seen intuitively that this is only possible if defects join up in the form of a lone pair. (The charges are not likely to be so strongly localized, but are drawn that way for ease of understanding).

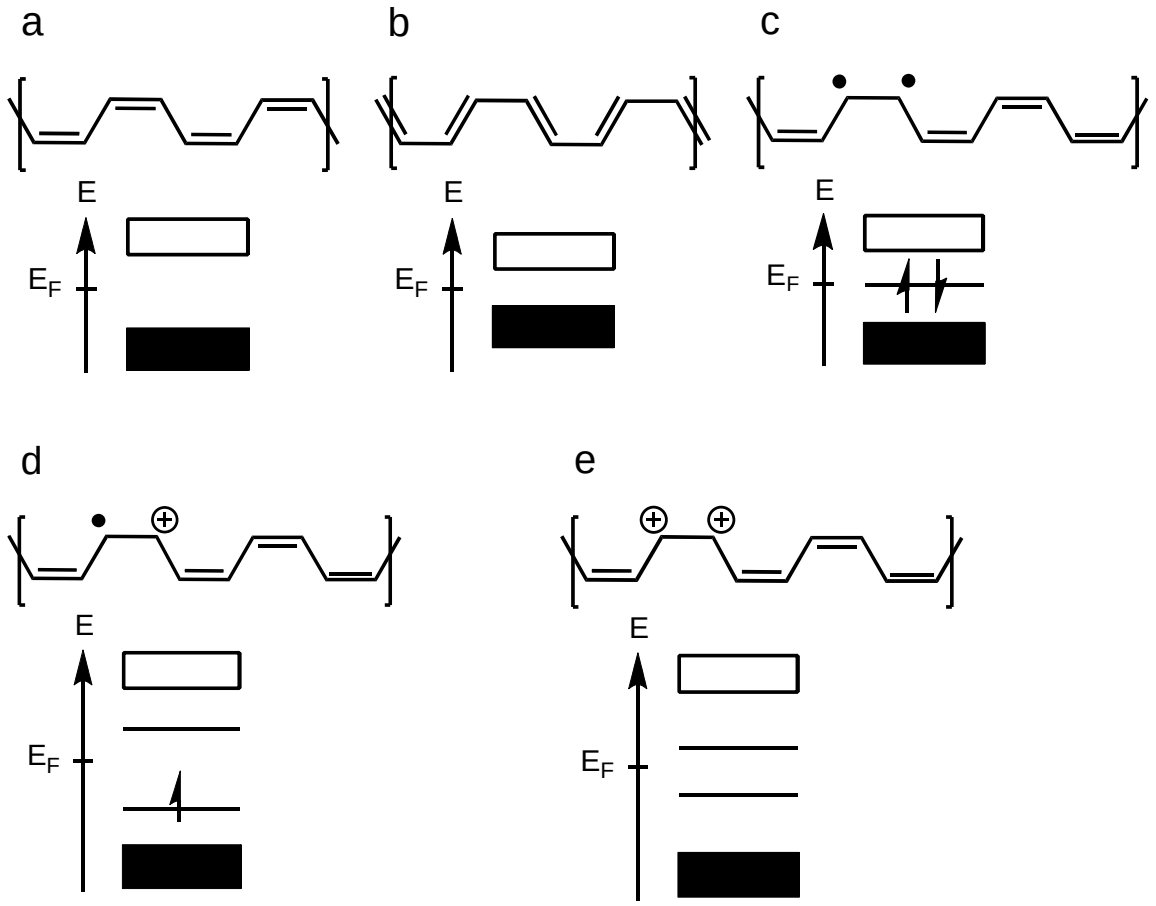

Figure II-8. Cis polyacetylene. Panel a: neutral, insulating, polymer. Panel b: non-degenerate bond alteration pattern of neutral, insulating polymer. Panel c: kink-antikink pair. Panel d: singly charged hole polaron. A polaron results from the ionization of one member of the kink-antikink pair and causes the midgap level to split. Panel e: bipolaron. A bipolaron is the result of ionizing the remaining radical electron of a singly charged polaron, or by the meeting of two singly charged polarons. The midgap energy levels are shifted towards the center of the gap.

Charged defects in conducting polymers can be understood in terms of the ionization of one member of the kink-antikink pair, or alternatively a member of a lone pair, for example, to form a hole and a radical electron.[34] The name for the charged

defect is a polaron.[35] To restate, the ground state of a polaron is symmetrical. That is, the bond alteration pattern is identical on either side of the polaron. Formally, the dimerization pattern of the polaron is formed by taking linear combinations of the two soliton dimerization patterns.[34] In summary, a (singly charged) charge carrier in a conjugated polymer is associated with an excess radical electron and is localized by a deformation of the polymer chain, and the nature of the carrier can be described in terms of the structural deformation.

From a chemistry point of view, it seems odd that a radical state of a semiconducting polymer would be the most stable charged configuration. It seems intuitive that two radical electrons would form a lower energy state by paring to form a doubly charged polaron, more often referred to as a bipolaron (see figure II-8 panel e). Theoretical calculations and solution electrochemical data,[36,37] suggest that this is possible. However, the existence of bipolarons in the solid state has not been unambiguously verified.

C.2) Methods of polymer charging

In order to study charged excitations of a semiconducting polymer, methods of charge induction must be devised. One of the earliest employed methods is treatment with iodine or bromine vapor. This is a strictly chemical process where the neutral diatomic vapor will withdraw an electron from the neutral polymer chain, forming a hole which can participate in conduction.[28] Another way to oxidize a conjugated polymer film is to change the electrochemical potential of the polymer through the application of a

voltage in an ionic solution. For example, negatively charged perchlorate ions from solution can be incorporated into the polymer matrix, via the application of an electrochemical potential, stabilizing holes in the polythiophene.[38] Thirdly, charges can be induced by changing the chemical potential of the polymer with an electric field gradient, stabilizing charges in the polymer without the presence of ions. This is called field doping, and is the basic operating mechanism in the organic field effect transistor. [39] Also, carriers can be induced by optical excitation, and is often done in the context of photoinduced absorption measurements.[40] Several of these mechanisms will be discussed in further detail in section E.

C.3) Interactions in the solid state

Ultimately, it is the solid state of the polymer which is most technologically useful. Although the SSH formalism gives a complete description of the basic charged excitations on a conjugated polymer chain, the SSH Hamiltonian does not account for interactions present only the in the solid state. In a solid film, the interactions between polymer chains can give rise to important effects which are critical to the ability of the film to conduct electricity. This is intuitive when one considers the fact that the length of a single polymer chain about 100 times smaller than the average electrode spacing in a thin film device. Thus the ability of a polymer to conduct electricity will depend upon the ability of charge carriers to move from chain to chain.[41] This is often called interchain transport.

The process by which a charge carrier moves between polymer chains is in many ways similar to that which occurs in a molecular solid. Since the chains are not typically cross-linked, van der Waals interactions between the chains serve to mediate charge transfer. Similarly to small molecule organic semiconductors, improving the crystallinity of the polymer is an effective way to improve interchain interactions. This paradigm has driven the development of polymers which can easily form crystalline structures. For example regio-regular P3HT, PBTTT, and F8BT (see figure 6) all have rigid backbones and alkyl side chains and can form crystallites when deposited from solution.

However, increasing crystallinity does not, of necessity, increase the thin film mobility of a polymer semiconductor. Kline, et al.[42-44] demonstrated that low molecular weight RR-P3HT, although more crystalline, has a lower mobility than high molecular weight RR-P3HT. They attributed this difference to the increased interconnectivity of the crystalline domains by the longer chains of high molecular weight polymer. However, the effect on mobility of increasing molecular weight plateaus at extremely high molecular weight. Interestingly this is correlated with a plateau of the width of crystalline nanofibrils.[45]

One interesting implication of the strong interaction between polymer chains is its effect on the energetic position of the polaron levels. As stated above, the presence of van der Waals interactions between the π orbitals of neighboring polymer chains facilitates charge transfer between them. In fact, this interaction is strong enough to encourage the delocalization of charge carriers across multiple polymer chains.[40] This affects the energetic position of the polaron levels due the decrease in confinement, lowering the energetic position of the lowest polaron energy level and increasing the

energy of the highest polaron energy level. To restate, the interactions present between polymer chains in the solid state not only affects the charge transport properties, but also the energy of the charge carriers themselves. Thus, the role of crystallinity and morphology in polymer semiconductors remains an open avenue of investigation.

D) Optical Absorptions in Organic Semiconductors

The majority of the work undertaken as a part of this thesis concerns the optical spectroscopy of charge carriers in organic semiconductors, especially in the infrared and near infrared. In order to make correct spectral assignments, it is important to have an understanding of some of the possible features that may arise during an experiment. With that in mind, this chapter focuses on the connection between spectroscopic signatures typical of organic semiconductors and theories of electronic structure and molecular vibration. This section will, therefore, include some discussion on the transport properties of organic semiconductors, but a focus on optical absorption in general will be maintained. The types of optical absorption considered are those relating to the classical Drude theory of metals, the absorption of polarons in semiconducting polymers and the infrared active vibrational absorptions associated with them. Also, the more traditional infrared absorptions associated with molecular vibrational modes will be discussed.

D.1) Drude absorption

One of the most famous examples of light absorption in classical electromagnetic theory is often called Drude absorption, or free carrier absorption. This effect is a dominant feature in the absorption of light by metals, the materials most accurately described by Drude theory and the free electron gas theory. Briefly, light is absorbed by a conductive material because the oscillating electromagnetic fields transfer energy to

mobile charge carriers. The mobile charges oscillate in space, dissipating their energy via resistive losses.[46]

More specifically, charges are treated as damped harmonic oscillators and their motion under the oscillating field of an incident light wave can be treated with the Lorentz force equation. Relating the bulk polarizability to the size of the dipole moment created by the oscillating charges allows one to connect the frequency dependent oscillation amplitude of said carriers with the dielectric constant of the material. The dielectric constant is in general a complex quantity and can be related to the results of an optical absorption measurement by multiplying the imaginary part of the dielectric constant by the frequency of light. (See appendix A for additional constants that enter the expression).[47]

The shape of the absorption depends qualitatively on whether or not the electrons are free to resonate as their frequency goes to zero. In this case, the complex dielectric constant diverges at low frequencies. This is true in the case of metals, which can be described in terms of free electron theory. Therefore, the presence of free-electron or Drude absorption is sensitive to whether or not a sample is metallic. Below is the equation for Drude absorption for metallic samples in terms of the complex dielectric constant $\varepsilon(\omega)$, the dielectric constant of free space, (ε_0) and the scattering time from Drude theory (τ). The plasma frequency also appears, ($\omega_P^2 = ne^2m^{-1}\varepsilon_0^{-1}$) and is related to the number of electrons (n) their mass (m) and their charge (e).[46]

(11) $$\frac{\varepsilon_D(\omega)}{\varepsilon_0} = i\frac{\omega_P^{\ 2}}{\omega\left(\tau^{-1} - i\omega\right)}$$

Converting the dielectric function of equation 11 into an absorption coefficient yields a function which does not diverge at low frequencies, but rather converges to a single value. This result is plotted in figure II-9.

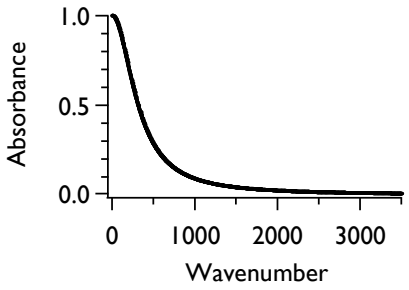

Figure II-9. Drude absorption. Theoretical prediction for absorbance experiment of a free electron metal. The width of the feature depends upon the relaxation time of the electrons.

In terms of organic semiconductors, Drude absorptions are not often observed because of a small degree of localization that occurs, restricting the ability of charge carriers to absorb light at low frequencies, presumably due to disorder.[48] Two recent observations are exceptions,[49,50] and debate concerning the nature of the highly conductive state in heavily doped conducing polymers is a continuing source of debate.[51] It is clear, however, that Drude absorption is not a major signature in the case of light and moderately doped organic semiconductor samples.

D.2) Polaron absorptions

Polarons are self localized charges which occur when charges are introduced into a polymer semiconductor.[34] The creation of a polaron significantly modifies the electronic structure of a material and brings about an entirely new set of absorptions (see figure II-8 and figure II-10). It is important to note that while six possible transitions

exist for a polaron, only three independent transitions are usually observed.[34] The three observable electronic transitions for a polaron are ω_1, ω_2, and the interband transition(HOMO→LUMO). It is perhaps worth mentioning that polaron creation can disrupt the local band structure, and can bleach the interband transition.[38,52]

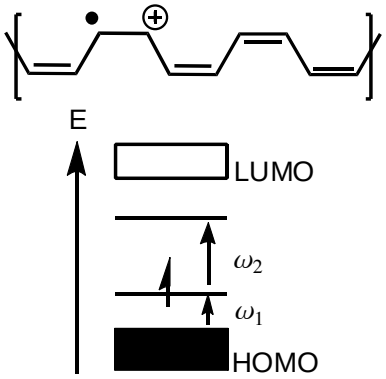

Figure II-10. Polaron absorptions. Only three allowed transitions exist for a singly charged polaron. The two that can be seen in the mid and near infrared are labeled ω_1 and ω_2. The transition across the band gap from the HOMO to the LUMO causes absorptions in the visible range.

As stated previously in section C.3, interchain interactions play a large role in polaron energetics; this is naturally reflected in the absorption spectrum. The interchain interactions allow a degree of 2-D delocalization, and the lowest polaron energy level decreases in energy due to decreasing kinetic energy.[53] This separation in energy can also be understood in terms of a linear combination of orbitals, whereby the bottom polaron level is split into a doublet. Since the polaron energy levels are symmetric about the center of the gap,[34] there is a corresponding splitting in the highest polaron level. Thus, ω_1 decreases in energy while ω_2 increases in energy, creating a distinct absorption spectrum from chains without strong interchain interactions.[40,54]

More recently, attempts to describe strong interchain interactions in terms of the Marcus theory of electron transfer have been relatively successful.[55] However, one would expect a certain similarity between the interchain polaron and the weakly localized

two dimensional carrier found in experiments on single crystal rubrene [23] for example. To date, a complete understanding of the nature of delocalized carriers in organic semiconductor has not been achieved.

Singly charged polarons are not the only excitations which are allowed in polymer semiconductors; two polarons can meet and lower their energy by sharing a single lattice distortion, forming a bipolaron. Much research has been devoted to working out the consequences of bipolaron formation.[56] However, the existence of bipolarons in the solid state is very much under debate.[36,37,50,51] In the case when two polarons combine to form a bipolaron, the set of observable excitations changes. In a hole bipolaron, the lowest polaron state is unoccupied, making the transition between the two polaron states (ω_2) impossible to access. The bipolaron states will be shifted towards the center of the gap, changing the energy of the ω_1 transition. The electron-hole symmetry of the polaronic states should also hold in the case of a two electron bipolaron requiring that again, ω_1 is the only observed transition.[34]

D.3) Infrared active vibrational modes (IRAV)

Polarons are charges which have been localized through their interactions with and polarization of the polymer chain. This means that there is a strong coupling between the excess charge and the motions of atoms on the chain. The electron-phonon coupling can manifest itself in ways other than the modification of the electronic structure of the polymer. One of the other ways that electron phonon coupling is observed in polymer is through the appearance of infrared active vibrational modes

(IRAV). Not all vibrational modes of the polymer are infrared active as some vibrations do not change the dipole moment of the bond. However, these modes can interact with the charge density of the polaron to produce an oscillation of the charge cloud. This can change the dipole moment of the vibration and cause the previously invisible vibrational mode to become a potent infrared absorber and appear in the spectrum.[57,58,59]

D.4) Vibrational absorptions

The collective vibration of atoms in a molecule is a dominant absorption mechanism in the infrared, and organic semiconductor molecules are no exception. The simplest model for molecular vibrations is the quantum mechanical harmonic oscillator. The Hamiltonian of the harmonic oscillator can derived from the force on a Hooke's law spring with a force constant (K), being translated a direction parallel to the axis of the spring (x).

(12) $$H = \frac{p^2}{2m} + \frac{kx^2}{2}$$

The allowed vibrational energies of a harmonic oscillator are evenly spaced and the magnitude of the energy spacing depends upon the spring constant of the oscillator.

(13) $$E = \hbar\omega\left(n + \tfrac{1}{2}\right)$$

Where ω is the natural frequency of the classical oscillator given by equation 14.

(14) $$\omega = \sqrt{\frac{K}{m}}$$

In terms of molecular properties, the spring constant of the oscillator is comparable to bond strength and the harmonic potential attempts to describe the change in energy to a chemical bond caused by altering the internuclear distance.[4]

A more accurate description of a vibrating molecule recognizes that a molecule is not merely a collection of oscillators, but that it is a collection of *interacting* oscillators. This is taken into consideration by what is called normal mode analysis, where the collective vibrations are decoupled into a set of generalized coordinates orthogonal to one another.[4] Each peak in an infrared absorption measurement of a real molecule is related to an energetic transition of one orthogonal mode.

E) Transistors, Capacitors, and Electrochemical Cells

A significant part of the results section is dedicated to understanding the charge injection mechanisms operating in organic semiconductor/polymer electrolyte devices via spectroscopic methods. As a result, it is necessary to develop a basic familiarity with the terminology and operating principles of the electrical devices themselves. Although this theme has appeared briefly and periodically throughout the introduction, this section is devoted to a more careful treatment of the subject. More specifically, it discusses the transistor, the metal insulator capacitor and the electrochemical cell.

E.1) Transistors

A basic schematic of a transistor is pictured in figure II-11 and is comprised of two different materials (gate dielectric and semiconductor) and three terminals which are connected to external circuitry (source, drain, and gate electrodes). As stated earlier, a transistor can be viewed as a switch. When a voltage is applied between the source and drain electrodes, current will flow through the semiconductor between the source and drain electrodes. The magnitude of that current is determined by the conductance of the semiconductor; often called the channel conductance. Applying a voltage to the gate electrode can increase the channel conductance by orders of magnitude, switching the device on.[3]

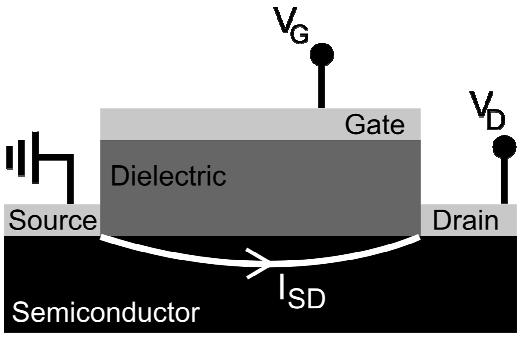

Figure II-11. Transistor schematic. Current (I_{SD}) is driven across the semiconductor layer by a voltage difference between source and drain electrodes (V_D). The magnitude of the current is modulated by the application of a voltage to the gate electrode (V_G) which changes the number of charge carriers.

Many processes control the level of the on current in a transistor, but two are of particular interest in the context of the work presented here. The first is the intrinsic charge transport properties of the semiconductor layer, which can be approached in terms of Drude's law. Applying a gate voltage increases the number of charge carriers, (n) and the channel conductance (σ) rises in direct proportion.[3]

(15) $\sigma = ne\mu$

This understanding is oversimplified, especially in terms of organic thin film transistors for the following reason: mobility can itself be a function of the number of charge carriers. In an electrochemical transistor, this dependence is quite strong, while in a field effect transistor this dependence is weaker.[60] However, the basic idea behind the transistor remains: more carriers, higher conductance.

The knowledge that higher channel conductance is the result of higher charge carrier densities does not fully answer the question of how a transistor works; it is important to have an account of how increased charge carrier density arises when the gate voltage is applied. Two methods of increasing the density of charge carriers will be addressed. The first method is field effect doping, also known as electrostatic doping,

and the second is electrochemical doping. Actually, one need not use a transistor to study the charging process at all. Field effect charging of a semiconductor can be studied by using a capacitor structure, and electrochemical doping can be studied using an electrochemical cell. Thus the remainder of the section will be devoted to the metal-insulator-semiconductor (MIS) capacitor, and the electrochemical cell.

E.2) MIS capacitors

To study the field effect charging process in the channel of a transistor, one can construct a capacitor by placing a dielectric between a metal electrode and a semiconductor. Placing an additional electrode on the semiconductor completes the device and allows it to be connected as part of a circuit. In the absence of any internal potential in the device, for example, as a result of a work function between the metal electrodes and the semiconductor, the amount of charge induced in the semiconductor ($q=ne$) is simply related to the applied voltage (V) by the capacitance of the dielectric layer (C).

(16) $q = CV$

The voltage drop across the device can be described as having two major physical components; the voltage drop across the dielectric, and the voltage drop the charged region of the semiconductor. The voltage drop across the dielectric is related to its capacitance, which for a linear dielectric varies inversely with the thickness of the dielectric.[3] The accumulation of charge near the semiconductor/dielectric interface is the cause of the remainder of the voltage drop in the device, and is a result of the altered

chemical potential of the electronic states near the dielectric interface.[5] The ability of MIS structures to accumulate charge in a predictable way has enabled the use of metal insulator organic semiconductor structures to study the concentration of trapped carriers.[61]

E.3) Electrochemical cells

Another way to induce charge carriers in an organic semiconductor device is to construct an electrochemical cell. A simple electrochemical cell consists of a metal electrode coated with a film of organic semiconductor, a metal counter electrode, and an electrolyte solution, all of which are in series with a power source. Charge is induced in the semiconductor film by applying an electric potential between the organic semiconductor and the counter electrode. The applied potential changes the position of the Fermi level (electrochemical potential) of the organic semiconductor with respect to the electrolyte solution and the semiconductor charges in order to maintain thermodynamic equilibrium.[62] In some ways, the process is similar to that of a MIS capacitor; an applied potential changes the internal potential energy of electrons in the organic semiconductor and the material accumulates charge. However, the mechanism of charge induction in an electrochemical cell is more complicated than in the case of a capacitor constructed with a linear dielectric. The two following possibilities will be examined: electrostatic double layer charging and mass transfer at the electrolyte/semiconductor interface.

The term “electrostatic double layer” describes the accumulation of charge at one side of an interface, and a corresponding accumulation of the opposite charge on the opposite side of the interface. For example, applying a negative potential to a mercury electrode in a NaF solution will cause the mercury electrode to accumulate electrons and become negatively charged. Conversely, in the solution, Na^+ ions become concentrated near the mercury electrode. Several models describing the ion concentration profile exist, but most predict that elevated ion concentrations extend 20 nm or less into the solution (for moderate to high ion concentrations). Because electric potential is constant throughout the bulk of the solution, potential only changes near the interface. The rapid change in potential gives the electrostatic double layer an unusually high capacitance, often on the order of 10 μF cm^{-2}.[62]

Developing methods to take advantage of the extremely high capacitance of the electrostatic double layer has been a point of interest in the organic semiconductor literature.[63-69] Perhaps the most important of these reasons is low voltage operation of organic transistors. This is especially compelling given that most uses for organic transistors are likely to focus on low cost, large area applications. Such applications will require low voltage operation as basic design specification.

The second mechanism of charge induction discussed here deals with mass transfer at the electrolyte interface. The intercalation of ions into the solid electrode of an electrochemical cell is not typically seen in systems with standard metal or crystalline inorganic semiconductor electrodes. These electrodes are for all practical purposes, impermeable to the ions of the electrolyte phase. However, not all materials are equally impermeable. Examples of permeable films include, clays, zeolites, solid polymer

electrolytes, polyelectrolytes, and porous metal films.[62] Lastly, and most importantly, semiconducting polymers are permeable to ions.[70]

Using an electric potential to drive ions into a semiconducting polymer causes the reduction or oxidation of the polymer by changing its electrochemical potential. In this way, an entire polymer film can be doped and made conductive although the bulk of the polymer is charge neutral due to the presence of counterions. Throughout the remainder of this thesis, the process of driving ions into the bulk of an organic semiconductor with an applied electric potential will be referred to as electrochemical doping.

This thesis is directed at developing a better understanding regarding organic field effect transistors (OFET) as well as organic thin film transistors (OTFT). The results of the original research found in this thesis will attempt to sharpen the distinction between the two. Simply put, charge carriers in an organic field effect transistor are induced by an electric field at the semiconductor/dielectric interface, while in an organic thin film transistor the means of inducing charges is unspecified. In this sense, the organic thin film transistor is the more general concept; it does not make reference to the mechanism of device operation.

F) References

[1] Gersten, J.I.; Smith, F.W.; *The Physics and Chemistry of Materials,* John Wiley and Sons: Danvers, MA, 2001.

[2] Kittel, C. *Introduction to Solid State Physics*, 8th ed.; John Wiley and Sons: Danvers, MA, 2005.

[3] Sze, S.M.; Ng, K.K. *Physics of Semiconductor Devices*, 3rd ed.; John Wiley and Sons: Hoboken, NJ, 2007.

[4] Shankar, R. *Principles of Quantum Mechanics*, 2nd ed.; Plenum Press, New York, 1994.

[5] Kittel, C.; Kroemer, H. *Thermal Physics*, 2nd ed.; W.H. Freeman and Company: New York, 2003.

[6] Gersten, J.I.; Smith, F.W. *The Physics and Chemistry of Materials*, John Wiley and Sons: Danvers, MA, 2001; pp 189.

[7] Kittel, C. *Introduction to Solid State Physics*, 8th ed.; John Wiley and Sons: Danvers, MA, 2005; pp 139.

[8] Kittel, C. *Introduction to Solid State Physics*, 8th ed.; John Wiley and Sons: Danvers, MA, 2005; pp 151.

[9] Mott, N.F. *Metal-Insulator Transitions*, 2nd ed.; Taylor and Francis: New York, 1990.

[10] Cheng, Y.C.; Silbey, R.J.; da Silva Filho, D.A; Calbert, J.P.; Cornil, J.; Bredas, J.-L. *J. Chem. Phys.* **2003**, 118, 3764-3774.

[11] Sanchez-Carrera, R.S.; Coropceanu, V.; Kim, E.-G.; Bredas, J.-L. *Chem. Mater.* **2008**, 20, 5832-5838.

[12] Pasveer, W.F.; Cottaar, J.; Tanase, C.; Coehoorn, R.; Bobbert, P.A.; Blom, P.W.M.; de Leeuw, D.M.; Michels, M.A.J.; *Phys. Rev. Lett.* **2005**, 94, 206601.

[13] Shkolvskii, B.I.; Efros, A.L. *Electronic Properties of Doped Semiconductors*, Springer-Verlag: New York, 1984.

[14] Mott, N.F.; Kaveh, M. *Adv. Phys.* **1985**, 34, 329-401.

[15] Bao, Z.; Locklin, J. *Organic Field Effect Transistors*, CRC Press: Boca Raton, FL, 2007 pp 46-48.

[16] Arkhipov, V.I.; Bassler, H. *J. Non-cryst. Solids* **1996**, 198-200, 242-245.

[17] Arkhipov, V.I.; Heremans, P.; Emelianova, E.V.; Adriaenssens, G.J.; Bassler,G. *Phys.Rev. B* **2005**, 72, 235202.

[18] Dhoot, A.S.; Wang, G.M.; Moses, D.; Heeger, A.J. *Phys. Rev. Lett.* **2006**, 96, 246403.

[19] Facchetti, A. *Mater. Today*, **2007**, 10, 28-37.

[20] Campbell, R.B.; Robertson, J.M.; Trotter, *J. Acta Cryst.* **1961**, 14, 705.

[21] Siegrist, T.; Besnard, C.; Haas, S.; Schiltz, M.; Pattison, P.; Chernyshov, D.; Batlogg, B.; Kloc, C. *Adv. Mater.* **2007**, 19, 2079-2082.

[22] Vikram, S.C.; Zaumseil, J.; Podzorov, V.; Menard, E.; Willett, R.L.; Takao, S.; Gershenson, M.E.; Rogers, J.A. *Science* **2004**, 303, 1644-1646.

[23] Li, Z.Q.; Podzorov, V.; Sai, N. Martin, M.C.; Gershenson, M.E.; Di Ventra, M.; Basov, D.N. *Phys. Rev. Lett.* **2007**, 99, 016403.

[24] Podzorov, V.; Menard, E.; Borissov, A.; Kiryukhin, V.; Rogers, J.A.; Gershenson, M.E. *Phys. Rev. Lett*. **2004**, 93, 086602.

[25] Krellner, C.; Haas, S.; Goldmann, C.; Pernstich, K.P.; Gundlach, D.J.; Batlogg, B. *Phys. Rev. B* **2007**, 75, 245115.

[26] Payne, M.M.; Delcamp, J.H.; Parkin, S.R.; Anthony, J.E. *Org. Lett*. **2004**, 6, 1609-1612.

[27] Brown, A.R.; Pomp, A.; de Leeuw, D.M.; Klaassen, D.B.M.; Havinga, E.E.; Herwig, P.; Mullen,K. *J. Appl. Phys*. **1996**, 79, 2136-2138.

[28] Chaing, C.K.; Fincher Jr., C. R.; Park, Y.W.; Heeger, A.J.; Shirakawa, H.; Louis, E.J.; Gau, S.C.; MacDiarmid, A.G. *Phys. Rev. Lett*. **1977,** *39*, 1098-1101.

[29] Heeger, A.J. *J. Phys. Chem. B* **2001**, 105, 8475-8491.

[30] Shirakawa, H. *Angew. Chem. Int. Ed*. **2001**, 40, 2574-2580.

[31] MacDiarmid, A.G. Rev. Mod. Phys. 2001, 73, 701-712.

[32] Pople, J.A.; Walmsley, S.H. *Mol. Phys.* **1962**, 5, 15-20.

[33] Su, W.P.; Schrieffer, J.R.; Heeger, A.J. *Phys. Rev. Lett*. **1979**, 42, 1698-1701.

[34] Fesser, K.; Bishop, A.R.; Campbell, D.K. *Phys. Rev. B* **1983**, 27, 4804-4825.

[35] Campbell, D.K.; Bishop, A.R. *Phys. Rev. B* **1981**, 24, 4859-4862.

[36] Bredas, J.-L.; Street, G.B. *Acc. Chem. Res.* **1985**, 18, 309-315.

[37] Apperloo, J.J.; Groenendaal, L.B.; Verheyen, H.; Jayakannan, M.; Janssen, R.A.J.; Dkhissi, A.; Beljonne, D.; Lazzaroni, R.; Bredas, J.L. *Chem. Eur. J*. **2002**, 8, 2384-2396.

[38] Hotta, S.; Rughooputh, S.D.D.V.; Heeger, A.J.; Wudl, F. Macromolecules **1987**, 20, 212-215.

[39] Newman, C.R.; Frisbie, C.D.; da Silva Filho, D.A.; Bredas, J.-L.; Ewbank, P.C.; Mann, K.R. *Chem. Mater.* **2004**, 16, 4436-4451.

[40] Osterbacka, R.; An, C.P.; Jiang, X.M.; Vardeny, Z.V. *Science* **2000**, 287, 839-842.

[41] Salleo, A. *Mater Today* **2007**, 10, 38-45.

[42] Kline, J.R.; McGhee, M.D.; Kadnikova, E.N.; Liu, J.; Frechet, J.M.J. *Adv. Mater.* **2003**, 15, 1519-1522.

[43] Kline, J.R.; McGhee, M.D.; Kadnikova, E.N.; Liu, J.; Frechet, J.M.J.; Toney, M.F.; *Macromolecules* **2005**, 38, 3312-3319.

[44] Kline, R.; McGehee, M. *Polym. Rev.* **2006**, *46*, 27-45.

[45] Zhang, R.; Iovu, M.C.; Jeffries-EL, M.; Sauve, G.; Cooper, J.; Jia, S.; Tristram-Nagle, S.; Smilgies, D.M.; Lambeth, D.N.; McCullough, R.D.; Kowalewski, T. *J. Am. Chem. Soc.* **2006**, 128, 3480-3481.

[46] Jackson, J.D. *Classical Electrodynamics*, 3rd ed; John Wiley and Sons: New York, 1999.

[47] Tolstoy, V.P; Chernyshova, I.V.; Skryshevsky, V.A. *Handbook of Infrared Spectroscopy of Ultrathin Films*, John Wiley and Sons: Hoboken, NJ, 2003.

[48] Lee, K.; Menon, R.; Yoon, C.O.; Heeger, A.J. *Phys. Rev. B* **1995**, 52, 4779-4787.

[49] Lee, K.; Cho, S.; Park, S.H.; Heeger, A.J.; Lee, C.-W.; Lee, S.-H. Nature 2006, 441, 65-68.

[50] Zhuo, J.-M.; Zhao, L.-H.; Chia, P.-J.; Sim, W.-S.; Friend, R.H.; Ho, P.K.H. *Phys. Rev. Lett.* **2008**, 100, 186601.

[51] Sai, N.; Li, Z.Q.; Martin, M.C.; Basov, D.N.; Di Ventra, M. *Phys. Rev. B* **2007**, 75, 045307.

[52] Brown, P.J.; Sirringhaus, H.; Harrison, M.; Shkunov, M.; Friend, R.H. *Phys. Rev. B* **2001**, 63, 125204.

[53] Beljonne, D. Cornil, J. Sirringhaus, H.; Brown, P.J.; Shkunov, M.; Friend, R.H.; Bredas, J.-L. *Adv. Funct. Mater.* **2001**, 11,229-234.

[54] Sirringhaus, H.; Brown, P.J.; Friend, R.H.; Nielsen, M.M.; Bechgaard, K.; Langeveld-Voss, B.M.W.; Spiering, A.J.H.; Janssen, R.A.J.; Meijer, E.W.; Herwig, P.; de Leeuw, D.M. *Nature*, **1999**, 401, 685-688.

[55] Chang, J.-F.; Sirringhaus, H.; Giles, M.; Heeney, M.; McCulloch, I. Phys Rev. B **2007**, 76, 205204.

[56] Street, R.A.; Salleo, A.; Chabinyc, M.L. *Phys. Rev. B* **2003**, 085316.

[57] Horovitz, B. *Solid State Comm*. **1982**, 41, 729-734.

[58] Carpinelli, J.M.; Weitering, H.H.; Plummer, E.W.; Stumpf, R. *Nautre* **1996**, 381, 398-400.

[59] Brown, S.; Gruner, G. Sci. Amer. 1994, 57, 50-56.

[60] Shimotani, H.; Diguet, G.; Iwasa, Y. *Appl. Phys. Lett*. **2005**, 86, 022104.

[61] Liang, Y.; Frisbie, C.D.; Chang, H.-C.; Ruden, P.R. *J. Appl. Phys.* **2009**, 105, 024514.

[62] Bard, A.J.; Faulkner, L.R. *Electrochemical Methods: Fundamentals and Applications*, 2nd ed.; John Wiley and Sons: Hoboken, NJ, 2001.

[63] Panzer, M.J.; Frisbie, C.D. *Adv. Funct. Mater.* **2006**, 16, 1051-1056.

[64] Panzer, M.J.; Newman, C.R.; Frisbie, C.D. *Appl. Phys. Lett*. **2005**, 86, 103503.

[65] Panzer, M.J.; Frisbie, C.D. *J. Am. Chem. Soc*. **2005**, 127, 6960-6961.

[66] Panzer, M.J.; Frisbie, C.D. *Appl. Phys. Lett*. **2006**, 88, 203504.

[67] Lin, F.; Lonergan, M.C. *Appl. Phys. Lett*. **2006**, 88, 133507.

[68] Dhoot, A.S.; Yuen, J.D.; Heeney, M.; McCulloch, I.; Moses, D.; Heeger, A.J. *Proc. Nat. Acad. Sci.* **2006**, 103, 11834-11837.

[69] Herlogsson, L.; Crispin, X.; Robinson, N.D.; Sandberg, M.; Hagel, O.-J.; Gustafsson, G.; Berggren, M. *Adv. Mater*. **2007**, 19, 97-101.

[70] Inzelt, G. *Conducting Polymers: a New Era in Electrochemistry*, Springer-Verlag, Berlin, Heidelberg, 2008.

III. Experimental

This chapter is dedicated to the detailed explanation of important concepts and methodology regarding the experiments carried out throughout the thesis research. More than any other, this chapter is written with the future graduate student in mind. Enough detail is included to give anyone a good chance at reproducing and improving the experiments. With that end in mind, the first section sets out to explain the technique of FTIR in enough depth to allow one to not only see how the technique works, but ways in which the current experimental apparatus is limited. The next section describes the infrared sampling technique used, describing not only how one goes about choosing a satisfactory optical material, but also how one can construct an optical piece from commercially available stock. Finally, the last and most detailed section covers the fabrication and testing of devices, including the highly specialized techniques that are glossed over in publication, but without which, the experiment would not work.

A) Fourier Transform Infrared and Near Infrared Spectroscopy

The research presented in this thesis is primarily comprised of spectroscopic data in the mid and near infrared spectroscopic range. To understand the data and make accurate spectral assignments, it is necessary to understand technique itself. In particular, it is necessary to understand the workings of an infrared spectrometer, the mathematical operations necessary to obtain a spectrum, and the potential sources of noise and artifacts.

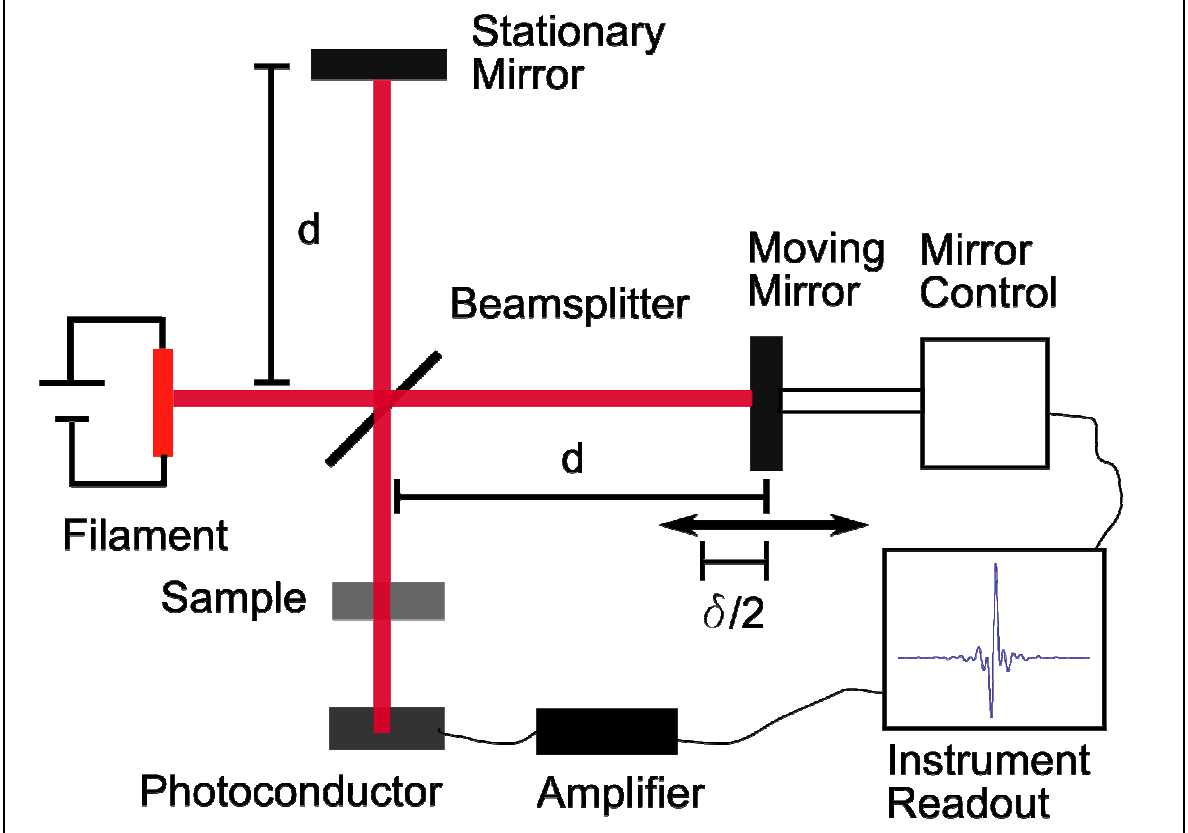

Figure III.1. FTIR Schematic. Infrared light is generated by passing current through a filament. The light reaches a beamsplitter where it is separated into two parts. One part travels a distance (d) to a stationary mirror. The other part is sent towards a moving mirror which can be offset by a distance (δ/2). The beams recombine at the beamsplitter and are sent towards the sample. After some of the light is absorbed by the sample, it reaches a photodetector, usually a photoconductive element. The resulting current is amplified and sent to control electronics which simultaneously monitor the position of the moving mirror. The data is used to construct an interferogram.

A.1) Infrared spectroscopy and the Michelson interferometer

One way to describe the workings of the spectrometer itself is to take the view of a group of photons as they are created and eventually converted into data. The discussion will rely on the schematic representation of the spectrometer found in figure III.1. At a brief glance, spectrometer operation can be described as a series of five steps. First, a beam of infrared light is generated and passed through a Michelson interferometer. Then, the beam reaches the sample where some of the light is absorbed. Lastly, the light enters a detector, which translates the flux of infrared photons into an electrical signal which can then be interpreted by a computer in order to generate an interferogram.

The generation of infrared light is typically done through the use of a resistively heated element. Passing current through a resistive element causes it to heat, and eventually it begins to glow, emitting a moderate flux of photons. The filament can be modeled as a blackbody, which allows for an estimate of the frequency spectrum of the emitted light.[1] The intensity of the light and its spectral shape both depend upon temperature,[2] thus the operating temperature of the infrared filament must be kept relatively constant to facilitate precise measurements.

After the infrared photons are generated, they are passed through an interferometer. The main purpose of this step is to allow the different frequency components of the light to be separated from one another. This separation begins with the use of an interferometer and is completed with the Fourier transform. In fact, interferometry can be thought of as a mechanical version the Fourier transform. This can be demonstrated with the aid of figure III.1 which shows a schematic of an

interferometer, and beginning with equation 1, which describes the spatially varying part of the electric field (E) in terms of its wavenumber (k), where E_0 represents the intensity of the field.[3]

(1) $$E = E_0 \exp[ikx]$$

After the beam enters the interferometer, it strikes a beamsplitter which separates the wave into two components, assumed here to be of equal intensity for the purpose of this discussion. One half of the beam is reflected towards a stationary mirror some distance, (d) away from the beamsplitter. The other half of the beam is transmitted towards a moving mirror which can translate by a distance ($\frac{1}{2}\delta$) from some average distance (d). When the beams recombine at the beamsplitter, they will have traveled different distances. The electric field propagating away from the beamsplitter is given by equation 2.

(2) $$E = \tfrac{1}{2} E_0 \left(\exp[ikx] + \exp[ik(x+\delta)]\right)$$

Factoring out the part of the plane which depends on x, shows that the electric field due to a particular frequency will go to zero when $k\delta = n\pi$ where n is any integer.

(3) $$E = \tfrac{1}{2} E_0 \exp[ikx]\left(1 + \exp[ik\delta]\right)$$

The intensity of the electric field now depends upon the product of the moving mirror position and the wavenumber of the incident radiation. Wavenumber information is thereby encoded in the sum of all moving mirror positions. When the signal is detected, the Fourier transform, in a sense, deduces the contribution from each

wavenumber component of the light by comparing the intensities at each moving mirror position.

In terms of spectrometer construction, the beam usually goes through the interferometer before reaching the sample. This is mostly out of convenience, not a formal requirement of the technique. In other words, the light absorbed by the sample is missing from the beam in the same proportion, regardless of whether it was absorbed before or after the beam entered the interferometer (assuming the linearity of the absorption process).

There are many ways to position a sample such that it can interact with the infrared beam and allow the beam to be collected. The simplest is transmission, whereby the beam is passed through the sample and collected on the other side. Other techniques include specular and diffuse reflection, and total internal reflection.[1] In the experiments presented in this thesis, the multiple total internal reflection technique is used exclusively. This technique will be discussed separately in section B.

After interacting with the sample, the beam is directed towards the detector. A typical infrared and near infrared detector is a photoconductive element, which monitors photon flux by measuring current response. Briefly, a photon having higher energy than the band gap of a material creates an electron-hole pair which can be separated by applying a voltage, creating an increased current.[4] The size of the band gap for a photoconductive element determines the minimum photon energy that can usefully be collected. Conversely, detectors also tend to become less sensitive at energies far above their band edge.[4] This imposes an upper energetic limit on photon energies that can be detected by a particular detector material. The overall effect is such that a detector has a

limited range of photon energies it can detect. It is therefore useful to employ multiple detector types to collect a wide spectral range.

To make the idea of the limits on a detector type, the three types of detectors used in this research will be discussed. The entire mid infrared range was detected by a liquid nitrogen cooled HgCdTe (MCT) detector which had a range 500-8000 cm^{-1}. Cooling the MCT with liquid nitrogen is especially important because its band gap must be quite small in order to detect radiation of such low energy, making it susceptible to thermal carrier production at room temperature. The mid to near infrared range was covered by a thermoelectrically cooled InGaAs detector with a range of 4000-15000 cm^{-1}. Although this detector is still somewhat sensitive above 11500 cm^{-1}, the sensitivity of the detector changes at higher energies, making it difficult to compare absorption intensities on either side of *11500* cm^{-1}. The near infrared to deep red visible part of the spectrum (*9000-15500* cm^{-1}) was collected by a thermoelectrically cooled silicon detector, whose upper limit is essentially dictated by the presence of the HeNe laser used for interferometer positioning.

After the beam strikes the detector and is converted into an electrical signal, the signal is electrically amplified and paired with the position of the moving mirror.[1] Repeating the process generates a data set of paired values of current versus moving mirror position. The name for this data is an interferogram and is the most basic data generated by the spectrometer. However, the interferogram itself is not normally useful in making spectral interpretations, requiring the employment of mathematical operations to convert the data into a useable form.

A.2) Mathematical data conversion

After the spectrometer obtains an interferogram, it must convert the plot of intensity versus moving mirror position, to a plot of intensity versus wavenumber. A computer program with the ability of taking a Fourier transform can complete the conversion. This process is normally done automatically by the spectrometer software, normally via the fast Fourier transform algorithm (FFT).[5] The operation generates a plot called a single beam spectrum which is the raw spectral data in frequency space, from which, more refined data analysis proceeds. The form of the single beam spectrum (R) is mostly due to three parts: the intensity of the light source, ($I_0(\omega)$) the response of the detector, ($F(\omega)$) and the contribution of absorbing species ($\exp[-\varepsilon(\omega)bc]$). Optical absorption is often described with the Beer-Lambert law which describes the exponential attenuation of the beam by a sample with a concentration of absorbing species c, having a molar absorbtivity of $\varepsilon(\omega)$. Also, the length of the beam path through the sample affects the amount of absorption and is given by b.[4,6,7]

(4) $$R \propto F(\omega) I_0(\omega) \exp[-\varepsilon(\omega)bc]$$

Often, data is presented in terms of absorbance, which is a method of subtracting details from the single beam spectrum not directly related to the absorbing species of interest. There are other ways of presenting the data, but the method almost exclusively employed throughout this research is given in equation 4, where A represents the absorbance, while R and R_0 represent the single beam spectrum containing the data of interest and the single beam spectrum containing only background information, respectively.

(5) $A = \ln R_0 - \ln R = \varepsilon(\omega)bc$

A critical point related to the computation of an absorbance spectra and a potential source of confusion results from the two different choices of background spectra used throughout the results section. Normally, when one takes the absorbance spectra of a sample, he or she is interested only in the absorptions of film as prepared. In this case, the background one would use contains only information relating to the detector response, the photon source, and the optical elements of the spectrometer, usually called a blank spectrum. However, during the course of in-situ spectroscopy, one will generally modify a parameter of the sample and monitor how the spectra changes as a function of that parameter. To be more concrete, when the voltage is modulated during the in-situ spectroscopic method employed here, the voltage induced changes are of interest. In order to isolate those changes, which can be somewhat small, the background subtracted belongs to the neutral sample. This will be referred to as a difference spectrum, and gives one the ability to directly observe the absorption spectra of charge carriers. In the interest of completeness, it is also possible to observe features opposite in sign due to a decreased absorbtivity of neutral portions of the film. This process is called spectral bleaching. To restate, two different types of spectra data are presented in the results section: absorbance spectra which use a blank background, and difference spectra which use the unbiased device as a background.

A.3) Artifacts and noise

Often, the magnitude of the spectral changes one wishes to observe is small.

Thus, it is important to understand the potential sources of noise and spectral artifacts that can enter into a data set to avoid a misinterpretation of the data. One can approach this problem by considering terms in equation 4 unrelated to the absorption of the sample. Often these and other factors can change in a manner out of the control of the experimenter. This point cannot be overemphasized; uncontrolled aspects of a spectroscopic experiment can cause artifacts that can be easily misinterpreted. Perhaps the easiest way to avoid this sort of error is to follow the maxim "Know how the spectrometer can lie to you." This knowledge comes from looking at a number of spectra in which no spectral features are expected. This is an important exercise, but the lessons learned from it are often dependent upon the exact spectrometer one is using. As a result, the rest of this section will include brief discussions of the physical sources of artifacts and noise resulting from specific components of the spectrometer. Most of the sources of noise and artifacts observed by me are related to IR intensity fluctuations, inherent current fluctuations in the detection electronics, and issues arising from detector warming and cooling.

One source of noise can be linked to changes in the intensity of the light source, represented in equation 4 as $I_0(\omega)$. Recalling that a typical infrared light source is roughly modeled as a radiating black body,[1,4] variations in the light intensity can be described in terms of variations in the temperature of the source. Temperature variations in the light source affect not only the intensity of the light, but its spectrum as well.[2] Thus spectral variations due to variable filament temperatures will have a broad, often curved shape. If the filament temperature is not explicitly controlled, long timescale power fluctuations in the power source can result in artifacts which consistently appear in

a similar form. One mechanism for power fluctuations occurring over hour timescales can be linked to the output of a wall outlet, for example.[8] Sources of noise that become more prominent at low frequencies, contribute to what is generally called *1/f*, or pink noise.[8]

Another major source of noise comes from the detector itself and the electronics connecting it to the rest of the spectrometer. Sources of noise in photoconductors are often linked to Brownian motion of charge carriers, the statistical distribution of photon flux with time, and the discreet nature of electrical current.[8] These are statistical fluctuations and tend to produce the familiar looking, rapidly oscillating, random fluctuations about the mean signal level. The level of the fluctuations can be decreased by averaging a larger number of measurements.[8] However, an arbitrarily large number of measurements cannot be averaged without taking steps to diminish the effects of *1/f* noise operating at long timescales.

Another source of *1/f* noise which is evident in FTIR experiments is due to detector warming and cooling. An infrared photoconductive element has by necessity, a small band gap. Thus the thermal excitation of carriers across the band gap can contribute significantly to the conductivity of the detector element. Thus, the detector must be cooled, usually with liquid nitrogen. Despite being connected to a vacuum insulated dewar, infrared detectors can warm slightly during the course of their operation, causing the baseline signal to drift over time, and eliminating the potential increase in the signal to noise ratio from averaging large numbers of spectra.

B) Attenuated Total Internal Reflection

As stated in the previous section, many spectroscopic sampling methods exist for infrared spectroscopy. However, the experiments done as a part of this thesis used one sampling technique exclusively. This technique is multiple attenuated total internal reflection (ATR) Fourier transform infrared spectroscopy (FTIR). In ATR infrared light is reflected inside of an optical waveguide, allowing the light to interact with a thin film of material on its surface (see figure III.2).[6] The optical waveguide can be constructed such that many reflections occur, allowing multiple sampling interactions, and increasing the overall signal level by an amount proportional to the number of reflections. The use of multiple internal reflections is a specific type of ATR, and is frequently also given the acronym MIR for multiple internal reflection.

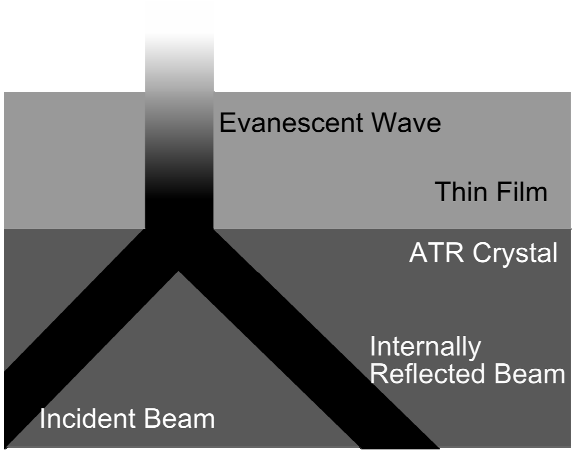

Figure III.2 Total internal reflection. An incident beam of light is reflected from the interface of two dielectric media. At the point of reflection, a rapidly decaying electric field propagates away from the interface. This phenomenon is commonly used for infrared sampling and is often referred to as ATR.

B.1) Snell's law and the evanescent wave

On the simplest level, the total internal reflection process is a consequence of Snell's law of refraction. Snell's law describes the change in the angle of an incident light beam changes as it passes from one non-absorbing medium to another. The change in angle is related to the change in a material property called the optical density, or more often, the index of refraction. The index of refraction has another important interpretation as the ratio of the speed of light in the vacuum and the speed of light in a non-absorbing medium, and is related to the complex dielectric function.[3] Equation 6 is a statement of Snell's law where θ_1 is the incident beam, θ_2 is the transmitted beam, n_1 and n_2 are the indices of refraction, or optical densities, for the two different materials (see figure III.3).

(6) $$\sin\theta_2 = \frac{n_1}{n_2}\sin\theta_1$$

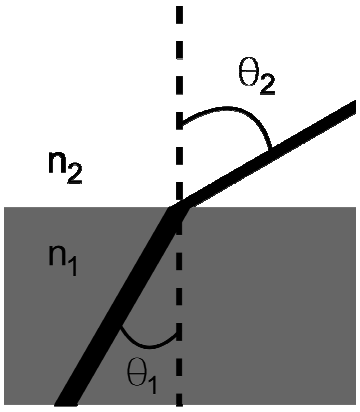

Figure III-3. Snell's Law. An incident light beam approaching the interface between two dielectric media with some angle from normal incidence (θ_1) is deflected to a new angle (θ_2) in proportion to the difference in the optical densities (n_1, n_2) between the two media.

Total internal reflection occurs as the right side of equation 6 becomes larger than one. That is, none of the beam is transmitted from the first to the second medium, and

the beam is completely reflected from the interface. This occurs when the incident angle is large and $n_1 > n_2$. The minimum angle necessary to facilitate total internal reflection (often called the critical angle, θ_C) is a function of the indicies of refraction of the two materials. Note that this angle decreases as n_1 increases and does not occur when $n_2 > n_1$.

(7) $$\theta_C = \sin^{-1}\left[n_2 / n_1 \right]$$

When the right side of equation 6 is greater than one, the angle of transmitted beam cannot be a real quantity, because the sine of a real number is always less than or equal to one. This is an important observation in the treatment of total internal reflection in terms of classical electromagnetic theory. The consequence of this observation becomes apparent when one writes a plane wave description of the electric field (E) in two dimensions (x,z) in terms of the angle of incidence (θ_1). In equation 8, the intensity of the electric field is given by E_0, and magnitude of the wavevector is given by k.[3]

(8) $$E = E_0 \exp\left[ikx\sin\theta_2 + ikz\cos\theta_2\right]$$

The cosine of angle can be obtained from the trigonometric identity associated the Pythagorean theorem. However, since the sine of the angle is greater than one, the cosine is no longer a real number.

(9) $$\cos\theta_2 = \sqrt{1-\sin^2\theta_2} = i\sqrt{\sin^2\theta_2 - 1}$$

Combining equations 6, 8, and 9 yields an equation for the electric field which penetrates into the second medium, but is exponentially attenuated.[3] This is called an evanescent wave, and is the mechanism responsible for the effectiveness of ATR as an infrared sampling technique. It is important to note that the attenuation factor is proportional to the wavenumber of light, and is of the same order of magnitude.

(10) $$E = E_0 \exp\left[-kz\sqrt{\left(\frac{n_1}{n_2}\sin\theta_1\right)^2 - 1}\right]$$

B.2) Choosing an ATR crystal

From the discussion above, it can be shown that there are a few practical considerations to take into account when choosing a material to serve as the optical waveguide. The first is that a good ATR element has a large index of refraction. This property is especially important if one wishes to make ATR measurements on a variety of films, some of which have a moderately high index of refraction. For example, an ATR measurement of a thick film with a large index of refraction would be impossible if the index of refraction of the ATR crystal is not higher still. Thus, the list of good choices for ATR crystal materials is immediately shortened. Typically, only inorganic semiconductors have real indicies of refraction which are high enough for this purpose.[9]

Another consideration when choosing an ATR crystal material is that it has a large tranmissive window. That is, a good ATR crystal will be transparent to a wide range of frequencies, especially the frequencies one is most interested in. This eliminates highly conductive samples, for example, metals and heavily doped semiconductors. For an inorganic semiconductor, the upper limit of the transparent window is dictated by the band gap of the material, while the lower limit is dictated by the onset of optical phonon absorption or free carrier absorption.[9,10] For example zinc selenide, is a wide band gap semiconductor, and is transparent even into visible frequencies, making it a natural choice for observing features in the near infrared.

Occasionally, one will wish to use a lightly doped semiconductor as an ATR substrate. This allows for the transmission of a wide range of frequencies, while simultaneously allowing the semiconductor to be used as an electrode. This is especially useful in the context of some of the in-situ spectroscopic methods applied here, in which the ATR crystal serves as one side of a capacitor. However, one must carefully choose the correct doping level so as to balance the transmission properties and electrical properties.

The optical properties of a lightly doped semiconductor at room temperature can be described by Drude absorption, using the dopant concentration as the number of free carriers.[12] This assumes that all of the dopants are ionized at room temperature, and at the very least, provides an upper bound to the absorption by the free carriers in the crystal. For most semiconductors, material specific constants found in Drude's law have been measured, allowing a quantitative measure of the crystal absorbance one can expect at each frequency.

Often the mechanical and chemical properties of the ATR material are a chief concern. For example, silicon crystals are mechanically robust and can be treated and cleaned with strong acids, most notably, a sulfuric acid/hydrogen peroxide mixture commonly referred to as piranha. Other ATR crystal materials are not nearly as stable. Germanium has a water soluble oxide and can therefore be dissolved in aqueous solutions of strong oxidizing agents, such as piranha. Zinc selenide, another useful ATR crystal material, will decompose into dihydrogen selenide, a poisonous gas, upon treatment with acid.[13]

Also of note is the poor mechanical stability of germanium and zinc selenide. Dropping the crystal a distance of 10 *cm* can deliver enough stress to shatter the crystal. This fact required the development of a few techniques for crystal handling, which although not remarkable in their ingenuity, significantly decreased the rate of ATR crystal breakage.

Frequently, ATR crystals were broke while manipulating them with tweezers. Accidents occurred most often while rinsing or drying the crystals, where the crystal was held against the flow of a gas or liquid. A solution to the problem is to wash and dry crystals while they were held in a test tube. Polyethylene tubes with holes drilled in the bottom were effective.

Crystal polishing was another activity which resulted in many broken crystals. Typically, ATR crystals were shipped as 1 *mm* thick plates, in the form of wafers (Ge,Si) or irregularly shaped stock (ZnSe). Thinner materials were tried without success. A local contractor was then used to dice the wafers to size. Typically, 1*cm* x 3.125 *cm* pieces were cut although 1*cm* x 5 *cm* pieces were also used. After obtaining the correctly sized crystals, they had to be polished into the shape of a parallelogram by hand. During this process, the crystals were placed in a specially designed holder, and held in place by a piece of poly(dimethoxy silane) (see figure 3). Despite efforts to the contrary, ATR crystals were often subjected to forces greater than they could withstand and would crack. This problem was resolved by encasing the crystal in acrylic prior to polishing. In the case of zinc selenide, thin metal supports were included near the crystal surface to add extra rigidity.

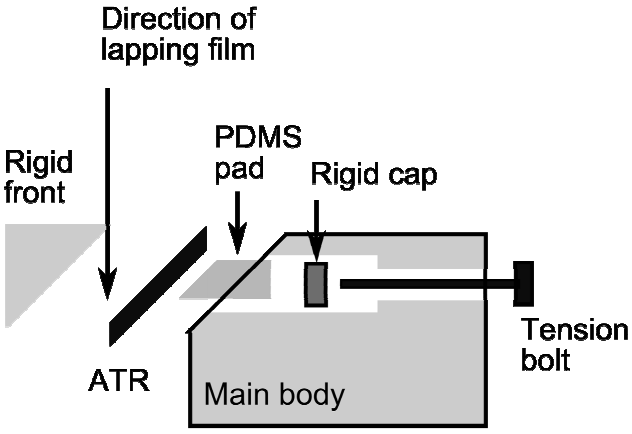

Figure III-4. Holder for ATR crystal polishing. Lapping film is used to polish a beveled edge. The crystal is held between the rigid front and the PDMS pad by a tension bolt which pushes a rigid cap against the PDMS. The rigid front is bolted to the main body.

In summary, ATR is a useful spectroscopic sampling technique that can make use of multiple reflections to increase the amount of signal detected in the experiment. The phenomenon of attenuated total internal reflection can be described by basic geometric optics and using the electromagnetic wave description of light. In choosing an appropriate ATR crystal material, one must take the following into consideration: the index of refraction, the breadth of the useful spectral window, the doping level, and the mechanical and chemical stability of the material. Poor chemical and mechanical stability are concerns which can be mitigated with careful technique.

C) In-situ Spectroscopy: Device Fabrication and Testing

In-situ spectroscopic measurements of charged organic semiconductors comprised the majority of the experimental data obtained throughout the course of the thesis research, and the basic methodology remained unchanged. The basic experimental methodology was to build a MIS capacitor on a waveguide enabling infrared and near infrared spectroscopic measurements to be made via the ATR technique (see figure III.5). From a device fabrication perspective, the differences from experiment to experiment can be related to changing some important parameters and/or materials used in each step of fabrication. Device fabrication can be broken down into three steps beginning with semiconductor deposition, followed by the placing of semiconductor electrodes, and completed with dielectric deposition. After the device was completed it was placed into the infrared or near infrared beam path and connected to a voltage source. The focus of this section is to discuss each step in detail.

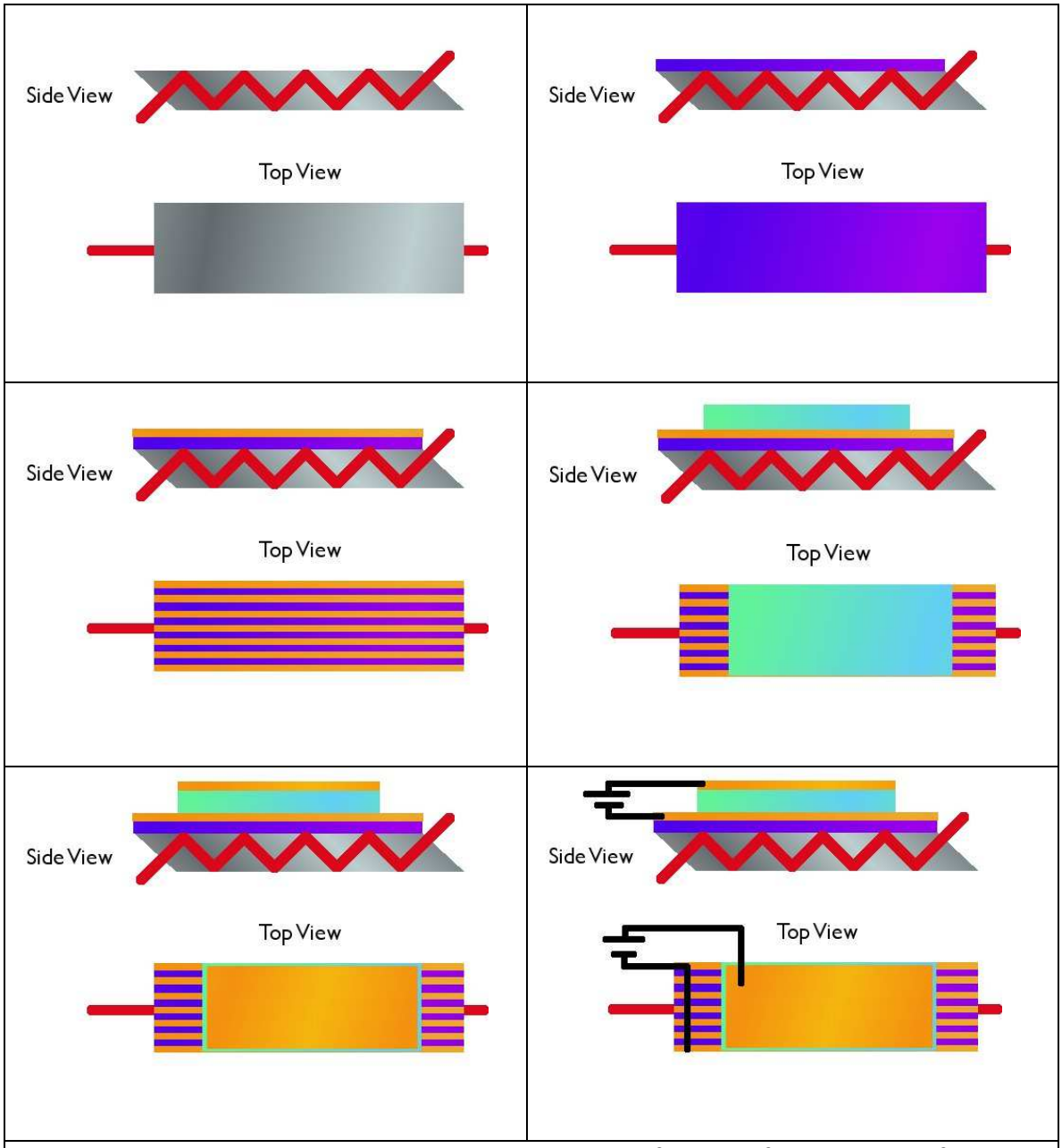

Figure III-5. Stepwise device construction. Steps are followed from right to left and top to bottom. Obtained an ATR crystal, took a background spectrum. Deposited a semiconductor thin film. Vapor deposited metal contacts . Deposited dielectric from solution or paste method. Affixed top electrode by metal vapor deposition or paste method. Grounded metal-semiconductor contacts and applied voltage to the top electrode while recording infrared and near infrared spectra.

C.1) Thin film deposition

The first step to fabricating a device is the deposition of a thin film of organic semiconductor. One way of accomplishing this task is by a spin coating process. Spin coating is a technique commonly used in polymer science to create a smooth polymer film by placing a liquid solution on a substrate and rotating the substrate fast enough to drive solution off of the substrate. If the surface energy is favorable, a thin liquid film will remain on the substrate. This film will dry leaving behind the polymer. The final thickness of the polymer film depends upon the thickness of the liquid film before drying and the concentration of the polymer in the film. Although these quantities are not independent, it allows one to intuitively grasp that the thickness of the polymer film decreases with increasing spin speed and decreasing concentration of the polymer film.[14]

Spin coating was the method used to deposit thin films of poly(3-hexylthiophene) (P3HT) on an ATR crystal, which serves as the substrate for an MIS device (see figure III-6 for the molecular structure of P3HT). The solutions were usually 20 *mg/ ml* of P3HT in 1,2 dichlorobenzene. Dichlorobenze was chosen as a solvent because it has a low vapor pressure and there is a correlation between low vapor pressure solvents and smooth P3HT film morphology, as well as improved transport characteristics.[15] The spin speed used was either 400 or 800 rpm, resulting in film thicknesses of 200 and 100 *nm*, respectively, as verified by profilometry and atomic force microscopy, by Travis Mills, and Matthew Goertz. The films were spun for 30-60 seconds and visually inspected for large scale inhomogeneities before being left to dry overnight. It was found

that the presence of large scale inhomogeneities could be minimized by making sure the substrate was as clean as possible. As a brief side note, it was found that treating the substrate with a hydrophobic monolayer of octadecyltrichlorosilane made spin coating difficult; the P3HT solution would not wet the substrate, instead forming droplets which easily moved off of the substrate.

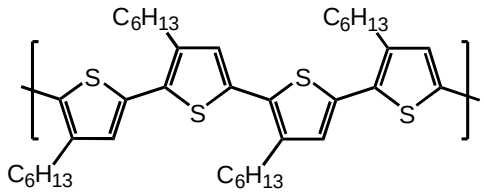

P3HT

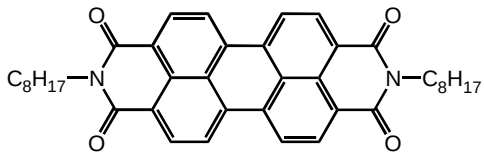

PTCDI-C8

Figure III-6. Organic semiconductors used for experiments. P3HT is a p-type polymer semiconductor deposited through spin coating. PTCDI-C8 is an n-type small molecule organic semiconductor deposited via physical vapor deposition.

The other method of organic semiconductor deposition used during this research was physical vapor deposition. The organic semiconductor molecules are sublimated under high vacuum by the use of a resistively heated furnace. The substrate, in this case an ATR crystal, is held above the furnace and the flux of sublimating molecules condenses on the substrate. The thickness of the film is measured by a quartz crystal microbalance which was calibrated by others in the Frisbie lab to calculate film thickness during the deposition process. The molecular semiconductor most frequently used was N,N dioctyl-perylene tetracarboxylic diimide (PTCDI-C8, see figure III-6). The conditions for deposition were taken from Chesterfield, et. al. [16] and are as follows: the furnace temperature was near 200 C^0, the substrate temperature was 100 C^0, and the

film thickness was usually 20-30 nm. Typically, the initial stages of film deposition were done more slowly (0.05 Å/s) than later ones (0.15 Å/s) for the purpose of improving film morphology.

It was found during the course of the research that evaporated films of organic semiconductor molecules, especially PTCDI-C8, adhere poorly to ATR crystal substrates. This can be especially problematic when large area devices are being fabricated, and the films are subjected to mechanical stress. The situation was improved dramatically through the use of self assembled monolayers (SAMs).

The idea behind the use of self assembled monolayers to improve the adhesion of vapor deposited organic semiconductors on an ATR crystal was to increase the hydrophobicity of the crystal. The energetic attraction between a surface and water is described as a hydrophilic interaction. When that interaction is unfavorable, a surface is described as hydrophobic. For example, the native oxide that naturally forms on a silicon surface is hydrophilic, that is, a water droplet naturally spreads across the surface, rather than appearing more spherical. The angle between the surface and the leading edge of the droplet is called its contact angle and can be used to gauge the hydrophobicity of the surface.[17]

Using self assembled monolayer chemistry, a single layer of organic molecules can be attached to the surface of a substrate, changing its wetting properties. For example, attaching a monolayer with a long alkyl chain to the previously mentioned silicon surface changes the surface from hydrophilic to hydrophobic. The thought behind doing SAM chemistry on ATR crystals was to make the organic semiconductor molecules wet and subsequently, adhere to the crystal surface more effectively. In the

case of PTCDI-C8 films, the strategy worked, as demonstrated by the scotch tape test (the semiconductor film remained on the crystal surface after the application and removal of a piece of scotch tape).

C.2) Self assembled monolayer chemistry

There are a variety of methods for attaching organic molecules to the surface of inorganic solids, and an in depth discussion of them would be more than a minor digression. Thus, the discussion will be limited to octadecyltrichlorosilane (OTS) monolayers on silicon oxide, and dodecyne monolayers on germanium.

OTS monolayers were grown on the surface of a silicon ATR crystal first by cleaning the crystal in boiling piranha (3:1 H_2O_2:H_2SO_4 by volume). After the crystal was removed from the solution, it was washed with water, then ethanol and dried under a stream of argon. Ethanol was used in order to speed the drying process, and was specifically chosen because it does not leave behind a residue as does acetone, for example. After the crystal was dry, it was immersed in a 0.01 *M* solution of OTS in bicyclohexyl and allowed to react for several hours. The crystal was then removed from the OTS solution, washed with toluene and sonicated in toluene for an additional 3-5 minutes. After sonication the crystal was washed with ethanol, water, then ethanol once more and dried under a stream of argon. The contact angle of a water droplet was measured by eye and found to be $90^0 \pm 10^0$. Additionally, an OTS film made by this procedure was examined by Vivek Kalihari of the Frisbie lab using atomic force microscopy (AFM). The result is found in figure III-7.

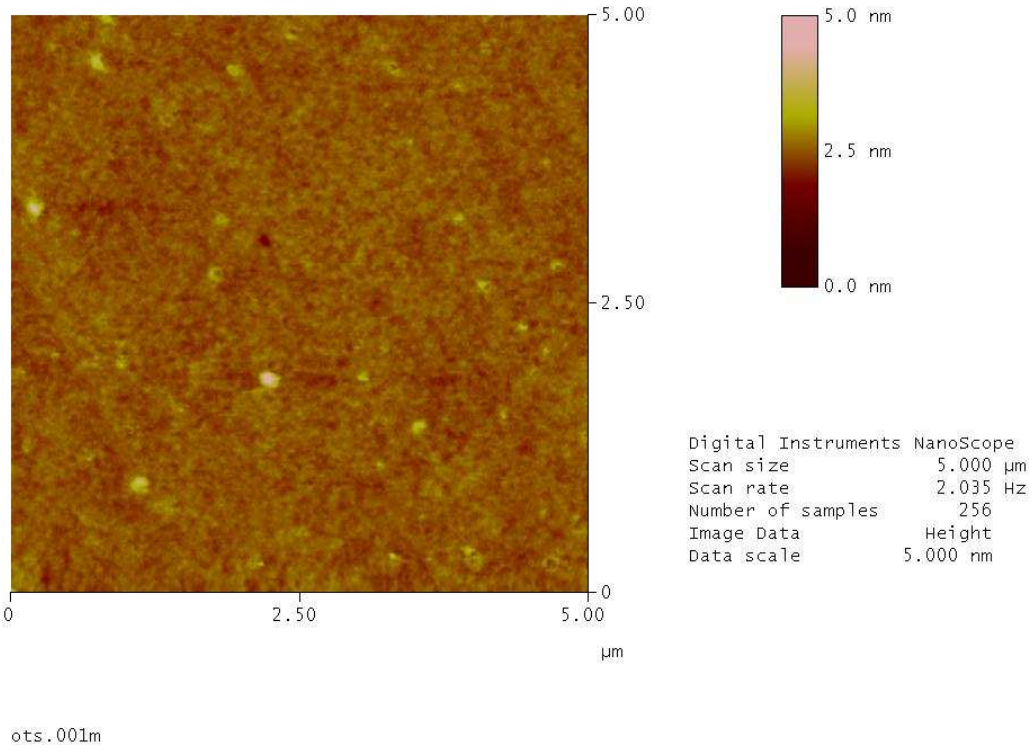

Figure III-7. AFM image of OTS on SiO_2. After treating the SiO_2 surface with OTS, objects with a height of 5 nm or less were prevalent on the surface. The remainder of the film appears homogenous with feature sizes of about 1 nm.

Monolayers of dodecyne were also grown on germanium ATR crystals. The procedure follows that of Choi et. al.[18] and begins with cleaning the crystal in a mild solution of hydrogen peroxide (30% in H_2O) for 1 minute, before rinsing with water and drying with argon. The crystal was then stripped of its native oxide by treatment in (10%) ammonium fluoride for 3 minutes, before rinsing with water and drying with argon. Ammonium fluoride is a particularly hazardous reagent; care should be exercised during this step. After treatment with ammonium fluoride, the crystal is immersed in a 25% v/v solution of dodecyne in mesitylene. The crystal is placed inside of a clean Teflon sheath to prevent it from chipping against the glass reaction vessel. The vessel is purged with argon, stirred, and heated to 190 C^0, and allowed to react overnight. After cooling the reaction vessel, the crystal is rinsed with dichloromethane then ethanol, and dried under argon. The contact angle of water on the crystal was found to be (80 ± 10^0). As a basis of comparison, the contact angle of water on a clean Ge surface is (25^0). While a more rigorous evaluation of the effectiveness of the surface chemistry would have provided clearer evidence that the monolayer attachment was successful, the change in contact angle is a measure of the surface property that is most relevant in improving organic semiconductor adhesion.

C.3) Metal contact deposition

After the semiconductor layer has been deposited on the ATR crystal, metal contacts are deposited upon the organic. In this thesis, gold was used exclusively as a metal contact. In the case of transistor fabrication, depositing metal electrodes on top of

an organic semiconductor film is referred to as a top contact configuration.[14] Vapor deposition is probably one of the most utilized methods of deposition metal contacts. One of the reasons for this is likely due to the fact that a vapor deposited metal layer will conform to the shape of the underlying material, making a good physical contact. The other reason, perhaps, is that it is relatively easy to obtain a desired pattern through the use of a shadow mask.

A shadow mask is simply a sheet with a pattern cut into it. The mask is placed in front of the substrate and selectively blocks the flux of metal vapor, ideally leaving the exact pattern in metal on the substrate. There are many ways of constructing shadow masks and many materials to construct them from. However, one of the most accurate methods is etching a pattern in a thin silicon wafer via lithographic techniques. However, thin silicon wafers are somewhat fragile, making thin steel sheet a reasonable alternative. During the experiments described in the results section, both methods were used.

The electrode pattern used in chapters V, VI, and VII is depicted in figure III-8. This pattern was through etched into a silicon wafer by Lage Matzke in the UMN nanofabrication center. The center of the pattern is the active area of the device. In the active area, the channel width is 500 μm and the length is 1.5 cm. The feature size is 300 μm, and the overall size of the pattern is 3.175 cm. The staggered pattern used was intended to allow every other electrode to be held at a different potential, opening the possibility of source-drain current measurements in a transistor configuration. This is a possibility for future work.

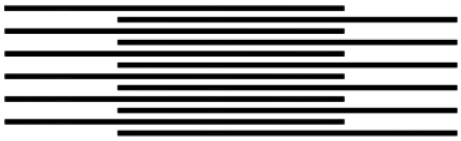

Figure III-8. 500 μm shadow mask. The electrode pattern used for the experiments of chapter V, VI, VII.

C.4) Dielectric deposition

After depositing the metal electrodes, the next step towards making a working device is to deposit the dielectric material. Most of the dielectrics studied share a common feature, namely that they are ion conductors comprised of poly(ethylene oxide) (PEO) and an electrolyte of some kind. Three electrolytes were examined: lithium perchlorate, poly(ethylene imidium) perchlorate, and lithium poly(styrene sulfonate). Recipies for making each and the physical methods of their deposition will be described.

C.4.1) PEO:$LiClO_4$

The first dielectric used in this research was a solution of lithium perchlorate in poly(ethylene oxide), referred to here as PEO:$LiClO_4$. The PEO used in this dielectric had a molecular weight of 100 kD and came in powered form. The PEO was mixed with $LiClO_4$ in a mole ratio of 16 ether oxygen atoms per lithium atom. This was found to be the ratio that maximized the ionic conductivity.[19] Both components were mixed in a solution of acetonitrile (3-6% m/m). Acetonitrile is a convenient solvent because is has a low boiling point which makes drop casting easier and is a non-aqueous solvent which dissolves both species.

The transistor research on which this research is based used mostly drop casting as a means of dielectric deposition.[14] However, problems were encountered when this methodology was extended to the fabrication of devices for in-situ spectroscopy. The problem encountered was a result of the unfavorable surface interaction between the PEO solution and organic semiconductor molecule PTCDI-C8, preventing the formation of a dielectric layer on top of the PTCDI-C8. In the transistor measurements, this problem was not encountered because the channel width was 200 μm, and the PEO had no trouble forming on top of gold.

The solution to the problem of surface energy mismatch was to mechanically hold the PEO solution on the active area of the channel, forcing the dielectric to form on the organic semiconductor. This was accomplished by the use of rubber die pictured in figure III-9. The ATR crystal was held against a plastic backing by putting pressure on the rubber die, and a seal was formed between the rubber and the crystal. The dielectric solution was introduced into the die and then left to dry overnight. Because the success of the procedure requires a good seal between the rubber die and the ATR crystal, the construction of the rubber die had to be rather exact.

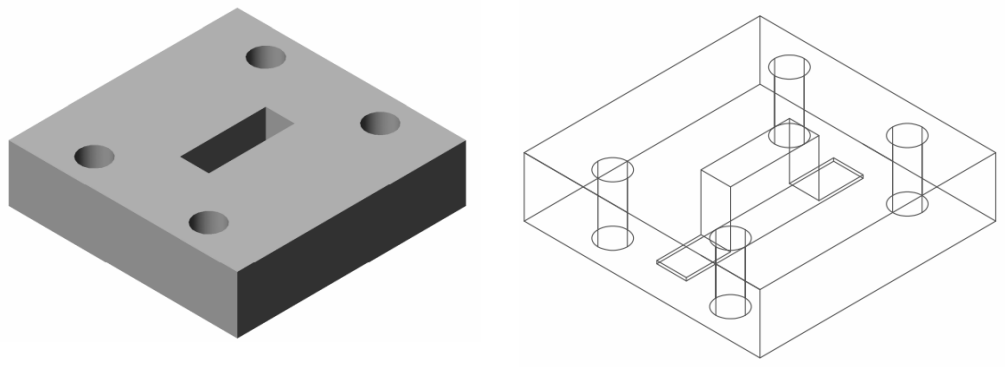

Figure III-9. PDMS die. Two representations of the PDMS piece used in die casting the PEO:$LiClO_4$ dielectric. The four holes on the outside edges are for bolts that hold the piece in place during casting. The rectangular hole in the center is where the PEO is cast. The place for the ATR crystal can be seen in the wire frame image.

The rubber die was constructed from poly(dimethoxy silane) (PDMS) obtained through the Dow Corning company. This material is flexible, but can hold even microscopic patterns on its surface.[20] After mixing the material with a curing agent, the PDMS solution was poured onto the plastic backing with a specially modified ATR crystal in place. To define the placement of the dielectric and provide a large volume for the PEO solution, a rectangular piece of aluminum was cut and glued with epoxy to a blank crystal. This crystal was put in place and the PDMS was poured around it and the plastic backing. After degassing the PDMS at -10 *psi* (gauge) for 20 minutes, the PDMS was cured at 80 C^0 1-2 hours, or until firm and not tacky. Once the PDMS die was prepared, it was treated with OTS vapor overnight. If this step is omitted, the PEO dielectric solution would adhere to the walls of the PDMS well enough to make its removal quite difficult once dried.

Using the PDMS die, it was possible to deposit a continuous dielectric layer across the surface of the device. Fortunately, the properties of the dielectric do not depend sensitively upon thickness, as the dielectric thickness was rarely uniform, varying between 0.1 and 0.5 *mm*. The device was finished by evaporating a metal contact on the top of the PEO dielectric. As previously observed,[14] it was important not to let the shadow mask used in the metal evaporation process touch the PEO dielectric during the metal evaporation process. This was usually accomplished by keeping the mask elevated from the sample by about 1 *mm*. The somewhat large spacing was tolerated because the accuracy with which the electrode was placed was not as critical of a parameter in the purely spectroscopic measurements.

C.3.2) PEO:PEIClO$_4$

Another dielectric formulation that was tried employed a polycation. The polycation chosen was poly(ethylene imidium perchlorate) (PEIClO$_4$), and is pictured in figure III-10. This molecule is only commercially available in as poly(ethylene imide) (PEI). However, charge state of the polymer is pH dependent, thus titration with and acid can be done to ensure that the majority of the polymer is positively charged. Perchloric acid was chosen for the task because it is a strong acid and the perchlorate ion is part of the lithium perchlorate dielectric mentioned in the previous section. The perchlorate solution was relatively dilute (0.1 *M* in water) because perchloric acid is a strong oxidizing agent and reactions using concentrated solutions can become dangerously exothermic.[21] The mole ratio of PEI to perchloric acid is between 2:1 and 1:1 to

ensure that PEI is in excess. The resulting solution is then rotovaped and heated to 100 C^0 under vacuum to drive off as much moisture as possible. The resulting polymer is a fluffy yellow solid.

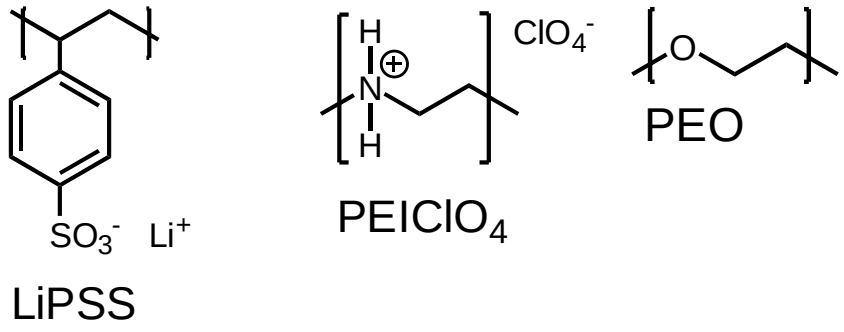

Figure III-10. Dielectric polymers. All dielectric materials described in the text used PEO as an ion conductor. $PEIClO_4$ is designed to gate n-type materials, while LiPSS is designed to gate p-type organic semiconductors.

After the $PEIClO_4$ is made, it is mixed with PEO. The mole ratio of PEO to PEI monomers was 16:1, although it is likely that this ratio could be better optimized. The molecular weight of PEO was chosen to achieve a viscosity similar to that of peanut butter. This was done in order to facilitate deposition by the paste method.[22] In the paste method, an electrode is constructed with metal foil and the dielectric is placed on the foil. The device is completed by gently pressing the dielectric against the semiconductor. The paste method is explained in further detail in section C.3.3.

C.3.3) PEO:LiPSS

A dielectric material using a polyanion was made from lithium poly(styrene sulfonate) (LiPSS), pictured in figure 8. This material is commercially available as a 30% wt solution in water. Because the presence of water is harmful to device performance, the LiPSS must be carefully dried. This was done by first using a rotovap, then by heating under vacuum to 100 C^0. The resulting polymer was off white and flaky. LiPSS is not soluble in a large variety of non-aqueous solvents, methanol and ethylene glycol being exceptions. The dried polymer was dissolved in methanol and mixed with molecular sieves in order to remove more water. Other chemical drying agents were avoided for fear that they may introduce trace ionic impurities and disrupt device performance. The solution was left to set overnight.

Once the LiPSS solution was decanted from the molecular sieves, it was mixed with PEO. As was the case with the other polyelectrolyte, the molecular weight of PEO was chosen such that the viscosity of the dielectric solution was compatible with the paste method.[22] Several formulations were made and tested, and although no consistent differences were noted, good results were obtained from the following mixture: 3% LiPSS, 93% PEO (0.3 kD), 4% PEO (100 kD) by mol of monomer.

As stated before, dielectric deposition was done via the paste method. This method came to be preferred because of the challenges with solution casting outlined in section C.3.1 on the PEO:$LiClO_4$ dielectric. The paste method works by coating a foil electrode with dielectric and pressing the dielectric against the semiconductor layer.

However, there are ways of making the foil electrode which make this process easier and more robust. The first suggestion is to use gold coated foil. Gold is not as reactive as other electrode materials (copper, aluminum, sliver) and its lack of a native oxide also makes it a good choice for electrical reasons.[23] However, gold foil is quite expensive, thus developing a useable alternative to pure gold foil is worthwhile. After some experimentation, it was found that ordinary aluminum foil coated first with a chromium adhesion layer followed by a relatively thick gold layer was mechanically stable (the gold did not flake off when strained.)

Another suggestion for creating a workable electrode for the paste method is to include a plastic backing behind the foil.[22] This was accomplished by using double side sticky tape to affix the gold coated foil to a small piece of polystyrene sheet. The sheet used was the kind typical of overhead projector slides. Once the gold coated foil was attached to the polystyrene backing, a thin copper wire was soldered onto the backside of the foil to help in connecting the device to an electrical circuit.

C.4) Integrating spectroscopy with electrical measurements

After the completion of a device it needs to be positioned for spectroscopic measurements while simultaneously being connected to an electric circuit. While this is not a feat of engineering in and of itself, there are better and worse ways of accomplishing the task. In addition, it is advantageous to control the atmosphere in which the experiments are conducted, as organic semiconductors are prone to chemical degradation. The evolution of the experimental methodology will be presented

chronologically to describe the experimental conditions used for each experiment in addition to describing the experimental challenges encountered and the methods used to circumvent them.

Results from first set of successful experiments are presented in chapter IV. The sample was contained in an acrylic box with a top which could be fastened, and was inherited from previous researchers, the last of which was Yongseok Jun. This design allowed the removal of atmospheric water and carbon dioxide by purging the container with house nitrogen. Both water and carbon dioxide have a large absorption cross section in the infrared, and removing them cleans up the spectrum. To that end, the design was effective, reducing CO_2 and water levels below the limits of detection with the spectrometer. However, the atmosphere inside the enclosure could not be classified as an inert atmosphere, because oxygen levels were not measured directly and were not likely to be in the ppm range.

The method of making electrical contact to the device was to solder copper wires to the gold contacts using a liquid metal as a cold solder. The liquid metal employed was gallium-indium eutectic, which does not wet either metal surface well, but well enough to facilitate contact. This method of making connection requires patience. The thin copper wires are somewhat difficult to control and the eutectic provides only a small amount of adhesive action. Also, the eutectic coated wires also have a tendency to place eutectic on areas where it is not wanted, for example on the surface of mirrors. Given a little time, however, connection between the voltage source and the device can be made. The voltage source originally used was controlled manually and the voltage read from a hand held voltmeter.

The next set of published experiments (chapter VII) was conducted inside of an inert atmosphere glove box. The glove box came equipped with an oxygen sensor which had a detection limit of 0.1 *ppm*. The atmospheric control contributed to the reproducibility and reversibility of the experiments. In addition, a new spectrometer was purchased which allowed an extended spectral range and provided better stability and signal to noise ratio. Apart from the general concerns of setting up a new piece of equipment, bringing an infrared beam into a glove box required the design of a KBr window to be placed over an auxiliary port on the glove box. This was done by Travis Mills.

A strange challenge to overcome during the process of setting up the new spectrometer was designing a method of delivering ultrapure liquid nitrogen into the glove box. It was found that the IR detectors should be placed inside the box, however the MCT detector is cooled with liquid nitrogen, and it defeats the purpose of using a glove box if anything but pure liquid nitrogen is introduced into the box. The method designed to accomplish this was to take pure nitrogen gas from a high pressure tank and liquify it in a copper condenser. The condenser was placed into a dewar of liquid nitrogen and the pressure of gas in the line was made to be significantly greater than atmospheric pressure. This raised the boiling point of the gas in the line and allowed liquid nitrogen to be used as the cryogen in the dewar. Once liquefied, the fluid can be pumped into the box. Some liquid will be lost along the way from imperfect insulation of the line and from the drop in pressure as the fluid enters the box, but this technique allows the delivery of liter quantities of ultrapure liquid nitrogen into the glove box. As with any experiment using pressurized liquid cryogen, pressure release valves are a

necessary safety measure. Also, pressures inside the glove box during the procedure can become quite large, potentially damaging the box and anything in it. However, this can be handled by keeping the inside door of the load lock open and using the mechanical pump to directly regulate the pressure.

Moving the experiment into the glove box was a good opportunity to redesign the way that electrical connection was made to the sample. The solution to improving the technique was to more directly integrate the sample holder with the electrical measuring apparatus. The current sample holder design is pictured in figure III-11 and shows how this was accomplished. The two vertical posts indicated by an arrow in the figure can be wrapped with a conductive material the making it much easier to contact the ATR device by means of an alligator clip. It is worth noting that a more careful design of the wrapping material should enable many electrodes to be contacted individually should more sophisticated electrical measurements become necessary.

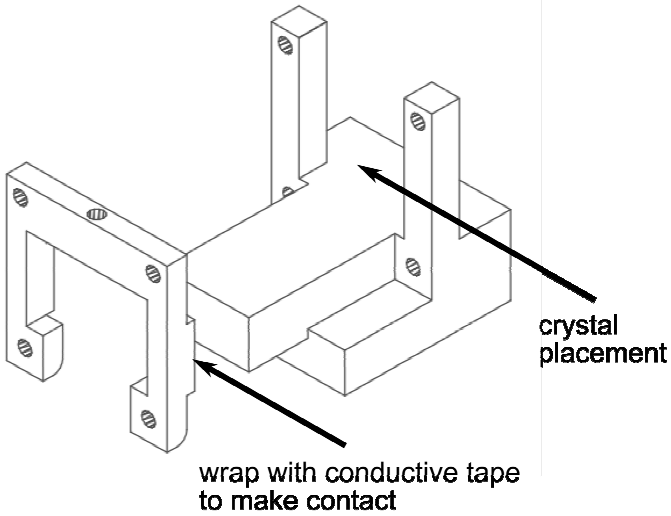

Figure III-11. ATR sample stage. This configuration is designed to both hold the sample in place while making electrical contact. In order to do so, electric contacts on the device must be facing the horseshoe shaped part which must be wrapped in a conductive tape (copper tape has been used).

Contact to the top electrode was at first accomplished by the use of copper tape or wire and gallium indium eutectic. However, performing experiments inside a glove box reduces the manual dexterity of the researcher, making this a less than ideal method. A more sophisticated method was developed through the use of the paste technique described in section C.3.4 of this chapter. The top electrode was made such that it already contained a copper wire soldered to it, consistently enabling good electrical contact to the power source.

The power source used starting with chapter V, was a digital instrument (Kiethley 6517A) enabling a better control of the applied voltage and eventually simultaneous displacement current measurements. This was achieved through the development of control software in LabView. A fuller integration between the electrical components and the spectrometer is achievable in principle, and is another direction in terms of instrument development.

In summary, one of the main challenges of in-situ spectroscopy is the seamless integration of spectroscopy with other external controls. This only occurs when all levels of the process are directed towards that integrated goal. Contrast this with what might be called a Frankenstein approach, where dissimilar techniques are unhappily stitched together via brute force. Although this set of adjectives characterizes the earliest attempts of this research, modest progress in the integration of both techniques has been made, and future directions appear promising. In short, device fabrication, sample positioning, and control software all have to be designed with the unique requirements of both techniques in mind. In so far as that was accomplished, the moniker of in-situ spectroscopy applies to this research.

D) References

[1] Brugel, W. *An Introduction to Infrared Spectroscopy*, Methuen: London, U.K., 1962.

[2] Kittel, C.; Kroemer, H. *Thermal Physics*, 2nd ed.; W.H. Freeman and Company: New York, 2003.

[3] Griffiths, D.J. *Introduction to Electrodynamics*, Prentice Hall: Upper Saddle River, NJ, 1999.

[4] Rieke, G.H. *Detection of Light: From the Ultraviolet to the Submillimeter*, 2nd ed.; Cambridge University Press, Cambridge, U.K., 2003.

[5] Kauppinen, J.; Partanen, J. *Fourier Transforms in Spectrscopy*, Wiley-VCH, Berlin, 2001.

[6] Tolstoy, V.P; Chernyshova, I.V.; Skryshevsky, V.A. *Handbook of Infrared Spectroscopy of Ultrathin Films*, John Wiley and Sons: Hoboken, NJ, 2003.

[7] Smith, B.C. *Fundamentals of Fourier Transform Infrared Spectroscopy;* CRC Press: Boca Raton, FL, 1996.

[8] Skoog, D.A. *Principles of Instrumental Analysis*, CBS College Publishing: New York, 1985.

[9] Harrick, N.J. *Internal Reflection Spectroscopy*, John Wiley and Sons: New York, 1967.

[10] Klingshirn, C.F. *Semiconductor Optics*, Springer-Verlag: Berlin, Heidelberg, 1995.

[11] Kittel, C. *Introduction to Solid State Physics*, 8th ed.; John Wiley and Sons: Danvers, MA, 2005.

[12] Jackson, J.D. *Classical Electrodynamics*, 3rd ed; John Wiley and Sons: New York, 1999.

[13] *Zinc Selenide*; MSDS No. 96485; Sigma-Aldrich: Saint Louis, MO, Dec 29, 2008.

[14] Panzer, M.J *Polymer Electrolyte-Gated Organic Field-Effect Transistors.* PhD. Thesis, University of Minnesota, Minneapolis, MN, May 2007.

[15] Kline, R.; McGehee, M. *Polym. Rev.* 2006, *46*, 27-45.

[16] Chesterfield, R.J.; McKeen, J.C.; Newman, C.R.; Ewbank, P.C.; da Silva Filho, D.A.; Bredas, J.-L.; Miller, L.L.; Mann, K.R.; Frisbie, C.D. *J. Phys. Chem. B* **2004**, 108, 19281-19292.

[17] Zangwill, A. *Physics at Surfaces;* Cambridge University Press: Cambridge, U.K, 1988.

[18] Choi, K.; Buriak, J.M. *Langmuir* **2000**, 16, 7737-7741.

[19] Gray, F. M.; *Solid Polymer Electrolytes: Fundamentals and Technological Applications*; VCH Publishers: New York, 1991.

[20] Menard, E.; Bilhaut, L.; Zaumseil, J.; Rogers, J.A. *Langmuir* **2004**, 20, 6871-6878.

[21] *Perchloric Acid*; MSDS No. 311421; Sigma-Aldrich: Saint Louis, MO, March 2, 2009.

[22] Cho. J.H.; Lee, J.; He. Y.; Kim, B.-S.; Lodge, T.P.; Frisbie, C.D. *Adv. Mater.* **2008**, 20, 686-690.

[23] Ulman, A. *J. Mater. Educ.* **1989,** 11, 205-280.

IV. Vibrational Spectroscopy Reveals Electrostatic and Electrochemical Doping in Organic Thin Film Transistors Gated with a Polymer Electrolyte Dielectric*

We apply attenuated-total-internal-reflection Fourier transform infrared (ATR-FTIR) spectroscopy to directly probe active layers in organic thin film transistors (OTFTs). The OTFT studied uses the n-type organic semiconductor, N-N'dioctyl-3,4,9,10-perylene tetracarboxylic diimide (PTCDI-C8) and a polymer electrolyte gate dielectric made from polyethylene oxide (PEO) and $LiClO_4$. FTIR spectroscopy of the device shows signatures of anionic PTCDI-C8 species and broad polaron bands when the organic semiconductor layer is doped under positive gate bias (V_G). There are two distinctive doping regions: a reversible and electrostatic doping region for $V_G \leq 2$V and an irreversible and electrochemical doping regime for $V_G \geq 2$V. Based on intensity loss of vibrational peaks attributed to neutral PTCDI-C8, we obtain a charge carrier density of $2.9 \times 10^{14}/cm^2$ at $V_G = 2$ V; this charge injection density corresponds to the conversion of slightly over one monolayer of PTCDI-C8 molecules into anions. At higher gate bias voltage, $V_G \geq 2$V, electrochemical doping involving the intercalation of Li^+ into the

* This chaper contains published material from the following reference: L.G. Kaake, Y. Zou, M.J. Panzer, C.D. Frisbie, X.-Y. Zhu, *J. Am Chem. Soc.* 2007, 129, 7824. See appendix for copyright information.

organic semiconductor film can convert all PTCDI-C8 molecules in a 30 nm film into anionic species. For comparison, when a conventional gate dielectric (polystyrene) is used, the maximum charge carrier density achievable at V_G = 200 V is ~4.5x10^{13}/cm^2, which corresponds to the conversion of 18% of a monolayer of PTCDI-C8 molecules into anions.

A) Introduction

Charge transport at or across interfaces is central to the operation of a wide variety of molecule-based devices, including organic light-emitting diodes, organic thin film transistors, (OTFT) organic photovoltaic cells, and nanoscopic molecular junctions based on single molecules or a small assembly of molecules. In each of these devices, the critical charge transporting interfaces are *buried interfaces* (*e.g.*, organic-insulator, organic-metal, or organic-semiconductor heterojunctions), which are not readily accessible to conventional structural or spectroscopic probes. Though there have been tremendous advancements in molecule-based electronics in the last a few years, the difficulty in determining structure-property relationships at buried interfaces has produced a knowledge gap that is a key obstacle to future development. Gaining rigorous and verifiable knowledge of the molecular states involved during the build up and movement of charge would help to close that gap. More specifically, the relationship between polarons and molecular ions is in need of exploration.

In an attempt to address these questions, we fabricate OTFTs on top of an IR waveguide and apply ATR-FTIR spectroscopy to measure the vibrational spectra (and

thus the structure and conformation) of molecules at the buried interfaces, particularly the critically important organic semiconductor/gate-dielectric interface. We have demonstrated this approach before for recording vibrational spectra of metal-molecule-metal or metal-molecule-semiconductor tunnel junctions, but without the application of bias voltage.[1] Here, we record FTIR spectra under gate voltage to identify spectroscopic signatures unique to gate-induced charge in organic semiconductor thin films.

Infrared spectroscopy has been used in the study of chemical doping[2,3] and electrochemical doping[4,4] of conducting or semiconducting polymers in the bulk form. Two recent studies have applied FTIR to active OFET devices to gain insight into the conduction mechanisms of OFETs under the application of a gate voltage; these studies revealed chemical species responsible for charge trapping at the dielectric/semiconductor interface[6] and polaron formation within organic semiconductor layers.[7] Optical absorption in other wavelength regions has also been used to probe operating OTFTs, particularly polaron bands from charge injection under gate bias.[8,9] Note that, in principle, there is a Stark effect in the vibrational peak position when an intense electric field is applied to a molecular sample;[10] it is too small, however, to be of significance to the kind of experiments presented in this report.

The present study focuses on the identification and quantification of charge carrying species in OTFTs based on multiple reflection ATR-FTIR. We chose multiple reflection ATR-FTIR[1,6] because it is more sensitive than transmission based techniques. Charge carrying and trapping species are minorities in an organic semiconductor film. In a typical OTFT device, gate-injected charge carrier density is

usually on the order of 10^{13}/cm^2, which is more than 10^2 times lower than the number density of organic semiconductor molecules in an OTFT. To increase charge carrier density for better characterization by ATR-FTIR, we use a polymer electrolyte gate dielectric, lithium perchlorate in poly(ethylene oxide) (PEO). This approach was successfully demonstrated recently to achieve charge carrier densities as high as 10^{15}/cm^2 in OTFTs.[11-13] Such a high charge carrier density results from the high capacitance on the order of 10 μF/cm^2 due to the presence of mobile ions in the polymer electrolyte dielectric. For comparison, the capacitance of a typical polymer or inorganic dielectric layer is on the order of 10 nF/cm^2. We choose N-N'dioctyl-3,4,9,10-perylene tetracarboxylic diimide (PTCDI-C8) as a model system because: 1) it is a known n-type conductor; 2) it possesses distinctive IR signatures (C=O stretches) that are sensitive to the charge state of the molecule; and 3) it has been successfully demonstrated in polymer electrolyte gated OTFTs with charge carrier density as high as 6.4x10^{14}/cm^2.[14]

When a charge carrier is injected into an organic semiconductor, there is a strong tendency for carrier localization.[15] There are two competing trends for an excited electron in a molecular solid: delocalization and localization. The driving force for delocalization is the resonant electronic interaction characterized by the electron transfer integral between neighboring molecules, β, which determines the electronic band width $\Delta\varepsilon_B$ ($\Delta\varepsilon_B \approx 4\beta$ in the tight-binding approximation). β is of the order of $10^{1\text{-}2}$ meV in typical molecular solids.[15] The Uncertainty Principle dictates that localization of the electron from a delocalized state is associated with an energetic penalty of δE_{del}, which is approximately equal to half of the electronic bandwidth (~2β). This is because construction of a localized wavefunction requires the superposition of all delocalized *k*

states, corresponding to an average energy approximately in the middle of the conduction band. The driving force for localization comes from polarization in electronic and nuclear coordinates. Electronic polarization occurs on the time scale of the inverse of the Bohr frequency, i.e., $\tau_e \approx 10^{-16} - 10^{-15} s$, which is shorter than the time scale for the electron to hop from one molecular site to the other ($\tau_h \approx \hbar / J_M \approx 10^{-14} s$), and results in an energetic gain of the order of ~1 eV in typical molecular solids. Polarization of nuclear subsystems occurs on a longer time scales depending on whether it is intramolecular or lattice motions. Polarization of intra-molecular coordinates results in a *small polaron or molecular polaron*, with a typical interaction energy of a molecular polaron is 0.1 - 0.2 eV. The molecular polaron usually forms because the molecular vibration time scale (τ_v ~ $2x10^{-15}$ - 10^{-14} s) is on the order of or shorter than τ_h. In contrast, a *lattice polaron* does not form because the time scales of optical and acoustic phonons are typically longer than 10^{-13} s, with is not competitive with electron hopping time (τ_h). The electronic and intramolecular polarization effects lead to an energy gain for localizaion, δE_{pol}, which is dominated by the electronic part. Due to the narrow bandwidth of most molecular solids, the $|\delta E_{del}| < |\delta E_{pol}|$ inequality is usually satisfied. As a result, the formation of a molecular polaron is the norm rather than exception in organic semiconductors.

What do we expect to observe in an IR absorption spectrum for an OTFT under gate bias? To answer this question, let's consider the band structure diagram in figure IV-1. When an electron is injected into the conduction band, the strong tendency to localize (thick dashed arrow) leads to a small or molecular polaron, whose energy is independent of the momentum vector (k). This is essentially an anion with the excess electron in the lowest unoccupied molecule orbital (LUMO) of the molecule. Even if localization occurs

initially in bandgap defect states, we also expect polarization to yield a molecular polaron. Thus, we expect two features in IR absorption. The first is vibrational signature unique to an anion; the intramolecular vibrations of an anion are different from those of the neutral molecule due to the changed molecular geometry and force constants. The second is the broad optical absorption (thin dot-dashed arrows) from the lower-lying polaron state to the delocalized conduction band. This polaron band can extend from the IR to the visible region, depending on the extent of polaron stabilization.

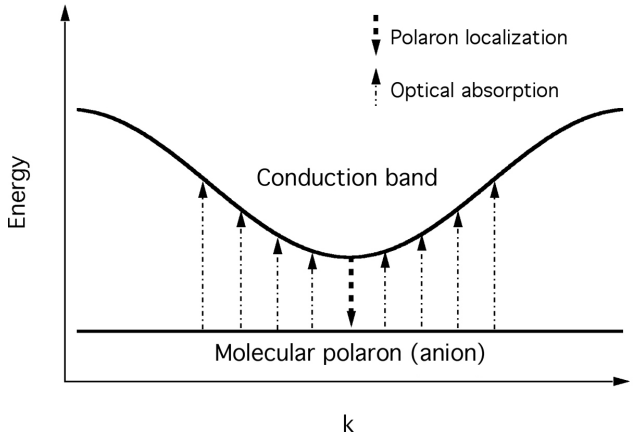

Figure IV-1. Schematic illustration of a conduction band resulting from delocalized LUMO in an organic semiconductor and a molecular polaron state. The thick dashed arrow represents self-trapping and the thin dot-dashed arrows illustrate optical absorption in the polaron band.

B) Experimental

OTFTs were fabricated on Si or Ge semiconductor crystals that served as waveguides for multiple internal reflection ATR-FTIR. Each Si or Ge ATR crystal (10mm x 50mm x 1mm) was cut from a Si (100 mm OD, 1mm thick, two side polished, 8-12 $\Omega \cdot cm^{-1}$, EL-CAT Inc.) or Ge (100 mm OD, 1mm thick, two side polished, undoped, MTI Corp.) wafer. Each semiconductor crystal was polished to the shape of a parallelogram with 45^{o} angles forming the two ends of the parallelogram. The Si ATR

crystal is transparent for $\bar{\nu} \geq 1500$ cm^{-1} while the Ge crystal is transparent down to 500 cm^{-1}.

Thin film transistors were fabricated on the ATR crystals. The surface of each ATR crystal was passivated to provide a hydrophobic wetting layer for organic semiconductor growth. On native oxide terminated silicon, the passivation layer was an octadecyltrichlorosilane self-assembled monolayer (SAM) while on germanium the monolayer was formed from a dodecyne hydrogermylation reaction.[16] N-N' dioctyl 3,4,9,10 perylene tetracarboxylic diimide (PTCDI-C8) was vapor deposited on the passivated Si or Ge surfaces at a rate of 0.05 Å/s to a thickness of 50 Å. Deposition continued at a rate of 0.15 Å/s for an additional 250 Å giving a total thickness of 300 Å. Gold source and drain electrodes (300 Å thick) were deposited through a shadow mask onto the PTCDI-C8 film at a rate of 0.5 Å/s. The gate dielectric used was an electrolyte solution of $LiClO_4$ in polyethylene oxide (mw = 10^5) in a ratio of 16 ether oxygen atoms to one lithium ion. The constituents of the dielectric were dissolved in acetonitrile and passed through a 0.2 μm PTFE filter. The solution was then drop cast onto the transistor assembly. Because acetonitrile and PTCDI-C8 repel each other due to the high surface energy at their interface, drop casting occurred in a polydimethoxysilane die. The drop casting procedure produced a PEO film which was close to 100 μm thick. After the dielectric was allowed to dry under high vacuum overnight, a 300 Å thick gold gate electrode was deposited onto the dielectric at a rate of 0.5 Å/s. In an attempt to minimize leakage current between the gate and the source or drain electrode, each was aligned to avoid spatial overlap in the horizontal direction.

As a comparison to devices with polymer electrolyte gate dielectric, we fabricated a bottom gate transistor with a conventional polymer gate dielectric layer, polystyrene (PS). In this device, the Si-ATR crystal served both as a waveguide for FTIR spectroscopy and as a gate electrode (with an Al/Au ohmic contact). A 400 nm thick polystyrene film was spin cast on the native oxide terminated silicon surface to serve as the dielectric layer. A 30 nm thick PTCDI-C8 film was vacuum deposited onto the polystyrene surface as described above. This was followed by the deposition of Au source and drain electrodes through a shadow mask.

The top insets in figure IV-2 show the device with polymer electrolyte gate dielectric. The total PTCDI-C8 film area was 4.0 cm^2 while the gate area was 2.4 cm^2. The devices fabricated on ATR crystals had source-drain channel dimensions of ~ 7 mm x 40 mm. For measurement under bias, the sample was connected to a power source and placed in a dry N_2 purged FTIR spectrometer (MIDAC) which was modified for multiple internal reflection with a liquid N_2 cooled MCT detector. During FTIR measurement, a constant voltage (V_G) was applied to the gate electrode with reference to the source electrode. Due to the large channel width, it was not possible to drive a current across the channel without causing a significant leakage current. Consequently, the source and drain electrodes were not biased relative to one another. The gate voltage was cycled between a maximum and minimum voltage in fixed increments. At each step, the voltage was held at a particular value for 6 min. Each FTIR scan took 5 min and was initiated 1 min after the voltage was applied. All FTIR spectra were collected at an instrument resolution of 1 cm^{-1}. The evanescent wave from the IR light decays exponentially outside the ATR crystal with decay length on the order of the light wavelength. It therefore

probes both the PTCDI-C8 layer and the dielectric layer. As an example, figure IV-2 shows an FTIR spectrum of the device with polymer electrolyte dielectric at a gate bias of V_G = 0 V. The spectrum mainly consists of vibrational peaks due to PTCDI-C8 and PEO molecules. Some of the most distinctive peaks assigned to PTCDI-C8 and PEO are labeled on the spectrum. Details will be discussed later.

The transistor properties of smaller devices were measured in order to better correlate the observed spectral changes with electrical transport measurements. Transistors were fabricated in a manner identical to the procedure described above, with the exception the channel dimensions and the substrate. The channel length was 500 μm, the width was 50 μm, and the substrate was oxide terminated silicon. More details on the transistor and its properties were published by Panzer and Frisbie.[14] During measurements, source, drain, and gate currents were measured independently from one another as the gate voltage was swept. Figure IV-3 shows the result of 2 separate experiments in which V_{SD} = 0.5 V. In one experiment, the gate voltage was swept from -1 V to 1.5 V, and in the other, the gate voltage was swept between -3 V and 3 V. The scan rate of the measurements was 8.5 x 10^{-2} V/s. This is two orders of magnitude faster than the comparable infrared scans. In the low voltage sweep, a reproducible transistor curve in which the source and drain currents were nearly identical was observed. The higher voltage sweep showed very different transport properties. The source and drain currents show a peak in the current, a noticeable disagreement between source and drain currents, a large hysteresis in both source and drain currents, and a gate current which is an order of magnitude larger than the low voltage sweep. These observations can be interpreted with the aid of infrared spectroscopy and will be discussed later.

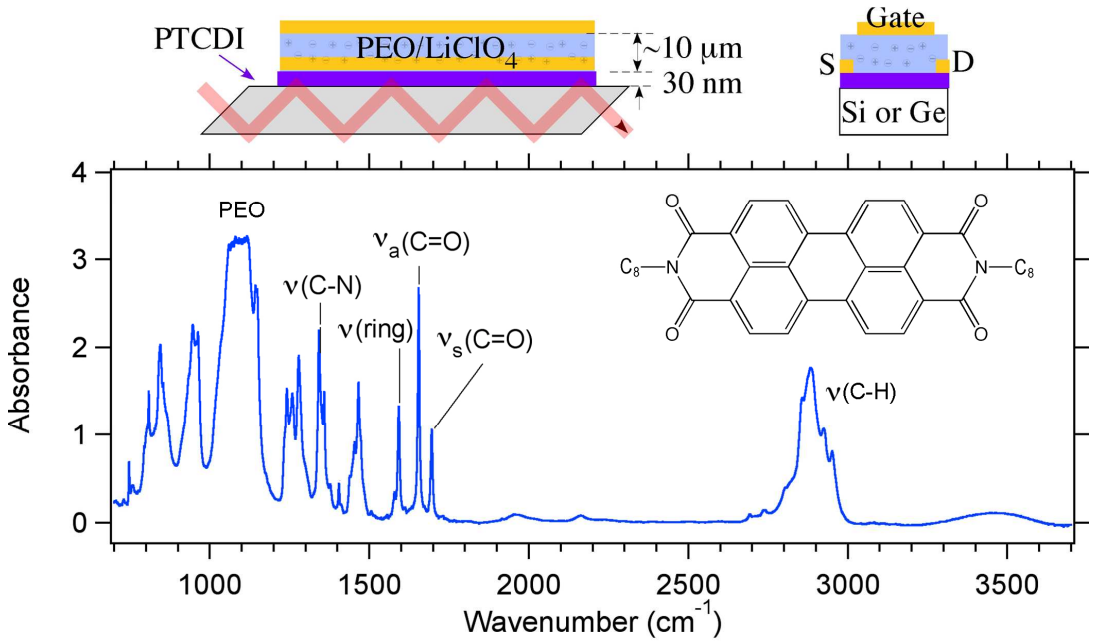

Figure IV-2. FTIR spectrum for the electrolyte gated device with V_G = 0 V. The inset is the molecular structure of PTCDI-C8. Top: Schematic illustration of the device fabricated on Si or Ge ATR crystals. The device consists of a top gate contact and a $PEO/LiClO_4$ dielectric.

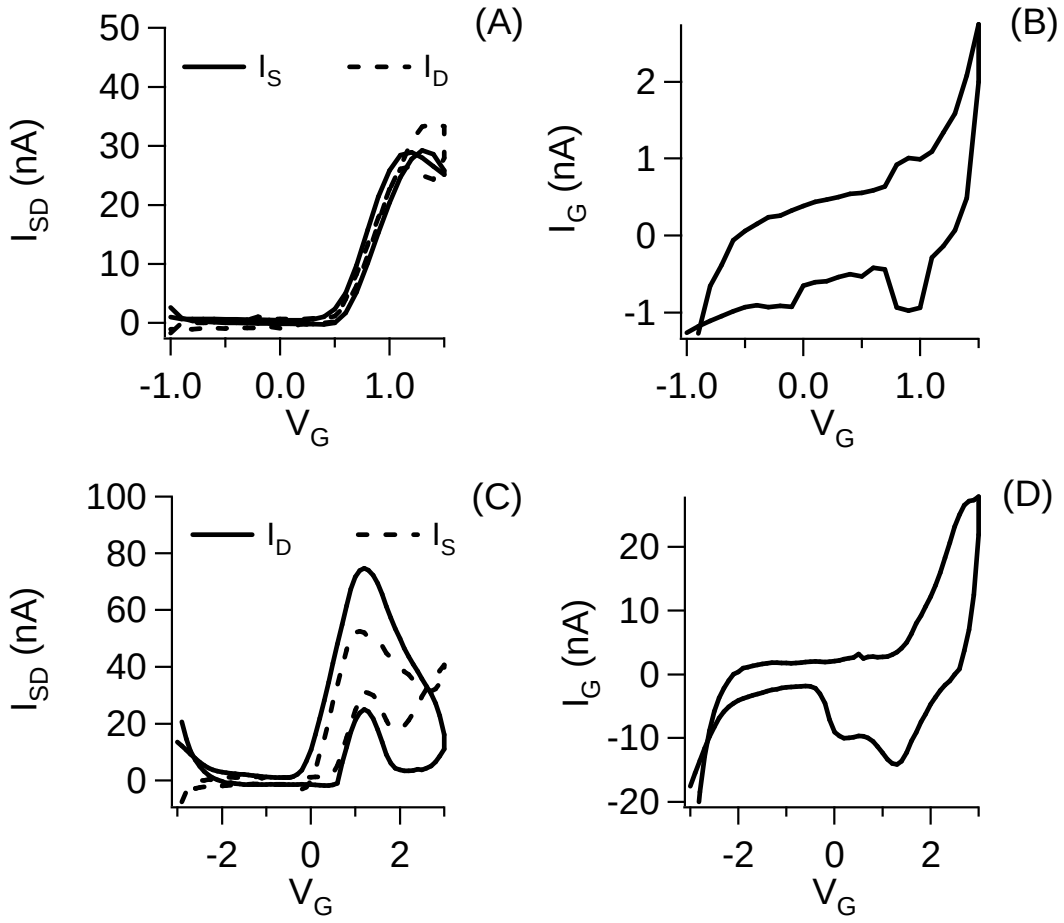

Figure IV-3. Transistor measurements as a function of gate voltage. Panel A,C describes the source and drain current. Higher current levels are achieved on the reverse sweep of panel C. Panel B,D describes the gate current. The measurements of panel A,B were taken prior to those in panel C, D.

C) Results and discussion

Perhaps the first and most notable observation is the very high effective gate capacitance afforded by the polymer electrolyte dielectric results in a transistor with a turn-on voltage of about V_G = +0.5 V. The positive V_G corresponds to n-channel conduction, *i.e.*, gate-induced electron injection into the PTCDI-C8 layer. An estimate of the injected charge density (θ_e) based on gate current measurement gives θ_e = $6.4x10^{14}/cm^2$ at V_G = 2.0 V.[14] At $V_G \geq$ 2 V, an increase in gate current was observed and irreversible changes occurred to the OTFT. As we show in the following from FTIR measurements that the low gate bias region ($V_G \leq$ 2 V) corresponds to electrostatic doping of the PTCDI layer while the high voltage region ($V_G \geq$ 2V) corresponds to electrochemical doping.

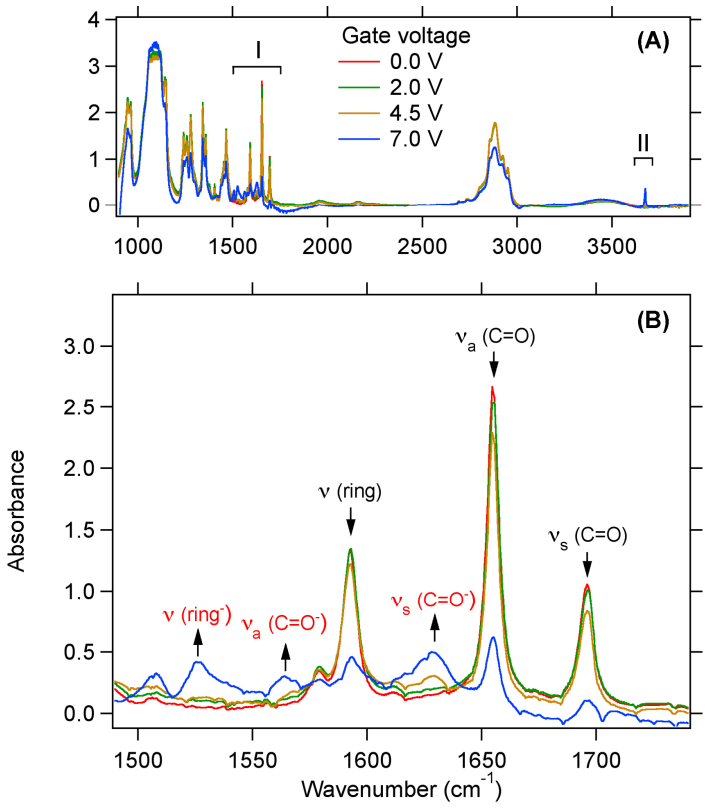

Figure IV-4. FTIR spectra of the polymer electrolyte gated PTCDI-C8 TFT under various gate bias voltage (red, green, orange, and blue for V_G = 0.0, 2.0, 4.5, and 7.0 V, respectively). Peaks labeled with downward arrows decrease with increasing V_G while those with upward arrows increase with V_G. Panel B is a magnified view of region "I" in the upper panel.

PTCDI-C8		PTCDI-C8 anion	
Peak/cm^{-1}	Vibrational mode	Peak/cm^{-1}	Vibrational mode
1696	Symmetric C=O stretching	1629	Symmetric C=O stretching
1655	Antisymmetric C=O stretching	1564	Antisymmetric C=O stretching
1593	Perylene ring stretching	1526	Perylene ring stretching
1439	Perylene ring stretching	1508	Perylene ring stretching
1405	Perylene ring stretching	1416	Perylene ring stretching
1345	C-N stretching	1325	C-N stretching
1259	C-H perylene bending		
PEO modes (cm^{-1}): 2162, 1960, 1473,1466,1453,1412,1358,1343,1279,1242,1145,1100, 965			

Table 1. Vibrational peak frequencies obtained from FTIR spectra in figures IV-1 & IV-3.

Figure IV-4 shows FTIR spectra obtained under various gate biases (V_G = 0, 2.0, 4.5, 7.0 V) for a PTCDI-C8 OTFT with a polymer electrolyte dielectric. There are two regions of the spectra that are most sensitive to V_G: I) 1500 – 1800 cm^{-1}, corresponding to the C=O stretching and perylene ring stretching modes; and II) a sharp peak at 3677 cm^{-1} which appears at high gate bias. We initially focus on region I, which is expanded in the lower panel. Table 1 summarizes major vibrational peaks of neutral PTCDI-C8 (at V_G = 0 V), along with those of PEO. The assignments for neutral PTCDI-C8 are from Antunes, et. al.[17] For PEO, only peak frequencies are shown and assignments are taken from the literature.[18,19] As shown in Panel B of Figure IV-4, the intensities of the C=O stretching and perylene ring stretching modes associated with the neutral PTCDI-C8 molecule decrease with increasing V_G. This is accompanied by the appearance and growth of a set of new peaks (labeled with red upward arrows) with increasing gate voltage. Following previous solution phase spectroelectrochemical experiments performed on other diimide molecules,[4] we assign these peaks to the singly charged anion of $[PTCDI\text{-}C8]^-$. The two C=O stretching peaks shift downward by 67 and 91 cm^{-1}, respectively, when the neutral PTCDI-C8 molecule is charged with one electron. For comparison, in solution phase experiments, these peaks shift downward by 78 and 116 cm^{-1} in a smaller model compound, pyromellitic dianhydride-N-butylimine (PMDA-N-Bu), when it is reduced to the singly charged anion form $[PMDA\text{-}N\text{-}Bu]^{-1}$.[4] Further reduction of PMDA-N-Bu to $[PMDA\text{-}N\text{-}Bu]^{2-}$ results in a triplet of C=O stretching peaks, with frequency decreases of more than 160 cm^{-1}.[4] Based on this previous study of model diimide compounds, we find no evidence of doubly charged $[PTCDI\text{-}C8]^{2-}$ in the V_G range investigated. All the new peaks that appeared under positive gate bias and

assigned to $[PTCDI\text{-}C8]^-$ are listed in Table 1. As expected from the conversion of neutral PTCDI-C8 to anionic PTCDI-C8 from electron injection under positive gate bias, the decrease in peak intensity associated with neutral PTCDI-C8 peaks are correlated with the increase of the anionic peaks. From repeated sweeping of V_G, we find that there are two regions of V_G in terms of reversibility of the vibrational spectrum: a nearly reversible region for $V_G \leq 2$ V and an irreversible region for $V_G \geq 2$ V.

In the reversible region, we sweep the gate voltage between 2V and -2V. Panel A in Figure IV-5 plots the absorbance (*Abs*) of the ν_a(C=O) peak for neutral PTCDI-C8 as a function of V_G for three consecutive cycles of V_G sweeps. Within experimental uncertainty, the absorbance change with V_G is reproducible from sweep to sweep. We make two important observations. The first observation is the complete recovery of the ν_a(C=O) peak intensity when the gate voltage is decreased from 2V to – 2V, indicating that all PTCDI-C8 anions are converted back to the neutral molecules. The second observation is the presence of significant hysteresis; the *Abs* vs. V_G data points during the reverse sweep (2 → 0 V) are below those of the forward sweep (0 → 2 V). Complete recovery only occurs when V_G is swept into the negative region. These observations are consistent with electrostatic doping of the PTCDI-C8 film gated by the polymer electrolyte dielectric in which time dependent diffusion occurs over observable timescales. Upon the application of a gate bias voltage, the positive Li^+ ions must diffuse to the PEO/PTCDI-C8 boundary to establish the electric field at the dielectric/organic semiconductor interface. The field-induced diffusion of ions in the polymer electrolyte is a slow process and the observed hysteresis reflects diffusion kinetics. In addition, the sample geometry used in the present study amplifies hysteresis: the area of the organic

semiconductor film under gate bias is 60% of the total area and polarization of PTCDI-C8 molecules outside the gated area may be a slow process. A hysteresis of a similar size in source-drain current sweeps was not observed in transistor measurements found in Panel A of Figure IV-2. This is likely due to the presence of multiple timescales of operation in the polymer electrolyte. Note that measurements in this reversible region were carried out on a newly fabricated device and V_G never exceeded the (-2 → 2V) range.

Based on changes in absorbance, we can calculate the density of gate-induced charge in the PTCDI-C8 film, given the proportionality relationship between absorbance and molecular concentration. As shown in panel A in figure IV-5, the application of V_G = 2 V results in the conversion of 4.6±0.2% neutral PTCDI-C8 molecules to the anionic form. The total area of PTCDI-C8 film sample is 4 cm^2 while the gate size is 2.4 cm^2. Assuming charge injection induced by electrostatic field only occurs under the gate, 7.7% of the PTCDI-C8 film is reduced. Since the density of PTCDI-C8 molecules in a monolayer is $2.5x10^{14}$ cm^{-2} and the inter-plane distance of the PTCDI-C8 film is 20 Å,[20,21] the calculated film density is $1.25x10^{21}$ cm^{-3}. Given a total PTCDI-C8 film thickness of 30 nm, we calculate a charge injection density of $2.9\pm0.2x10^{14}$ cm^{-2}. The charge injection density achieved here is equivalent to the complete conversion an entire monolayer of PTCDI-C8 molecules at the interface. For comparison, the injected charge density estimated from the integrated gate current in electrical measurement was of $6.4x10^{14}$ cm^{-2} at V_G = 2V.[14] We believe the electrical measurement may overestimate the charge injection density due to possible presence of gate leakage currents.

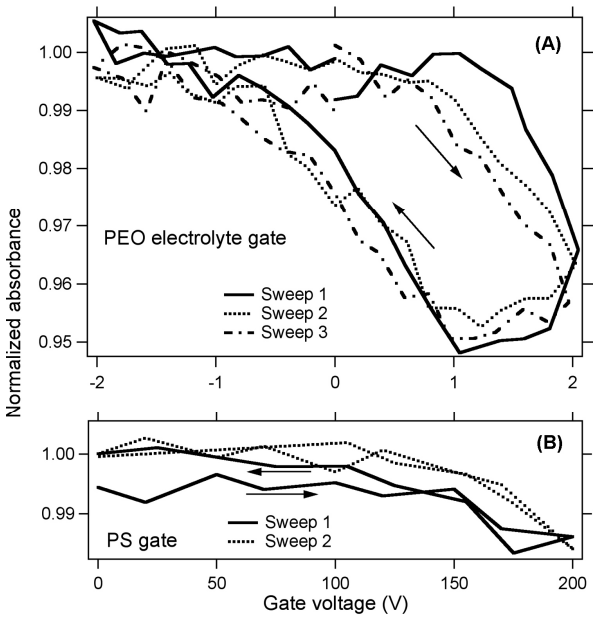

Figure IV-5. Normalized absorbance of the ν_a(C=O) mode of neutral PTCDI-C8 as a function of gate voltage for the polymer electrolyte gated TFT (Panel A) and the polystyrene gated TFT (Panel B). The arrows indicate the sweep directions. There are three VG sweeps (0 → 2 → 0 → -2 → 0 V) in Panel A and two sweeps (0 → 200 → 0 V) in Panel B.

As a comparison to the polymer electrolyte gated OTFT, we also carried out FTIR measurements for a PTCDI-C8 TFT with a 400 nm thick polystyrene dielectric and bottom gate. As expected, the amount of change in FTIR spectra under gate bias is significantly smaller than that seen for the polymer electrolyte gated OTFT. Panel B in figure IV-5 plots the absorbance of the ν_a(C=O) peak for neutral PTCDI-C8 as a function of V_G up to 200 V, above which dielectric breakdown is observed. At the maximum gate voltage of V_G = 200 V, 1.2±0.3% of the neutral molecules have been converted to anions, corresponding to a charge injection density of $4.5\pm2\times10^{13}$ cm^{-2}. This maximum doping level is equivalent to the conversion to anions of 18% of a monolayer of PTCDI-C8 molecules at the interfaces, over 5x lower than the charge injection density in the PEO system at V_G = 2 V.

When the gate voltage exceeds 2 V for the polymer electrolyte gated device, FTIR shows irreversible changes, and a large hysteresis in the source and drain current appears.

This is illustrated in Figure IV-6. Panel A shows a set of FTIR spectra taken as V_G is cycled in the range 0 → 7 → 0 → -6 → 0 V, with ±1 V steps (each data point corresponds to the voltage held for 5 min). The corresponding peak intensities (integrated and normalized to the maximum value) of ν_s(C=O) for the neutral and anionic PTCDI-C8 species are shown in the lower panels. As V_G increases above 3 V, the sharp decrease in the intensity of the neutral PTCDI-C8 peak is accompanied by a sharp decrease in the intensity of the anionic peak. The concentration of the neutral PTCDI-C8 molecule decreases to 18% of its starting value at V_G = 6-7 V. Since 40% of the PTCDI-C8 molecules are not directly under the gate electrode, this result indicates that reduction occurs for not only all PTCDI-C8 molecules under the gate electrode but also some PTCDI-C8 molecule beyond the gated area.

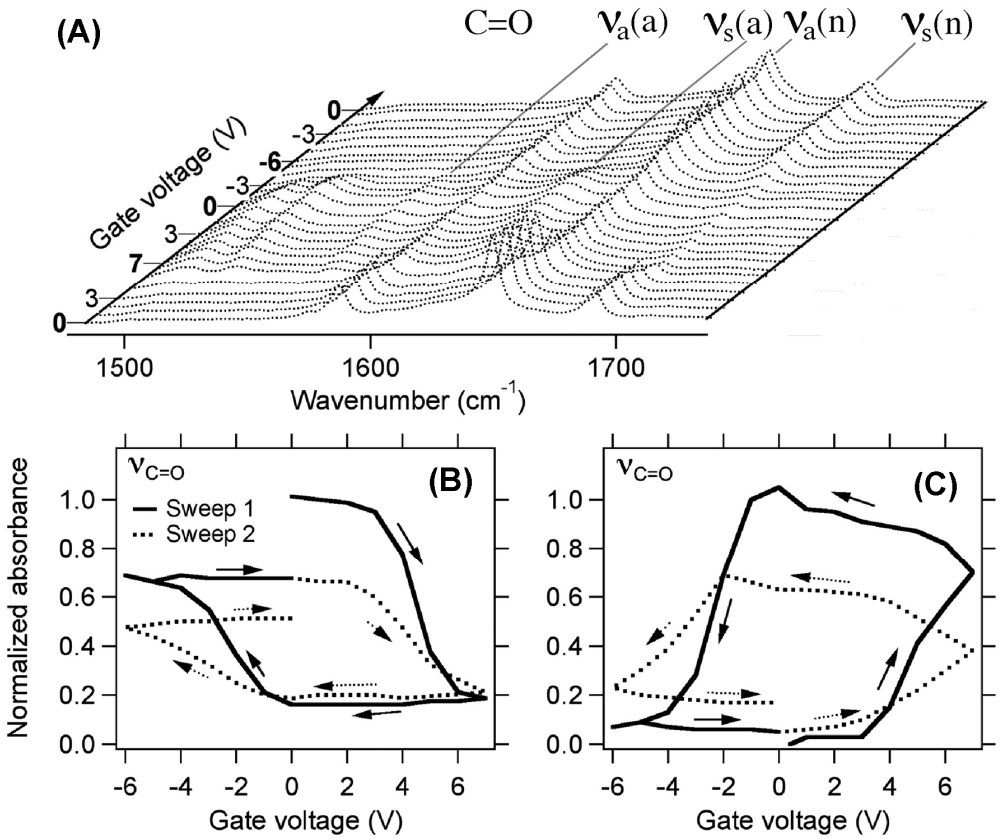

Figure IV-6 (A): FTIR spectra in carbonyl stretching region for a complete V_G sweep (0 → 7 → 0 → -6 → 0 V). The symmetric & asymmetric C=O stretching peaks are labeled and (n) and (a) stand for neutral and anionic PTCDI-C8, respectively. Normalized absorbance of the symmetric C=O stretching peaks of neutral (Panel B) and anionic (Panel C) PTCDI-C8 as a function of V_G for two sweeps. The arrows indicate the sweep direction.

There are two types of irreversibility in the *Abs* vs V_G plots in Figure IV-6. The first is the large hysteresis in the neutral and anionic peak intensities within each V_G sweep (0 → 7 → 0 → -6 → 0 V). After the nearly complete reduction of PTCDI-C8 at V_G = 6-7 V, the neutral species showed virtually no sign of recovery until the gate voltage is less than 0 V. At negative V_G, partial recovery occurs, as shown by the increase in neutral peaks and the decrease in anionic peaks. The second type of irreversibility is the change from cycle to cycle. As shown by the neutral PTCDI-C8 peak intensity in Panel B in Figure IV-6, 30% of the neutral PTCDI-C8 intensity is lost after V_G is returned to zero after negative bias. Following the second sweep, another 20% of the intensity is lost. Interestingly, the loss in the intensity of neutral PTCDI-C8 molecules from sweep to sweep is not compensated for by a gain in that of anionic species. In fact, there is less anionic PTCDI-C8 intensity formed in the second sweep than that is the first sweep.

The irreversible loss of C=O stretching peak intensities for both neutral and anionic PTCDI-C8 molecules following each cycle of V_G sweep must be due to chemical reaction. Supporting this conclusion, we find a sharp peak at 3677 cm^{-1} which appears at $V_G \geq 5$ V (see region II in panel A of Figure IV-4). This peak is the O-H stretching mode in a lithium hydroxide molecule (LiOH).[22] Figure IV-7 shows in detail the O-H stretching region of FTIR spectra during the first sweep of gate voltage. The broad peak present in all spectra is the O-H stretching mode of hydrogen-bonded water in the PEO electrolyte. When $V_G \geq 5$ V, the sharp LiO-H vibrational peak appears. Repeated cycling of the voltage causes only small changes in LiOH concentration, as shown by the small change in absorbance following the second cycle of V_G sweep, lower panel. This LiOH molecule giving rise to the 3677 cm^{-1} peak must be located in the PTCDI-C8 film;

otherwise, it should dissociate in the PEO electrolyte layer. We arrive at two conclusions: 1) Li^+ must diffuse into the PTCDI-C8 thin film at sufficiently positive V_G; and 2) there is a chemical degredation reaction which occurs in the PTCDI-C8 layer to form LiOH.

The intercalation of Li^+ into layered solids is well known, particularly for materials used in lithium ion batteries. It is not surprising that, under sufficiently positive gate bias, Li^+ diffuses into the layered solid of PTCDI-C8. In order to form a LiOH molecule, the presence of H_2O is required and water is a readily available impurity in the hydrophilic PEO layer. It is then likely that as Li^+ ions diffuse into the PTCDI-C8 layer at $V_G > 2$ V, they carry water molecules along with them in the form of a hydration shell. In view of the loss of C=O stretching peak intensity in both neutral and anionic PTCDI-C8 and the irreversible formation of LiOH, we propose the following reaction mechanism, equation (1). In this reaction, the PTCDI-C8 anion reacts with H_2O impurities to give OH^-, which readily associates with Li^+ to form the LiOH molecule.

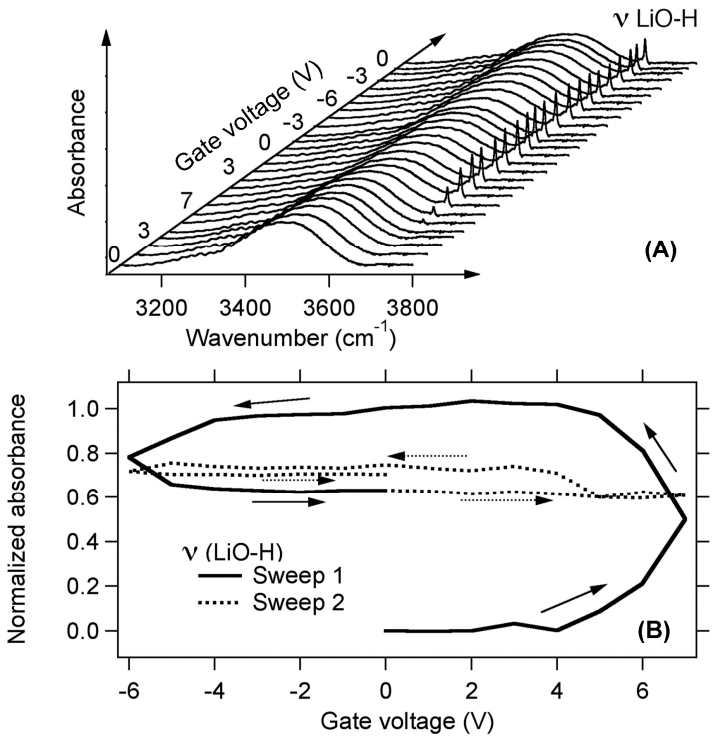

Figure IV-7. Panel A: FTIR spectra in the OH stretching region as a function of gate voltage. The broad peak centered at about 3500 cm^{-1} is assigned to hydrogen bonded water in PEO. The sharp peak at 3677 cm^{-1} is assigned to LiO-H. Panel B: Normalized (to the maximum) absorbance of the ν(LiO-H) peak as a function of V_G for two voltage sweeps. The arrows indicate the V_G sweep directions.

(1) 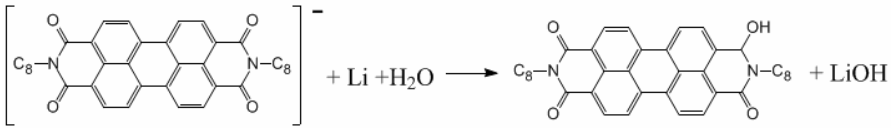

The mechanism for PTCDI-C8 anion formation in the irreversible region at V_G > 2 V is completely different than the electrostatic mechanism at $V_G \leq 2$ V. At $V_G > 2$ V, we essentially have electrochemical reduction of PTCDI-C8 molecules with Li^+ as counter ions. Thus, this is called electrochemical doping. The existence of two distinctively different regimes of doping is most obvious in the first part of the voltage sweep (0 → 7 V) in figure IV-6. The rate of conversion from neutral to the anionic species (as a function of V_G) increases dramatically when V_G exceeds 3 V. The negative slope of the

Abs vs V_G plot for neutral PTCDI-C8 (panel B of figure IV-6) or the positive slope for PTCDI-C8 anion (panel C of figure IV-6) is proportional to the capacitance of the dielectric. The capacitance of the dielectric is basically constant for V_G = 0-2 V. This is the electrostatic doping region. For V_G > 2 V. the effective capacitance (slope) increases in a discontinuous fashion and reaches a value which is more than one order of magnitude larger than that in the electrostatic doping region. This is because, in addition to electrostatic doping, the more efficient electrochemical doping mechanism is turned on for V_G > 2 V. The transition from the electrostatic to the electrochemical doping region is irreversible due to structural deformation of the PTCDI-C8 film.

The spectroscopic evidence for the two doping regions observed here in a polymer electrolyte gated OTFT are consistent with previous electric measurements that established the two doping regions: 1) the electrostatic (also called ion-blocking or non-Faradaic[23]) region[11-14] where the ionic double layer at the electrolyte-organic semiconductor interface is responsible for charge injection into the first a few layers of the organic semiconductor at the dielectric interface; and 2) the electrochemical (also called ion-permeable or Faradaic[25]) region[24,25] involving the oxidation/reduction of the whole organic semiconductor thin film and the intercalation of counter ions into the organic semiconductor layer. A transition between these two regions has also been reported recently by Lin and Lonergan in electrical measurement of a liquid electrolyte gated TFT of polyacetylene as the active organic semiconductor layer.[25]

E) Conclusions

We successfully applied ATR-FTIR spectroscopy to directly probe active layers in organic thin film transistors (OTFTs). For a PTCDI-C8 TFT with a PEO/$LiClO_4$ polymer electrolyte gate dielectric, FTIR spectroscopy showed the formation of anionic PTCDI-C8 species from electron injection under positive gate bias. There were two distinctive different doping regions: a reversible and electrostatic doping region for $V_G \leq$ 2V and an irreversible and electrochemical doping regime for V_G > 2V. In the electrostatic doping region, the injected electron density at V_G = 2 V was $2.9\pm0.2 \times 10^{14}$ cm^{-2}, corresponding to the conversion of slightly more than one monolayer of PTCDI-C8 molecules into anions. Transistor measurements taken in this regime are reversible with little hysteresis. In the electrochemical doping region at V_G > 2V, we observed the diffusion of Li^+ into the organic semiconductor film and the conversion of all PTCDI-C8 molecules into anionic species. In addition, we observed a chemical reaction between anionic PTCDI-C8 and impurity water molecules. Transistor measurements in this regime have unusual hysteresis and discrepancies in source and drain currents, the latter stemming primarily from a large gate current. For comparison, we also probed a PTCDI-C8 TFT with a conventional polystyrene gate dielectric; the maximum charge carrier density under electrostatic doping at V_G = 200 V was $4.5\pm2 \times 10^{13}$ cm^{-2}, corresponding to the 18 % conversion of one monolayer of PTCDI-C8 molecules into anions.

E) Acknowledgements

This work was supported by US Department of Energy Office of Basic Energy Sciences and the US National Science Foundation MRSEC Program under award number DMR 0212302.

F) References

[1] Jun, Y.; Zhu, X.-Y. *J. Am. Chem. Soc.* **2004,** 126, 13224-13225.

[2] Chaing, C.K.; Fincher Jr., C. R.; Park, Y.W.; Heeger, A.J.; Shirakawa, H.; Louis, E.J.; Gau, S.C.; MacDiarmid, A.G. *Phys. Rev. Lett.* **1977,** 39, 1098-1101.

[3] Kim, J.-Y.; Kim, E.-R.; Sohn, D.; Sakamoto, A.; Tasumi, M. *Bull. Korean Chem. Soc.* **2001**, *22*, 833-836.

[4] Viehbeck, A.; Goldberg, M.J.; Kovac, C.A *J. Electrochem. Soc.* **1990,** 137, 1460-1466.

[5] Costantini, N.; Lupton, J. M. *Phys. Chem. Chem. Phys.* **2003**, *5*, 749-757.

[6] Chua, L-L.; Zaumseil, J.; Chang, J-F.; Ou, E.C-W.; Ho, P.K-H.; Sirringhaus, H.; Friend, R.H. *Nature* **2005,** 434, 194-199.

[7] Li, Z.Q.; Wang, G.M.; Sai, N.; Moses, M.C.; Martin, M.C.; Di Ventra, M.; Heeger, A.J.; Basov, D.N. Nano Lett. **2006,** 6, 224-228.

[8] Ziemelis, K.E.; Hussian, A.T.; Bradley, D.D.C.; Friend, R.H.; Ruhe,J.; Wegner, G. *Phys. Rev. Lett*. **1991,** 66, 2231-2234.

[9] Deng, Y. Y.; Sirringhaus, H. *Phys. Rev. B* **2005**, *72*, 045207.

[10] Andrews, S. S.; Boxer, S. G. *J. Phys. Chem. A* **2000**, *104*, 11853.

[11] Panzer, M.J.; Newman, C.R.; Frisbie, C.D. *App. Phys. Lett.* **2005,** 86 103503-103503.

[12] Panzer, M.J.; Frisbie, C.D. *Adv. Funct. Mater.* **2006,** 16, 1051-1056.

[13] Dhoot, A.S.; Yuen, J.D.; Heeney, M.; McCulloch, I.; Moses, D.; Heeger, A.J. *P.N.A.S.* **2006,** 103, 11834-11837.

[14] Panzer, M.J.; Frisbie, C.D. *J. Am. Chem. Soc.* **2005,** 127, 6960-6961.

[15] Silinsh, E. A.; Capek, V. *Organic molecular crystals: interaction, localization, and transport phenomena* (**1994**, AIP Press, Woodbury, NY).

[16] Choi, K.; Buriak, J.M.; *Langmuir* **2000,** 16, 7737-7741.

[17] Antunes, P.A.; Constantino, C.J.L.; Aroca, R.; Duff, J. *Appl. Spec.* **2001,** 55, 1341- 1346.

[18] Papke, B. L.; Ratner, M. A.; Shriver, D. F. *J. Electrochem. Soc.* **1982**, *129*, 1434.

[19] Yoshihara, T.; Tadokoro, H.; Murahashi, S. *J. Chem. Phys.* **1964**, 41, 2902.

[20] Chesterfield, R.J.; McKeen, J.C.; Newman, C.R.; Ewbank, P.C.; Demetrio, A. S. F.; Bredas, J-L.; Miller, L. L.; Mann, K.R.; Frisbie, C.D. *J. Phys. Chem. B.* **2004**, 108, 19281-19292.

[21] Hadicke, E.; Graser, F. *Acta Cryst.* **1986,** C42, 189-195.

[22] Wikersheim, K.A. *J. Chem. Phys.* **1959,** 31, 863-869.

[23] Lin, F.; Lonergan, M.C. *Appl. Phys. Lett.* **2006,** 88, 133507-133510.

[24] Ofer, D.; Crooks, R.M.; Wrighton, M.S. *J. Am. Chem. Soc.* **1990,** 112, 7869-7879.

[25] Taniguchi, M.; Kawai, T. *Appl. Phys. Lett.* **2004,** 85, 3298-3300.

V. Time Dependent Operating Mechanisms in Ion Gel Gated Organic Thin Film Transistors*

We applied in-situ infrared spectroscopy on a metal-insulator-polymer semiconductor capacitor to understand the mechanism responsible for the high carrier densities achieved in ion gel gated organic thin film transistors. The ion gel used is a mixture of a triblock copolymer, poly(styrene-b-methylmethacrylate-b-styrene), and an ionic liquid, 1-ethyl-3-methylimidazolium bis(trifluoromethylsulfonyl)imide. It was found that the primary charging mechanism at low frequencies is the introduction of ions into the semiconductor layer. The kinetics of this process was characterized and used to specify the maximum operating frequency for the device as an electrochemical transistor. Any device operating at faster timescales can be thought to work via the formation of an electrostatic double layer.

A) Introduction

Organic thin-film transistors (OTFTs) have been investigated extensively due to their potential importance as critical current and voltage modulating components of organic electronic circuitry.[1-5] In an OTFT, the organic semiconductor is insulated

* This chapter contains excerpts from the following published work: Lee, J.; Kaake, L.G.; Cho, J.H.; Zhu, X.-Y.; Lodge, T.P.; Frisbie, C.D. *J. Phys. Chem. C* **2009**, 113, 8972-8981. See appendix for copyright information

from the gate electrode by a dielectric layer, and the gate/dielectric stack is responsible for inducing the charge carriers in the semiconductor channel.[6] It is desirable for the gate dielectric to have a high specific capacitance, because higher capacitance results in more induced charges in the semiconductor and thus higher ON currents at lower gate voltages. Generally, a high capacitance dielectric layer can be attained by reducing its thickness, and several research groups have employed ultra-thin crosslinked polymer films [7-9] or self-assembled monolayers (SAM) [3,10-12] as dielectrics. The capacitances of these systems have reached 1 $\mu F/cm^2$, which allows low voltage OTFT operation.

Solid polymer electrolytes consisting of a salt dissolved in a polymer matrix offer another promising approach to achieving high capacitance values. The exceptionally high capacitance (*e.g.* C_i ~100 $\mu F/cm^2$) of solid polymer electrolytes results from the formation of an electrical double layer only nanometers in thickness at the electrolyte/gate electrode interface, when cations and anions move in response to the gate bias.[13,14] Several groups have demonstrated solid polymer electrolyte gated transistors based on organic single crystals,[15-18] organic semiconductor thin-films,[19-24] or carbon nanotubes.[25-28] These devices display good static device characteristics such as high ON currents and low operating voltages. However, they generally show poor dynamic characteristics, especially low switching frequency (*e.g.*, 1 Hz), resulting from the slow polarization response of the polymer electrolyte. High capacitance "ion gels," were demonstrated to improve the dynamic behavior of electrolyte gated transistors (GEL-OTFT).[29-31] Ion gels can be prepared from mixtures of an ionic liquid and a block copolymer, and can provide specific capacitances in excess of 10 $\mu F/cm^2$ and

switching speeds up to 1 kHz.[29-31] One of the best performing materials combination for GEL-OTFT uses 1-ethyl-3-methylimidazolium bis(trifluoromethylsulfonyl)imide [EMIM][TFSI] as the ionic liquid, poly(styrene-b-methylmethacrylate-b-styrene) (SMS) as the triblock copolymer, and poly(3-hexylthiophene) (P3HT) as the polymer semiconductor.[31] This combination of materials was studied exclusively in this report.

Although the utility of GEL-OTFTs ultimately depends upon their electrical performance, there remains a major question regarding the nature of the physical process that gives rise to the observed high carrier densities. More specifically, what is the relative importance of electrochemical doping (the penetration of ions into the bulk of the semiconductor) versus electrostatic doping (the accumulation of ions at the semiconductor interface and the subsequent large electric field they can produce)? In the context of electrochemistry, the two different doping mechanisms are referred to as Faradaic and non-Faradaic processes, respectively.[14] In principle, operation in the electrostatic, non-Faradaic, regime is more desirable as it avoids chemical change to the polymer semiconductor, change that might be only partially reversible.

B) Experimental

A metal/insulator/polymer semiconductor capacitor was constructed on a zinc selenide optical waveguide, a schematic of which is found in Figure V-1. Zinc selenide is transparent from 500 to 20,000 cm^{-1}, enabling attenuated total internal reflection Fourier transform infrared spectroscopy (ATR-FTIR) to be carried out while the capacitor device is charged and discharged. Device fabrication began with the spin

coating of a 200 nm thick P3HT film, followed by the thermal evaporation of a pattern of 30 nm thick gold drain electrodes. The electrode pattern created eleven active polymer semiconductor channels each having a width of 500 μm and a length of 16 mm. The device was finished by laminating a polyester-supported copper strip on top of an ion gel dielectric using [EMIM][TFSI] ionic liquid and the SMS triblock copolymer. The details concerning the making of the ion gel can be obtained from Lee, et. al.[31] The drain electrodes were grounded and a voltage was applied to the copper gate electrode. Simultaneously, infrared spectra were recorded on a Nicolet 6700 spectrometer with a mercury cadmium telluride (MCT) detector. All measurements were taken in a dry nitrogen environment to avoid semiconductor degradation which has been shown to limit the reversibility of repeated electrochemical doping experiments.[32]

C) Results and discussion

To examine the operating mechanism in GEL-OTFTs, we performed in-situ optical spectroscopy measurements on a model device, Figure V-1a. Some typical spectra are shown in Figure V-1, panel (b-d). The absorbance spectra are generated by subtracting a spectrum taken at $V_G = 0$ as the background, such that the observed spectral signatures are due to the presence of charge. Panels b and c show that upon application of a gate voltage, a broad feature appears centered at 3500 cm^{-1}, whose intensity increases as time unfolds. This feature is frequently called a polaron absorption and, in p-type semiconductors, is the result of an electronic transition from the extended HOMO of the conjugated polymer to a state within the HOMO/LUMO gap created by the presence of a

hole.[33] The intensity of this absorption is therefore directly related to the number of holes in the semiconducting film.

With an estimate of the number of holes in the semiconducting film during the doping process, it is possible to determine if the process is electrochemical in nature. Because electrochemical doping affects the bulk of the semiconductor, while electrostatic doping only occurs near the dielectric/semiconductor interface, the simplest signature of electrochemical doping is a charge density that is impossible to account for by electric double layer charging. Because the intensity of the polaron absorption is related to the number of holes in the film, a large polaron absorption is a reliable indicator of electrochemical doping.

The action of the electrochemical doping mechanism can also be more rigorously identified by examining absorption features of the neutral semiconductor.[32,34] At V_G = -1.25, after over 2000 seconds of steadily applied voltage, the thiophene ring stretching mode has been bleached by over 15 percent due to hole injection. Because the film is 200 nm thick, the smallest possible thickness of the accumulation layer is 30 nm. Such extensive doping cannot be accounted for by double layer charging, hence electrochemical doping plays an important role at and above these voltages. It is worth noting that electrochemical doping may play a role at lower voltages, but electrostatic doping and very light electrochemical doping cannot be unambiguously differentiated in this context.

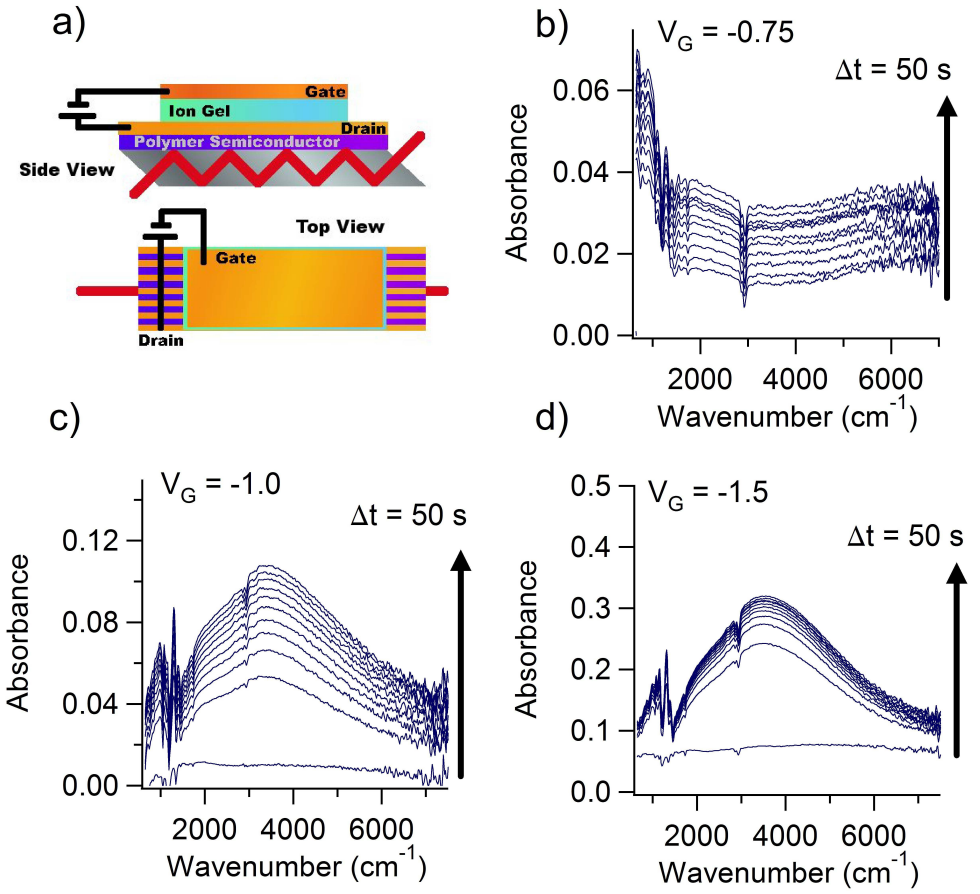

Figure V-1. (a) Schematic of the infrared spectroscopy experiment. Infrared light undergoes total internal reflection inside a ZnSe waveguide and probes the transistor as it charges. (b)-(d) Time evolving infrared spectra taken at different gate voltages. The background used to generate the spectra was that of the device at zero gate voltage. The broad polaron feature centered at 3500 cm^{-1} was present at all V_G > -0.75, while the feature peaked at 1000 cm^{-1} was more representative of lower voltage spectra.

A more interesting question to address in the context of the high switching speeds of GEL-OTFTs is the kinetics of electrochemical doping. That is, do GEL-OTFTs depend upon electrochemical doping to modulate charge density in the active channel of the device at high frequencies? To answer this question, we examined the time dependence of device charging at different gate biases by applying a gate voltage and taking spectra at regular time intervals. To determine the amount of charge in the film at a given time, the polaron absorption depicted in Figure V-1 was integrated over the interval 600 to 8000 cm^{-1}. The resulting uptake curve for V_G = -1.5 V is shown in Figure V-2 and is characterized by a rapid initial uptake, followed by a gradual increase in charge density at longer times.

We modeled the diffusion process in order to interpret the charging curves and extract the relevant timescale for electrochemical doping.[35] As electrochemical doping occurs, hole polarons in the P3HT film are accompanied by the negatively charged [TFSI] ions and the polymer film is overall charge neutral. Upon the application of a negative gate voltage, [TFSI] is initially at a much higher concentration near the dielectric/semiconductor interface than in the bulk. Doping of the P3HT film is thus controlled by diffusion of [TFSI] ions into the polymer semiconductor. With this in mind, we write the diffusion equation for [TFSI], taking z as the direction perpendicular to the dielectric/semiconductor interface, and assuming that the diffusivity D is independent of ion concentration.

$$\frac{\partial [TFSI](z,t)}{\partial t} = -D\frac{\partial^2 [TFSI](z,t)}{\partial z^2} \quad (1)$$

Given the appropriate boundary conditions, solving this differential equation is straightforward.[36] In this case, the [TFSI] concentration at the

dielectric/semiconductor interface (z = 0) is assumed to be constant as suggested by the high ion conductivity of the ion gel. The second condition is the "no-flux" boundary condition for the semiconductor/ZnSe interface at z = a:

(2) $$\frac{\partial[TFSI](a,t)}{\partial z} = 0$$

where *a* is the thickness of the P3HT layer. This boundary condition states that the flux of [TFSI] into the zinc selenide waveguide beneath the P3HT film is zero. The solution to this differential equation is given by

(3) $$[TFSI](z,t) = [TFSI](z=0,t)(1-\frac{4}{\pi}\sum_{n}^{\infty} c_n \sin(\lambda_n z)\exp(-\lambda_n^2 Dt))$$

where *[TFSI](z=0,t)* is also the equilibrium concentration of [TFSI] as time approaches infinity (i.e., *[TFSI](z=0,t) = [TFSI](z,t=∞))*, and λ_n and c_n are constants which depend upon an integer which is the index of the infinite series.

(4) $$c_n = \frac{1}{(2n-1)}$$

(5) $$\lambda_n = \frac{\pi(2n-1)}{2a}$$

Because the *in-situ* infrared spectroscopic technique employed examines the entire P3HT film and is not sensitive to the z dependence of the hole diffusion profile, Equation 4 must be integrated with respect to *z* before it can be used to fit the data. However, it is worth noting that while ATR-FTIR is, in general, sensitive to the *z* position of the holes which it measures, this sensitivity only becomes important when the film thickness is on the order of the wavelength of light. This is not the case for a 200 nm film in an infrared study.

When the integrated form of Equation 3 is used to fit the data, we observe that the fit accurately describes the initial uptake of holes into the P3HT film, but deviates from the experimental data at longer timescales (not shown). There could be several reasons for this deviation from simple one-dimensional diffusion. For example, hole diffusion and ion diffusion are coupled; *i.e.*, an excess hole concentration creates a net positive charge which exerts an electrostatic force upon the negatively charged [TFSI] ions. Also, when the concentration of the negatively charged [TFSI] ions in the P3HT is sufficiently high, we expect structural changes in the P3HT film.[37,38] To quantitatively analyze the experimental uptake curve, we employed a linear combination of two solutions for Equation 4, each with a different diffusion constant. Such a two component diffusion model provides an excellent description of the experimental data, as shown in Figure V-2. Naturally, the faster term dominates at the initial stage. This diffusion constant is represented as a function of gate voltage in Figure V-2. At high gate voltages the diffusivity is only on the order of 10^{-12} cm^2/s, a rather low value. For comparison, Kaneto, *et al*. reported ClO_4^- diffusion constants of 10^{-12}-10^{-10} cm^2/s in a polythiophene film in contact with liquid electrolyte.[39]

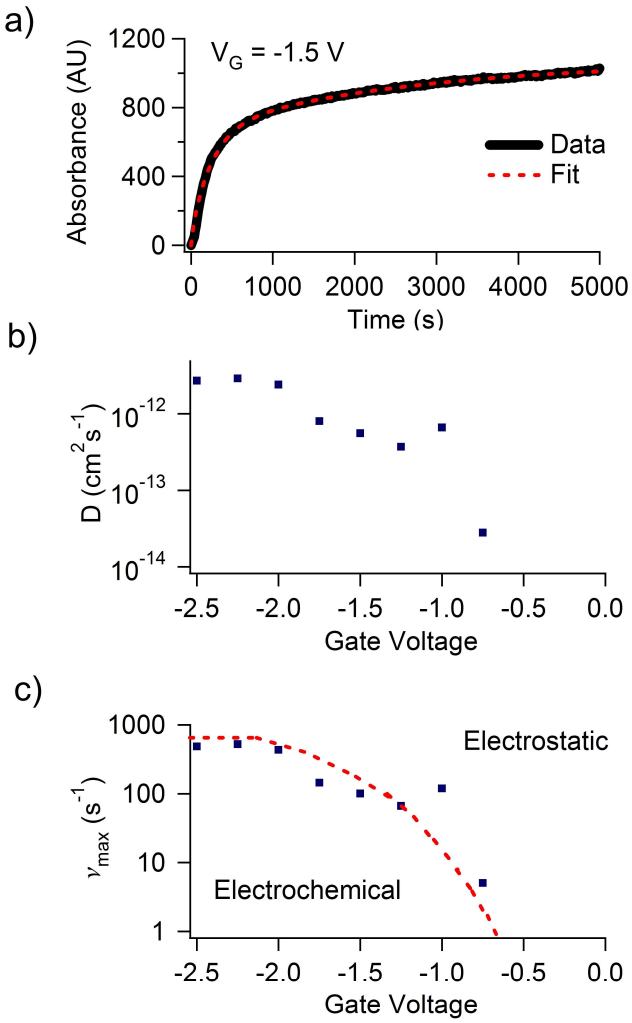

Figure V-2. a) Infrared spectra were integrated over the range 600 to 8000 cm^{-1} and the result is plotted as a function of time after the application of a gate voltage. The form of the fitting function is described by Equation 4. b) Extracted diffusivity of [TFSI] as a function of gate voltage. The estimate of diffusivity comes from the fastest component of a linear combination of Equation 4 using two diffusivities. c) Maximum operating frequency of a SOS[EMIM][TFSI] GEL-OTFT as an electrochemical device as a function of gate voltage. This value is estimated from the diffusivity plotted in panel b using Equation 10.

To further explore how ion diffusion influences the high switching speeds of a GEL-OTFT (*i.e.*, in the short diffusion time regime), the diffusion equation must be solved using boundary conditions which more accurately reflect the situation near the dielectric/semiconductor interface at short timescales. The boundary condition given in Equation 3 is changed such that the P3HT film is approximated as semi-infinite and then requiring that $[TFSI](z\rightarrow\infty,t) = 0$. Given this, Equation 1 can be solved exactly.

$$[TFSI](z,t) = [TFSI](z=0,t)\left(1 - erf\left[\frac{z}{2\sqrt{Dt}}\right]\right) \quad (6)$$

The right side of equation 6 can be integrated with respect to z over the limits of zero to infinity to yield the following:

$$\int_0^\infty \frac{[TFSI](z,t)}{[TFSI](z=0,t)} dz = \frac{2}{\sqrt{\pi}}\sqrt{Dt} \quad (7)$$

The concentration profile specified in the left hand side of Equation 7, is commonly approximated as linear with a thickness, *l*, that evolves at a rate of $\sqrt{Dt}$.[40]

$$\int_0^\infty \frac{[TFSI](z,t)}{[TFSI](z=0,t)} dz \Rightarrow \int_0^l 1 - \frac{z}{l} dz = \frac{l}{2} \quad (8)$$

Thus the thickness of the electrochemically doped layer is given by the following:

$$l = \frac{4}{\sqrt{\pi}}\sqrt{Dt} \quad (9)$$

To determine the time it takes for electrochemical doping to occur, it is useful to specify a definition for time dependent electrochemical doping. Namely, electrochemical doping can be considered to occur in the time it takes for the depth of the linear concentration profile to exceed the lattice parameter of the organic semiconductor in question. Using the previously published XRD parameters,[41] we set l=1.62 nm in Equation 9 and solve

for the time required to electrochemically dope a single layer of P3HT. This characteristic time can then be inverted to obtain the maximum frequency for which a GEL-OTFT can be thought to act as an electrochemical device. This result is plotted in panel c of Figure V-2. To restate, the data represented in Figure V-2c are the maximum timescales for which an SMS[EMIM][TFSI] GEL-OTFT operates as an electrochemical device.

The graph depicts the different regimes of operation, with devices operating at frequencies above the curve acting more as electrostatic (field effect) devices and those below the curve acting as electrochemical devices. Lee et. al.[31] measured transistor on/off current ratios in a nearly identical GEL-OTFT and found that at -2.5 V and 400 Hz, the ratio was 10x. The frequency at which the on and off current levels was indistinguishable was extrapolated to be 2.4 kHz. Although the on/off ratio was limited by increasing off current, the timescales suggested are in reasonable agreement with the results of figure V-2.

D) Conclusions

In situ optical spectroscopy was carried out on metal-insulator-organic semiconductor device to study the mechanism of device charging in the case of an OTFT employing an ion gel dielectric. At low frequencies the device was found to operate as an electrochemical cell. In other words, ion penetration into the semiconductor layer is a key aspect of device operation at low frequencies. The time dependence of the charging process was fitted by means of a diffusion model which allowed the extraction of a

diffusion constant for the [TFSI] ion in P3HT. The diffusion constant was found to depend on voltage, and was used to describe the maximum operating frequency for a similarly constructed electrochemical transistor. Reasonable agreement with published results[jpcc] was found. The results also suggest that at operation speeds greater than 1 kHz a GEL-OTFT can primarily be thought of as an electrostatic double layer device.

E) Acknowledgements*

This work was supported by the Korea Research Foundation Grant funded by the Korean Government (MOEHRD) (KRF-2006-214-D00061 for J. Lee and KRF-2006-352-D00107 for J. H. Cho), and by the University of Minnesota Materials Research Science and Engineering Center funded by the NSF (DMR-0212302). Additional funding was provided by NSF through Award DMR-0406656 (TPL) and by the Department of Energy through Award DE-FG02-05ER46252 (XYZ & CDF).

E) References

[1] Forrest, S. R. *Nature* **2004**, *428*, 911-918.

[2] Klauk, H.; Zschieschang, U.; Pflaum, J.; Halik, M. *Nature* **2007**, *445*, 745-748.

[3] Gundlach, D. J. *Nat. Mater.* **2007**, 6, 173 – 174.

[4] Someya T.; Kato, Y.; Sekitani, T.; Iba, S.; Noguchi, Y.; Murase, Y.; Kawaguchi, H.; Sakurai, T. *Proc. Natl. Acad. Sci. U S A* **2005**, *102(35),*12321-5.

* Acknowledgements were left unaltered from the original publication

[5] Sakamoto, Y.; Suzuki, T.; Kobayashi, M.; Gao, Y.; Fukai, Y.; Inoue, Y.; Sato, F.; Tokito, S. *J. Am. Chem. Soc.* **2004**, *126(26)*, 8138-8140.

[6] Sze, S. M. *Physics of Semiconductor Devices*, Wiley, New York, 1999.

[7] Yoon, M.-H.; Yan, H.; Facchetti, A.; Marks, T. J. *J. Am. Chem. Soc.* **2005**, *127(29)*, 10388-10395.

[8] Kim, S. H.; Yang, S. Y.; Shin, K.; Jeon, H.; Lee, J. W.; Hong, K. P.; Park, C. E. *Appl. Phys. Lett.* **2006**, *89*, 183516.

[9] Kim, C.; Wang, Z.; Choi, H.-J.; Ha, Y.-G.; Facchetti, A.; Marks, T. J. *J. Am. Chem. Soc.* **2008**, *130(21)*, 6867-6878.

[10] Yoon, M.-H.; Facchetti, A.; Marks, T. J. *Proc. Natl. Acad. Sci. U S A* **2005**, *102(13)*, 4678-4682.

[11] Halik, M.; Klauk, H.; Zschieschang, U.; Schmid, G.; Dehm, C.; Schütz, M.; Maisch, S.; Effenberger, F.; Brunnbauer, M; Stellacci, F, *Nature* **2004**, *431*, 963–966.

[12] Hur, S.-H.; Yoon, M.-H.; Gaur, A.; Shim, M.; Facchetti, A.; Marks, T. J.; Rogers, J. A., *J. Am. Chem. Soc.* **2005**, *127(40)*, 13808-13809.

[13] Gray, F. M.; *Solid Polymer Electrolytes: Fundamentals and Technological Applications*; VCH Publishers: New York, 1991.

[14] Bard, A. J.; Faulkner, L. R. *Electrochemical Methods: Fundamentals and Applications*, Wiley, New York, 1980.

[15] Takeya, J.; Yamada, K.; Hara, K.; Shigeto, K.; Tsukagoshi, K.; Ikehata, S.; Aoyagi, Y. *Appl. Phys. Lett.* **2006**, *88*, 112102.

[16] Shimotani, H.; Asanuma, H.; Takeya, J. *Appl. Phys. Lett.* **2006**, *89*, 203501.

[17] Shimotani, H.; Asunuma, H.; Takeya, J.; Iwasa, Y. *Appl. Phys. Lett.* **2006**, *88*, 073104.

[18] Panzer, M. J.; Frisbie, C. D. *Appl. Phys. Lett.* **2006**, *88*, 203504.

[19] Panzer, M. J.; Newman, C. R.; Frisbie, C. D. *Appl. Phys. Lett.* **2005**, *86*, 103503

[20] Panzer, M. J.; Frisbie, C. D. *J. Am. Chem. Soc.* **2005**, *127*, 6960-6961.

[21] Panzer, M. J.; Frisbie, C. D. *Adv. Funct. Mater.* **2006**, *16*, 1051-1056.

[22] Dhoot, A. S.; Yuen, J. D.; Heeney, M.; McCulloch, I.; Moses, D.; Heeger, A. J. *Proc Natl Acad Sci U S A* **2006**, *103*, 11834-11837.

[23] Panzer, M. J.; Frisbie, C. D. *J. Am. Chem. Soc.* **2007**, *129(20)*, 6599-6607.

[24] Herlogsson, L.; Crispin, X.; Robinson, N.D.; Sandberg, M.; Hagel, O.-J.; Gustafsson, G.; Berggren, M. *Adv. Mater*. **2007**, *19*, 97.

[25] Rosenblatt, S.; Yaish, Y.; Park, J.; Gore, J.; Sazanova, V.; McEuen, P. L. *Nano Lett.* **2002**, *2*, 869.

[26] Siddons, G. P.; Merchin, D.; Back, J. H.; Jeong, J. K.; Shim, M. *Nano Lett.* **2004**, *4*, 927-931.

[27] Ozel, T.; Gaur, A.; Rogers, J. A.; Shim, M. *Nano Lett.* **2005**, *5*, 905-911.

[28] Shimotani, H.; Kanbara, T.; Iwasa, Y.; Tsukagoshi, K.; Aoyagi, Y.; Kataura, H. *Appl. Phys. Lett*. **2006**, *88*, 073104.

[29] Lee, J.; Panzer, M. J.; He, Y.; Lodge, T. P.; Frisbie, C. D. *J. Am. Chem. Soc.* **2007**, *129(15)*, 4532-4533.

[30] Cho, J. H.; Lee, J.; He, Y.; Kim, B.S.; Lodge, T.P.; Frisbie, C.D. *Adv. Mater*. **2008**, *20*, 686.

[31] Lee, J.; Kaake, L.G.; Cho, J.H.; Zhu, X.-Y.; Lodge, T.P.; Frisbie, C.D. *J. Phys. Chem. C* **2009**, 113, 8972-8981.

[32] Kaake, L. G.; Zou, Y.; Panzer, M. J.; Frisbie, C. D.; Zhu, X-Y. J. *Am. Chem. Soc.* **2007**, *129*, 7824-7830.

[33] Heeger, A. J.; Kivelson, S.; Schrieffer, J. R.; Su, W.-P. *Rev. Mod. Phys.* **1988**, *60*, 781-850.

[34] Yuen, J. D.; Dhoot, A. S.; Namdas, E. B.; Coates, N. E.; Heeney, M.; McCulloch, I.; Moses, D.; Heeger, A. J. *J. Am. Chem. Soc.* **2007**,*129*, 14367-14371.

[35] Mills, T.; Kaake, L.G; Zhu, X.-Y. *Appl. Phys. A*, **2009**, 95, 291-296.

[36] Powers, D.L. *Boundary Value Problems, Third Edition;* Harcourt Brace Jovanovich: Orlando, FL, 1987; pp 136-139.

[37] Tashiro K.; Kobayashi M.; Kawai T.; Yoshino K.; *Polymer* **1997**, *38*, 2867-2879.

[38] Prosa, T.J.; Winokur, M.J.; Moulton, J.; Smith, P.; Heeger, A.J.; *Phys. Rev. B.* **1995**, *51*, 159-168.

[39] Kaneto, K.; Agawa, H.; Yoshino, K. *J. Appl. Phys.* **1987**, *61*, 1197.

[40] Geankoplis, C.J. *Mass Transport Phenomena, Sixth Printing;* Edwards Brothers: 1995; pp 182-184.

[41] Joshi, S.; Grigorian, S.; Pietsch, U. *Phys. Status. Solidi A* **2008**, *205*, 488-496.

VI. The Polyelectrolyte Dielectric/Polymer Semiconductor Interface: Electrostatics and Electrically Driven Mixing

We performed a study of a new dielectric material made up of a polyelectrolyte, lithium poly(styrene sulfonate), dissolved in an ion conducting polymer, poly(ethylene oxide), using both in-situ optical spectroscopy and transistor measurements. The dielectric was discovered to act as an electrostatic double layer capacitor with a polymer semiconductor over a well defined voltage range. At higher voltages, the charged polymer semiconductor, poly(3-hexylthiophene) (P3HT) dissolves into the dielectric. The mid and near infrared spectrum of P3HT at high charge carrier densities was obtained. The dielectric provides the unique ability to change the carrier density by a factor large enough to witness the preferential filling of different structural elements.

A) Introduction

One emerging subfield of organic semiconductor research is concerned with the development of high capacitance, solution processable, dielectric materials.[1-14] Although potentially of general use,[15] these materials are especially important in the context of organic thin film transistors, where a premium is placed upon low voltage device operation. Electrolyte dielectric materials are a promising methodology, and use

mobile ions to achieve large electric fields at an interface.[16,17] Resulting capacitance values can be as large as 10-100 μF cm^{-2}.

From a technological standpoint, the electrical characteristics of a transistor are the ultimate criteria for judging the effectiveness of a dielectric material. However, the use of electrolyte dielectric materials for organic transistor applications has been troubled by the possibility of electrochemical doping [18-20] where the mobile ions in the dielectric are incorporated into the semiconducting material. Electrochemical transistors, [21-22] particularly those based on ion gels, [13,14,20] may be equally as useful compared to field effect transistors which use a more conventional dielectric such as silicon oxide, or an insulating polymer. However, the introduction of ions into the semiconductor can cause morphological changes,[23,24] and the ions act as Coulomb wells which can reduce the mobility of charge carriers.[25,26] Ideally, one would like to use an electrolyte dielectric material that can be reliably demonstrated to operate as an electrostatic double layer capacitor with a polymer semiconductor.

Although kinetic considerations can limit the role of electrochemical doping in a polymer semiconductor system,[20] one would ideally like to have a system in which there is a thermodynamic barrier to ion inclusion in the semiconductor layer. One possible way to accomplish this is through the use of a polyelectrolyte, which should be too large to easily penetrate the semiconductor layer. The use of polyelectrolytes in an electrolyte dielectric system has been already shown to be an effective means of constructing an organic thin film transistor.[11,12] However, assessing the physical processes operating at the buried interface between a dielectric and a semiconductor can be difficult using electrical measurements alone.

In order to firmly establish the charging mechanism of a polyelectrolyte dielectric, and provide insight into the material attributes and physical processes responsible for device failure, we have characterized a polyelectrolyte dielectric using transistor measurements (see figure 1) and in-situ optical spectroscopy (see figure 2). This combination of characterization techniques has proven useful in the investigation of the semiconductor/dielectric interface in previous studies.[18-20,27-29]

B) Experimental

The polyanion, lithium poly(styrene sulfonate) (LiPSS) (see figure 1), was obtained from Aldrich as a 30% w/w solution in water. The water was removed first by rotovap, then by dissolving in methanol and mixing with molecular sives. Several cycles of freeze drying and heating under vacuum was the final step employed to remove as much water as possible. Poly(ethylene oxide) PEO (m_w = 300) was obtained from Aldrich and used without further purification. LiPSS was mixed with PEO at a 3% mol ratio in methanol. The methanol was driven off first by rotovap, then by several cycles of freeze drying. The resulting substance was a cloudy, viscous, liquid.

Poly(3-hexylthiophene) (P3HT) was obtained from Reike metals (mw = 76 kD and 45 kD) and was used without further treatment. Also, a lower molecular weight sample (mw= 15kD) of P3HT was synthesized using a modified version [30] of the Grignard metathesis (GRIM) polymerization originally developed by

the McCullough group.[31] No major difference between the three samples was observed; the conclusions and observations presented here apply to all three molecular weights.

The substrates used for transistor measurements are Si wafers with 3000 Å of thermally grown oxide, purchased from Silicon Valley Microelectronics (San Jose, CA), which were cut into ~ 1.5 cm x 1.5 cm pieces. In an inert atmosphere glovebox (MBraun) the Si/SiO_2 substrates were spin-coated (Laurel) with P3HT from a 20 mg/mL solution in dichlorobenzene (Aldrich) at 800 rpm for 120 sec. While still under inert atmosphere, the resulting films were baked on a hotplate at 105ºC for ~20 min. to drive off any residual solvent. Atop the P3HT film, Au source and drain contacts were thermally evaporated through silicon shadow masks, defining channel areas of either 200µm x 2000µm or 50µm x 2000µm (length x width). Under inert atmosphere, the polyelectrolyte dielectric was manually pasted over the channel region and a Pt mesh or Au foil gate electrode, with an area much larger than the channel, was laminated atop the dielectric. The devices were left to set 24 hours in nitrogen glove box.

Transistor measurements were made first by transferring the finished devices to a Desert Cryogenics (Tucson, AZ) vacuum probe station. Current-voltage measurements were carried out with two Keithley 236 source measure units and a Keithley 6517 electrometer. Measurements were preformed in the dark under nitrogen.

The devices used for in-situ optical spectroscopy were fabricated on ZnSe waveguides. The raw ZnSe was purchased from photonic supply. The 1mm thick material was cut into pieces 1cm x 3.175 cm by Syagrus Systems Inc. 45 degree Beveled edges were polished by hand, to enable the use of the attenuated total internal reflection

(ATR) technique. Voltages were applied by a Keithley 6517A electrometer, and spectra were collected with a Nicolet 6700 spectrometer using MCT, Si, and InGaAs detectors to cover the full range of the spectrum. Voltages were applied for 30 minutes, during which several spectra were taken. After applying the voltage, the device was allowed to set for 30 minutes. Spectra were collected during this time as well. Voltages were stepped in -0.2 *V* increments, starting with -0.2 *V*. A full set of voltage steps constituted a single day's experiments and each day only one detector was used, thus the full spectra represents three days of experiments on the same device. The experiments were conducted in an inert atmosphere glove box (MBraun) where oxygen levels never reached higher than 3 ppm during device operation.

Two different means of data presentation of the absorption spectra are shown. The difference between the two methods lies only in the spectrum subtracted as a background. Graphs labeled as A[AU] used a clean ZnSe crystal as the background spectra while graphs labeled as ΔA[AU] used the spectrum of the entire device before the application voltage. The two types of presentation styles are referred to as absorption spectra and difference spectra, respectively.

C) Results and discussion

Figure VI-1, panel a shows the output characteristic of a top-gated transistor assembled using an PEO:LiPSS dielectric and a P3HT semiconductor layer. Field effect mobilities were measured in the saturation regime for several devices and was found to be 0.1 ± 0.05 cm^2/Vs. Considering the roughness that is present on the top surface of a

spin coated polymer film, this mobility is relatively high. With that said, it must be noted that device response is particularly sluggish and suffers from relatively high leakage current (possibly due to the presence of water). Panel b of figure 1 shows the output characteristic of a device that is taken on a higher voltage excursion. The most obvious difference between the two measurements is the complete and irreversible destruction of channel conduction upon reaching a voltage of -2.0 *V*. One possible explanation of this result is as follows: the device operates in two regimes, one in which the charge injection mechanism is that of an electrostatic double layer. In that regime the polymer semiconductor interface remains intact. The second regime appears after a certain voltage threshold is reached and the polymers mix, irreversibly damaging the interface and destroying the conductivity of the channel.

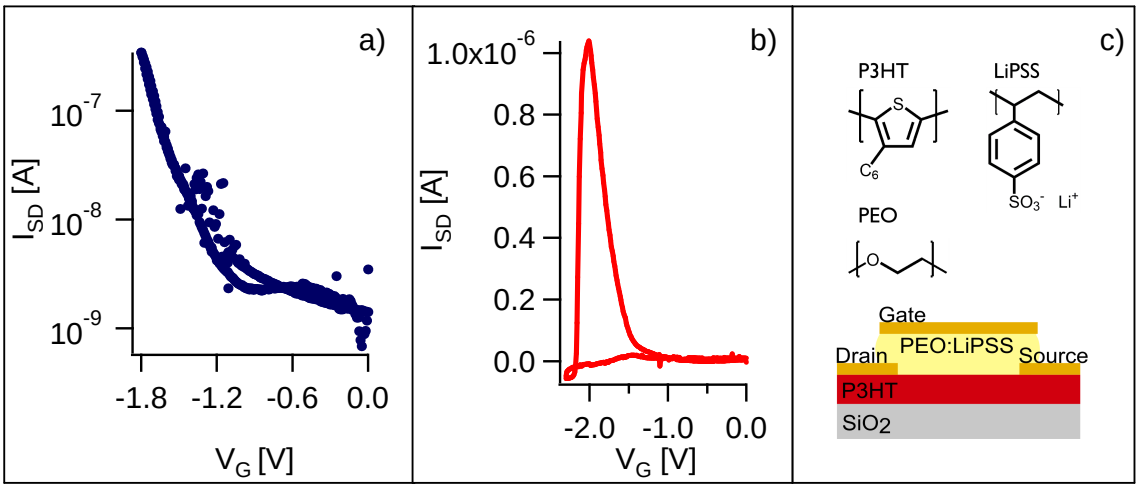

Figure VI-1. Representative transistor measurements. Panel a) reversible transconductance traces occur when the gate voltage is less than -2.0 volts. Panel b) irreversible loss of transconductance occurs as the gate voltage is brought past -2.0 volts. Panel c) schematic of top gate transistor geometry employed and chemical structures of materials employed in the study.

While it is reasonable to believe that the polyelectrolyte gated devices described here operate as electrostatic double layer transistors, this statement cannot be unambiguously verified on the basis of electrical measurements alone because of the slow response time of the dielectric. To verify and electrostatic double layer charging mechanism, spectroscopic measurements are also necessary; they provide an estimate of the total number of molecules which bear charge. Should this number exceed 1-2 monolayers of organic semiconductor molecules, the doping process cannot be accounted for by the field effect. For example, there are two types of absorptions sensitive to the presence of charge which can be used to estimate charge density: polaron absorptions and molecular vibrations of the neutral polymer.

The presence of charge carriers causes broad electronic absorptions to appear. These absorptions, often referred to as polaron absorptions are associated with the appearance of localized electronic states within the band gap of a polymer semiconductor.[32] Figure 2, panel a) shows a difference spectra of the device at a few voltages. Note the growth of a broad absorption centered at 4000 cm^{-1}. This feature is assigned as the lowest polaron absorption of the doped P3HT molecule. (See figure 4 for an energy diagram.) While the strength of a polaron absorption may or may not be directly linear with respect to the number of carriers, increases in the polaron absorption *are* associated with an increasing number of carriers.[27] With this in mind, it is important to note the logarithmic increase in polaron absorption as a function of voltage. (See figure 2, panel a) This is a clear indication of a large increase in the number of carriers as the voltage is increased from -1.6 *V* to -2.2 *V*.

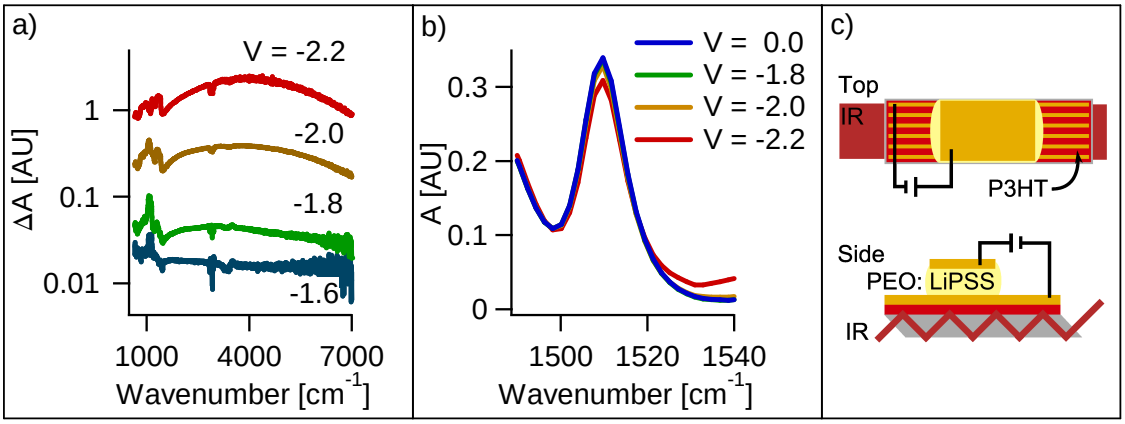

Figure VI-2. Representative in-situ spectroscopy measurements. Panel a) difference spectra in the mid infrared change with voltage. Note the logarithmic increase in intensity above -1.8 volts. Panel b) neutral ring stretching modes of P3HT change with applied voltage. Note that below -2.0 volts, changes are exceedingly small. Panel c) a schematic of the in-situ spectroscopic experiment showing a capacitor structure is fabricated on an optical waveguide.

To be completely rigorous, however, one must use signatures of the neutral molecule to prove or disprove a hypothesis involving a bulk doping process. The argument runs as follows: charging of an organic semiconductor disrupts spectroscopic signatures belonging to the neutral molecule. If more neutral molecules are disrupted than can be accommodated in 1-2 monolayers, the charging process involves the bulk of the material, and is called an electrochemical doping process. In order to firmly establish this statement, it is necessary to clarify against alternative hypotheses.

First, it is possible to imagine that electrochemical doping could be limited to the first several layers of the organic semiconductor. Previous reports showed that the electrochemical doping process is governed by the kinetics of ion diffusion within the semiconductor.[20] In the context of kinetic limitations, it is possible to imagine that electrochemical doping is limited to the first few layers of the semiconductor. However, once the ions have sufficient driving force to penetrate past the first few layers of the semiconductor, there is no thermodynamic reason to suppose that the ions will stop there. At long timescales, an electrochemical doping process will most likely involve the bulk of the material.

Secondly, it is possible to imagine that very light electrochemical doping can look like electrostatic double layer charging; both processes could potentially involve the same number of molecules. In order to differentiate between these two processes, it is necessary to perform transistor measurements under the same conditions. It was shown that light electrochemical doping leads to logarithmically lower mobilities than interfacial doping via the field effect.[25,26] Simply put, a lightly doped electrochemical device will not be especially conductive, and a heavily doped electrostatic double layer device

will. Thus, one can convincingly say that an electrolyte gated device operates with an electrostatic double layer mechanism when the threshold for transistor turn on is not nearly equal to the threshold for spectroscopically obvious bulk electrochemical doping.

When applying this technique and argument, it is important to note that not all spectroscopic signatures of the neutral molecule are disrupted by the presence of charge. However, the vibrational modes associated with the conjugated core of a molecule were shown to be strongly disrupted by device charging.[27,33] Figure 2, panel b) shows how the ring stretching mode of the thiophene monomer decreases with applied voltage. This absorption can be used to estimate the percentage of molecules or monomer units which bear some portion of charge.

For this purpose, it is useful to define a variable, *d,* which is equal to the ratio of molecules affected by the presence of carriers.

$$d = \left(1 - \frac{A_V}{A_{V=0}}\right)\frac{a_{tot}}{a_G} \quad (1)$$

In equation 1, A_V is the absorbance of a neutral mode at a particular voltage, here calculated as the integration of the ring stretching mode of a neutral thiophene. $A_{V=0}$ is the absorbance of the same mode when the voltage is equal to zero. The ratio outside the parenthesis is a correction that takes into account the fact that the gated area of P3HT (a_G) is less than the total area of the P3HT film (a_{tot}). Figure 3, panel a) shows a plot of *d* versus applied voltage for a P3HT capacitor with a PEO:LiPSS dielectric. Figure 3, panel a) also contains a plot of the integrated intensity of the lowest energy polaron absorption (shown in figure 2 panel a) as a function of voltage. Both values remain low throughout the entire operating regime of the transistor, and suddenly increase between *V = -1.8* and *V = -1.9*. This voltage correlates well with the observed sharp *decrease* in the

transconductance, unambiguously indicating that bulk doping of the semiconductor is not causing transistor turn on. Also, on figure 3 panel a) is a line indicating the value of *d* associated with the charging of 1 monolayer (ML) of P3HT. The value of *d* remains below that line during the entire stable operation regime of transistor, a further indication that the polyelectrolyte dielectric acts as electrostatic double layer capacitor over a well defined voltage range.

At higher voltages, the amount of charged polymer increases significantly. In addition, once the threshold voltage is breached, the dielectric mixture becomes dark red, indicating the presence of P3HT. Also, it is tough to imagine that a large polymer ion could penetrate into the organic semiconductor layer. Thus, the behavior observed at high voltages is attributed to the mixing of charged P3HT *into* the dielectric. This process could be termed electrically driven mixing and is schematically pictured in figure 3, contrasted with a schematic of electrostatic double layer charging. Thus it appears that there are two well defined, mutually exclusive, regimes of device operation: electrostatic double layer charging and electrically driven mixing.

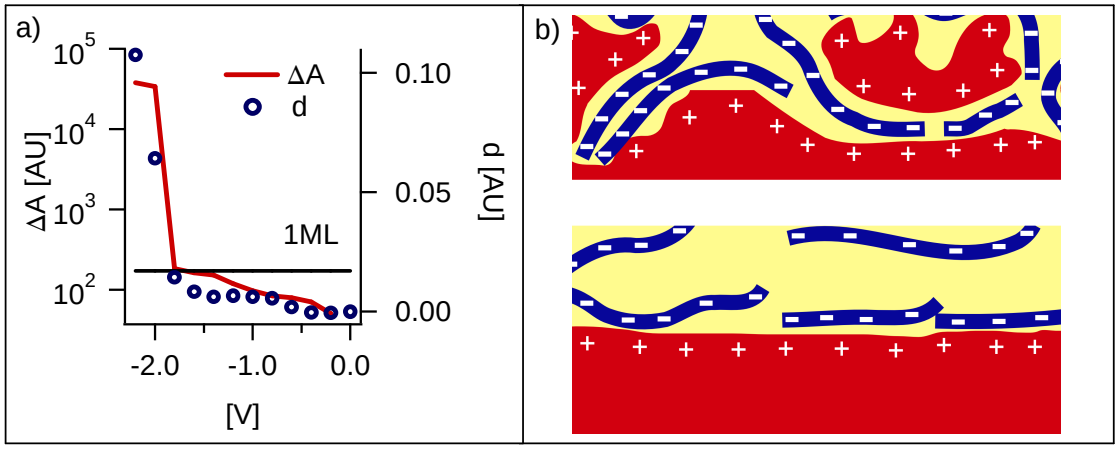

Figure VI-3. Voltage dependence of spectral changes. Panel a) voltage induced changes shown in figure 1@ are integrated and plotted as a function of voltage. Right axis: integrated spectral intensity from difference spectra over the entire mid infrared. Left axis: the quantity d, defined in equation 1 and obtained from the neutral ring stretching modes of P3HT as a function of voltage. A line labeled 1 ML indicates the expected value d would take for one completely charged monolayer of P3HT. Panel b) schematic of the two proposed regimes of device operation. Top: electrically driven mixing. Bottom: electrostatic double layer charging.

Although the previous statement is supported by the observations, the possible subtleties of the polyelectrolyte dielectric/organic semiconductor interface necessitate a thermodynamic argument for the clear separation of two distinct charging regimes. Theoretical work towards this aim based upon the thermodynamics of polymer mixing is ongoing.

Assuming a clear distinction between the two regimes can be made, the spectroscopic results regarding device charging below the mixing threshold can be discussed in terms of field effect doping. The results for -1.4 *V* and -1.6 V are presented in figure 4. These voltages were chosen because their signal levels are high enough to allow meaningful comparisons, and the voltages are well below the mixing threshold. For clarity the spectra are normalized with respect to their value at 800 cm^{-1} and then offset to make the change in the spectral shape with voltage more obvious. Comparison with the literature [34-37] allows the identification of the major features as belonging to polarons in the crystalline and the amorphous phases of P3HT. The energy level diagram for the two phases is schematically outlined in the right panel of figure 4.

Perhaps the most interesting observation of figure 4 is the more obvious presence of features belonging to amorphous polarons for -1.6 *V* than for -1.4 *V*. This suggests that the crystalline regions of P3HT fill before the amorphous regions. We suppose that the novel dielectric employed here allows us to modulate the charge density over a wide enough range to witness the preferential filling of the microcrystalline domains in P3HT before regions with only weak intermolecular interactions.

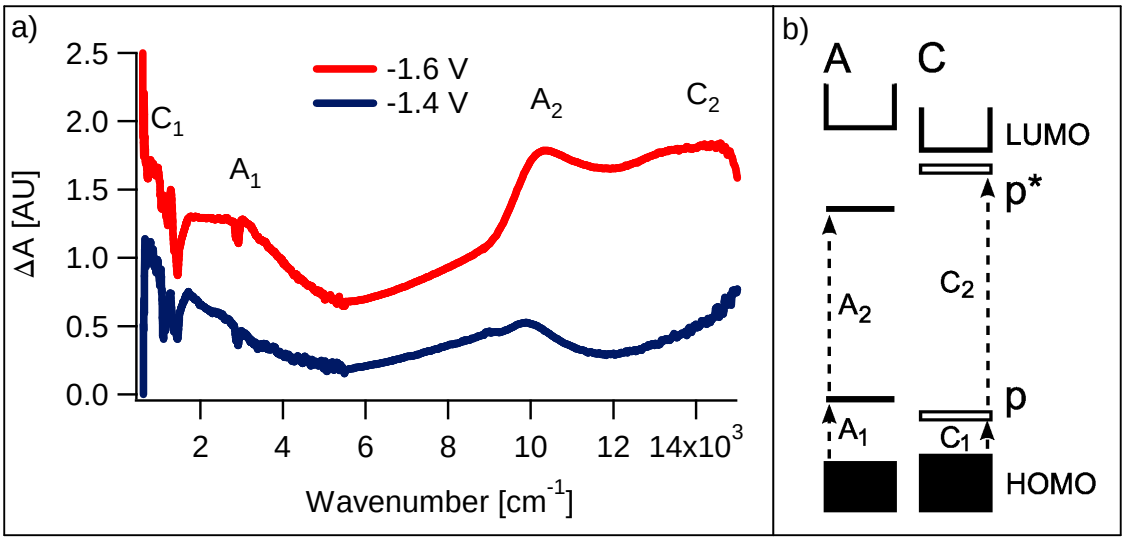

Figure VI-4. Full spectra from the electrostatic regime. Panel a) difference spectra showing the spectra obtained from the mid to the near infrared as the device was charged. Spectra are normalized to their value at 800 cm^{-1} and offset according to voltage. Note that A_1 and A_2 are more noticeable at -1.6 *V*. Panel b) schematic energy diagram of the observed electronic transitions.

D) Conclusions

In conclusion, we have developed a new dielectric material using lithium poly(styrene sulfonate). Organic thin film transistors using this material functioned sluggishly, but mobilities of 0.1 cm^2/Vs could be obtained. The polyelectrolyte was proven to function as an electrostatic double layer capacitor over a useful voltage range. At higher voltages, the polymer semiconductor dissolves into the dielectric. The dielectric was used to vary charge carrier density over a wide enough range to spectroscopically witness the preferential filling of crystalline regions in electrostatically gated P3HT.

E) Acknowledgements

The authors would like to thank Bryan Boudouris for providing P3HT, Prof. C.D. Frisbie for valuable suggestions and technical assistance, and also Prof. T.P. Lodge for valuable suggestions.

F) References

[1] Gundlach, D. J. *Nat. Mater.* 2007, 6, 173 – 174.

[2] Yoon, M.-H.; Yan, H.; Facchetti, A.; Marks, T. J. *J. Am. Chem. Soc.* 2005, *127(29)*, 10388-10395.

[3] Kim, S. H.; Yang, S. Y.; Shin, K.; Jeon, H.; Lee, J. W.; Hong, K. P.; Park, C. E. *Appl. Phys. Lett.* 2006, *89*, 183516.

[4] Kim, C.; Wang, Z.; Choi, H.-J.; Ha, Y.-G.; Facchetti, A.; Marks, T. J. *J. Am. Chem. Soc.* 2008, *130(21)*, 6867-6878.

[5] Yoon, M.-H.; Facchetti, A.; Marks, T. J. *Proc. Natl. Acad. Sci. U S A* 2005, *102(13)*, 4678-4682.

[6] Halik, M.; Klauk, H.; Zschieschang, U.; Schmid, G.; Dehm, C.; Schütz, M.; Maisch, S.; Effenberger, F.; Brunnbauer, M; Stellacci, F, *Nature* 2004, *431*, 963–966.

[7] Hur, S.-H.; Yoon, M.-H.; Gaur, A.; Shim, M.; Facchetti, A.; Marks, T. J.; Rogers, J. A., *J. Am. Chem. Soc.* 2005, *127(40)*, 13808-13809.

[8] Panzer, M. J.; Newman, C. R.; Frisbie, C. D. *Appl. Phys. Lett.* 2005, *86*, 103503.

[9] Panzer, M. J.; Frisbie, C. D. *J. Am. Chem. Soc.* 2005, *127*, 6960-6961.

[10] Panzer, M. J.; Frisbie, C. D. *Adv. Funct. Mater.* 2006, *16*, 1051-1056.

[11] Herlogsson, L.; Crispin, X.; Robinson, N.D.; Sandberg, M.; Hagel, O.-J.; Gustafsson, G.; Berggren, M. *Adv. Mater*. 2007, *19*, 97.

[12] Said, E.; Crispin, X.; Herlogsson, L.; Elhag, S.; Robinson, N.D.; Berggren, M. *Appl. Phys. Lett.* 2006, 89, 143507.

[13] Lee, J.; Panzer, M. J.; He, Y.; Lodge, T. P.; Frisbie, C. D. *J. Am. Chem. Soc.* 2007, *129(15)*, 4532-4533.

[14] Cho, J. H.; Lee, J.; He, Y.; Kim, B.S.; Lodge, T.P.; Frisbie, C.D. *Adv. Mater*. 2008, *20*, 686.

[15] Ahn, C.H.; Bhattacharya, A.; Di Ventra, M.; Eckstein, J.N.; Frisbie, C.D.; Gershenson, M.E.; Goldman, A.M.; Inoue, I.H.; Mannhart, J.; Millis, A.J.; Morpurgo, A.F.; Natelson, D.; Triscone, Rev. Mod. Phys. 2006, 78, 1185-1212.

[16] Gray, F. M.; *Solid Polymer Electrolytes: Fundamentals and Technological Applications*; VCH Publishers: New York, 1991.

[17] Bard, A. J.; Faulkner, L. R. *Electrochemical Methods: Fundamentals and Applications*, Wiley, New York, 1980.

[18] L.G. Kaake, Y. Zou, M.J. Panzer, C.D. Frisbie, X.-Y. Zhu, *J. Am Chem. Soc.* 2007, 129, 7824.

[19] J. D. Yuen, A.S. Dhoot, E.B. Namdas, N.E. Coates, M. Heeney, I. McCulloch, D. Moses, A.J. Heeger, J. Am. Chem. Soc. 2007, 129, 14368.

[20] J. Lee, L.G. Kaake, J.H. Cho, X.-Y. Zhu, T.P. Lodge, C. D. Frisbie, J. Phys. Chem. C 2009, 113, 8972.

[21] M. Taniguchi, T. Kawai, *Appl. Phys. Lett.* 2004, 85, 3298.

[22] H. Shimotani, G. Diguet, Y. Iwasa, *Appl. Phys. Lett.* 2005, 86, 022104.

[23] Tashiro K.; Kobayashi M.; Kawai T.; Yoshino K.; *Polymer* 1997, *38*, 2867-2879.

[24] Prosa, T.J.; Winokur, M.J.; Moulton, J.; Smith, P.; Heeger, A.J.; *Phys. Rev. B.* 1995, *51*, 159-168.

[25] Shimotani, H.; Digut, G.; Iwasa, Y. *Appl. Phys. Lett*. 2005, 86, 022104.

[26] Arkhipov, V.I.; Emelianova, E.V.; Heremans, P.; Bassler, H. *Phys. Rev. B* 2005, 72, 235202.

[27] Mills, T.; Kaake, L.G.; Zhu, X.-Y. *Appl. Phys. A* 2009, 95, 291-296.

[28] Li, Z.Q.; Wang, G.M.; Sai, N.; Moses, D.; Martin, M.C.; Di Ventra, M.; Heeger, A.J.; Basov, D.N. *Nano Lett*. 2006, 6, 224-228.

[29] Chua, L.-L.; Zaumseil, J.; Chang, J.-F.; Ou, E. C.-W.; Ho, P.K.-H.; Sirringhaus, H.; Friend, R.H. *Nature (London)* 2005, 434, 194-199.

[30] Boudouris, B. W.; Molins, F.; Blank, D. A.; Frisbie, C. D.; Hillmyer, M. A. *Macromolecules* **2009**, 42, 4118-4126.

[31] Loewe, R. S.; Khersonsky, S. M.; McCullough, R. D. *Adv. Mater*. **1999**, 11, 250-253.

[32] Fesser, K.; Bishop, A.R.; Campbell, D.K. *Phys. Rev. B* 1983.

[33] Kaake, L.G.; Zhu, X.-Y. *J. Phys. Chem. C* **2008**, 2008, 112, 16174-16177.

[34] H. Sirringhaus, P.J. Brown, R.H. Friend, M.M. Nielsen, K. Bechgaard, B.M.W. Langeveld-Voss, A.J.H. Spiering, R.A.J. Janssen, E.W. Meijer, P. Herwig, D.M. de Leeuw, *Nature* 1999, 401, 685.

[35] J.-F. Chang, H. Sirringhaus, M. Giles, M. Heeney, I. McCulloch, *Phys. Rev. B* 2007, 76, 205204.

[36] R. Osterbacka, C.P. An, X. M. Jiang, Z. V. Vardeny, *Science* 2000, 287, 839.

[37] D. Beljonne, J. Cornil, H. Sirringhaus, P. J. Brown, M. Skunov, R.H. Friend, J.-L. Bredas, *Adv. Funct. Mater.* 2001, 11, 229.

VII. Charge Transport, Nanostructure and the Mott Insulator-to-Metal Transition in Poly (3-hexylthiophene)[*]

We carried out in situ optical spectroscopy measurements of gate-doped poly(3-hexylthiophene) (P3HT) using a polymer electrolyte dielectric. At low doping levels, hole polarons are present in two distinct environments: crystalline and amorphous phases of P3HT. As carrier concentration increases to a region corresponding to the insulator-to-metal transition in transistor measurements, the two polaron states merge into a single state. We take this spectroscopic signature as evidence for strong carrier screening which removes the energetic barrier for polaron transfer from crystalline to amorphous domains; this is responsible for the insulator-to-metal transition in highly doped P3HT.

A) Introduction

Charge transport in organic systems has been the focus of a great deal of investigation since the report of conducting polyacetylene.[1] Early investigations into these materials centered on understanding the nature of individual charge carriers and their interaction with a single polymer chain.[2,3] More recently, it has become apparent that disorder and nano-crystalline structures are critical to the charge transport properties of conducting polymers.[4-7]

[*] This chapter contains published material from the following reference: Kaake, L.G.; Zhu, X.-Y. *J. Phys. Chem. C* **2008**, 2008, 112, 16174-16177. See appendix for copyright information.

Thin films of conducting polymers often consist of crystalline and amorphous domains; but how polymer conductivity is related to the degree of crystallinity remains an open question. A well-known example is regio-regular poly-3-hexyl-thiophene (RR-P3HT), which is among the most conductive polymers investigated to date. While the presence of nano-crystallinity in P3HT is critical to its higher conductivity over that of the amorphous regio-random (RRa) polythiophene, high conductivity also requires a fine balance between crystalline and amorphous domains. Highly crystalline thin films from low molecular weight RR-P3HT are less conductive than those of the less crystalline high molecular weight polymer samples, presumably because the coupling between crystalline grains of the low molecular weight RR-P3HT is poor.[5] A high molecular weight RR-P3HT thin film consists of nanocrystalline domains in an amorphous matrix. Each crystalline domain is essentially a two-dimensional (2D) conductor made of strongly interacting oligothiophene sheets separated by weakly interacting hexyl side chains. The amorphous regions are regarded as one-dimensional (1D) conductors due to the weak intermolecular interactions between oligiothiophene units. What makes high molecular weight RR-P3HT unique is that a single chain is long enough to bridge two crystalline regions via an amorphous polymer segment. Sufficient electronic interaction between the 2D and 1D regions is thus believed to be essential in coupling the 2D islands and providing high conductivity.[5] Recent experiments based on field-effect transistors have even provided evidence for the insulator-to-metal transition (IMT) in RR-P3HT at high doping levels.[8-11]

The Mott insulator-to-metal transition can be most simply described as a discontinuous transition in conductivity from zero to a finite level at $T = 0\ K$.[12] In

disordered materials, insulating behavior is typically interpreted in terms of charge carrier localization at the Fermi level, while metallic conduction is due to the population of extended states which allows charge transport to occur without thermal activation.[13] However, a P3HT thin film consists of both ordered crystalline domains and disordered amorphous regions. *How, then, do we understand metallic conductivity in such a structurally inhomogeneous system?* To answer this question, we carry out in-situ optical absorption study of P3HT at different doping levels as controlled by a gate voltage in transistor geometry. Optical absorption spectroscopy has been of critical importance in developing mechanistic understandings of organic semiconductor materials, as spectroscopic signatures of charge carriers are distinctively different from those of neutral species in terms of vibrational and electronic transitions.[9,14-16] We use a solid state solution of $LiClO_4$ in poly(ethylene-oxide) (PEO) as the gate dielectric in a transistor setup to induce high doping levels and the IMT, as demonstrated by Panzer and Frisbie.[10,11] In their experiments, the mobile ions in the PEO-$LiClO_4$ dielectric provided a very high capacitance which enabled a low transistor turn on voltage of V_G = -1.5 V. Temperature dependent measurements showed little thermal activation for charge transport in the on-state ($V_G \leq$ -1.5 V); this led to the suggestion that P3HT undergoes the insulator-to-metal transition as charge carrier density reaches a critical value. A similar conclusion was reached by Heeger and coworkers in a transistor measurement using the PEO-$LiClO_4$ dielectric and a different polythiophene.[9]

B) Experimental

The device structure used in this study is illustrated in the upper right of figure VII-1. Each device was fabricated on a ZnSe semiconductor crystal which served as a waveguide for multiple internal reflection Fourier transform infrared or near-infrared (MIR- FTIR or FTNIR) spectroscopy. Each ZnSe crystal (10mm x 32 mm x 1mm) was polished to the shape of a parallelogram with 45^{o} angles forming the two ends of the parallelogram. The ZnSe crystal is transparent between 500 and 20000 cm^{-1}. The model device is constructed layer by layer as follows: a 200 nm P3HT thin film (MW = 55 kD, Rieke Metals) was spin coated from 1,2 dichlorobenzene (Sigma) onto the ZnSe surface. A 30 nm Au source/drain electrode array (200 μm wide, 500 μm spacing) was then thermally evaporated onto the P3HT film. This was followed by the deposition of a 100 μm thick polymer electrolyte gate dielectric, $LiClO_4$ in PEO (MW = 10^5) in a ratio of 16 ether oxygen atoms to one lithium ion, via drop casting in acetonitrile. Finally, a 30 nm thick Au gate electrode was thermally evaporated onto the dielectric. The active area of the device consisted of eleven conducting channels, each having a width of 0.5 mm and a length of 15.9 mm. During spectroscopic measurements, the source and drain electrodes were both grounded while the gate voltage (V_G) was used to control the charge density in the P3HT layer. All spectroscopic measurements were carried out on a Nicolet 6700 FTIR-NIR spectrometer using either an MCT or Si detector. In all absorbance spectra presented below, we use the absorbance spectrum of each device at $V_G = 0$ as reference. All experiments were carried out in a glove box under a dry N_2 environment.

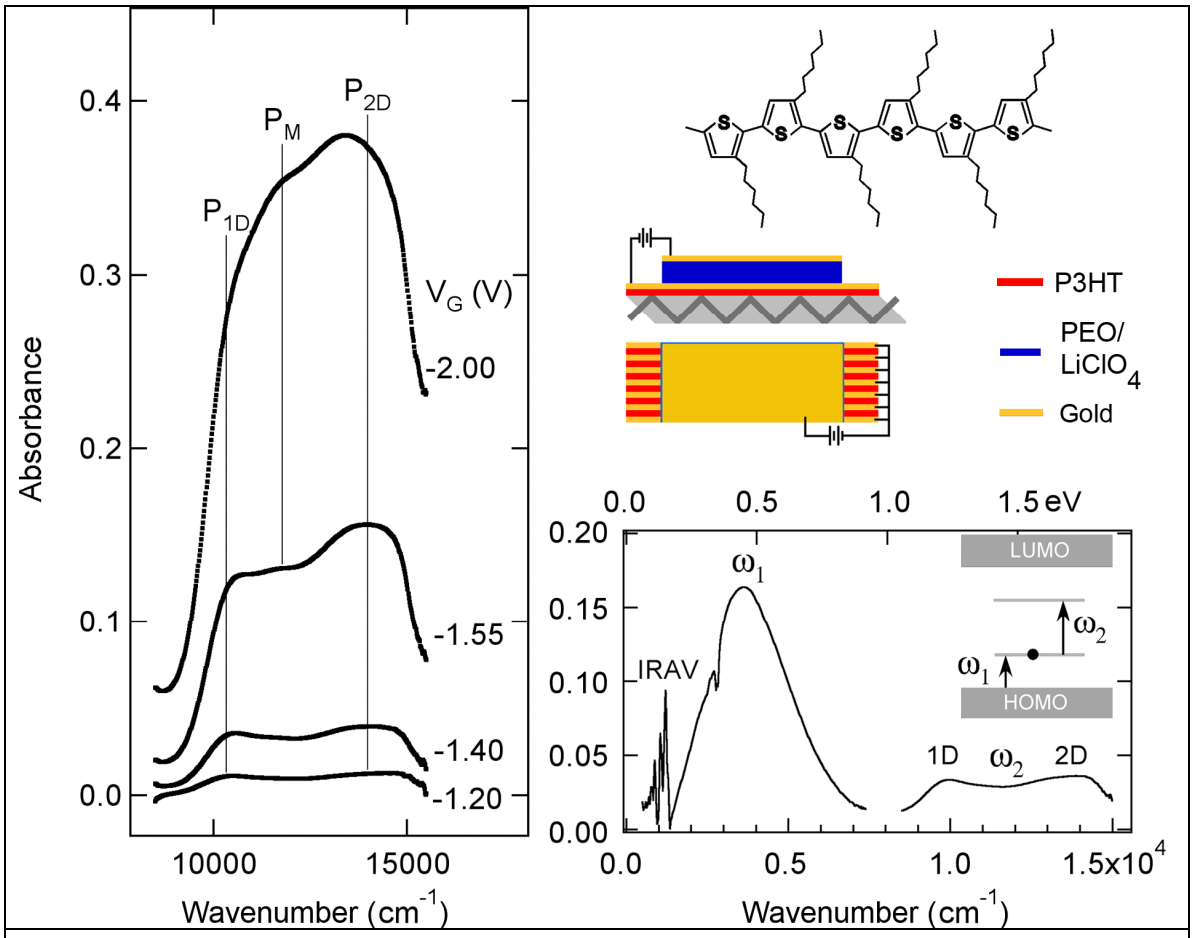

Figure VII-1. Lower-Right: FTIR-NIR spectrum of P3HT obtained at a gate bias of V_G = -1.35 V on a device shown on the top right. Also shown in the schematic is the molecular structure of P3HT. The two polaron transitions (ω_1 & ω_2) are illustrated schematically in the inset. The sharp features at the low-wavenumber end are IR active vibrational (IRAV) modes due to charge injection. Left: Spectra in the ω_2 region obtained as a function of gate bias. Each spectrum was obtained within 100 s after V_G is turned on.

C) Results and discussion

A typical absorbance spectra at V_G = -1.35 *V* is shown in the lower-right panel in figure VII-1. The spectrum shows three types of absorption features. In the lowest energy region are sharp infrared active vibrational modes (IRAV); these transitions are forbidden in the neutral state but become active in the presence of charge carriers (polarons).[17] At higher energies, there are two broad peaks from electronic transitions associated with a hole polaron. A hole polaron is a quasiparticle formed by the deformation of the neutral polymer backbone in the presence of an excess positive charge. The deformed polymer chain gives rise to electronic states which lie in the HOMO/LUMO gap [2]. The broad features found in figure VII-1 are the HOMO → lowest lying polaronic state (ω_1) and intra-polaron (ω_2) transitions, as established in previous studies of doped P3HT.[14,16] The intrapolaron transition, ω_2, is a doublet, corresponding to the two distinctively different local environments of the polymer chains. This doublet has been observed in previous studies of RR-P3HT;[14] the higher energy peak originates from a hole polaron in the crystalline phase (2D) while the lower energy peak is assigned to a hole polaron in the amorphous (1D) phase. The interchain coupling in the crystalline domain leads to two-dimensional (2D) delocalization of polaron states in the thiophene stacks, shifting the lower gap state towards the HOMO and the upper gap state to the LUMO; as a result, ω_2 is blue shifted. In the following, we focus on the ω_2 doublet as the P3HT film undergoes the insulator-to-metal transition.

The left panel in figure VII-1 shows spectra in the ω_2 region taken at different gate biases. For -1.5 V < V_G < 0 V, a voltage range corresponding to the off-state observed in

previous transistor measurements, [10] each spectrum clearly shows a doublet of polarons in the 1D amorphous (P_{1D}) and 2D crystalline (P_{2D}) domains. For V_G < -1.5 V, i.e., the on-state, a third feature (P_M) with energy intermediate between P_{1D} and P_{2D} appears. All spectra in figure VII-1 are recorded immediately (within 100s) after the application of the indicated gate bias. We find the intermediate polaron peak (P_M) becomes more pronounced in the absorption spectra as time unfolds and the device reaches equilibrium.

Panels a-c in figure VII-2 show FTNIR spectra in the ω_2 region taken as a function of time after the application of the indicated gate bias. The time interval between consecutive spectra is 100 s. Clearly, doping of the P3HT thin film is a very slow process and the time scale to reach equilibrium is on the order of hours at all gate bias voltages. This is clear evidence for electrochemical doping, as has been reported also by Heeger and coworkers recently for a polythiophene thin film transistor gated with the PEO-$LiClO_4$ dielectric.[9] Under gate bias, the mobile ions can reach the P3HT/PEO interface to exert a very high field and, thus, electrostatic-like doping of the active P3HT layer. However, the mobile ions (in this case ClO_4^-) can also diffuse into the semiconductor polymer on a longer time scale. In this case of electrochemical doping, the hole polarons in P3HT are electrostatically balanced by ClO_4^- counter ions. The process of electrochemical doping is much slower in comparison with the response time of the polymer electrolyte dielectric operating as an electric double layer capacitor. This is due to the much slower mobility of ions in the semiconducting polymer as compared with that in the ion conducting PEO.[18] As shown in figure VII-2, such a slow electrochemical doping process is seen below (V_G = -1.3 V), at (V_G = -1.5 V), or above (V_G = -2.0 V) the threshold voltage for transistor turn-on. The time-dependent spectra in figure VII-2

are quite different for gate bias below and above the threshold voltage. Below the threshold (V_G = -1.3 V), ω_2 remains a doublet of 1D and 2D polarons (P_1 & P_2). At the threshold (V_G = -1.5 V), the intermediate peak (P_M) grows with increasing doping level

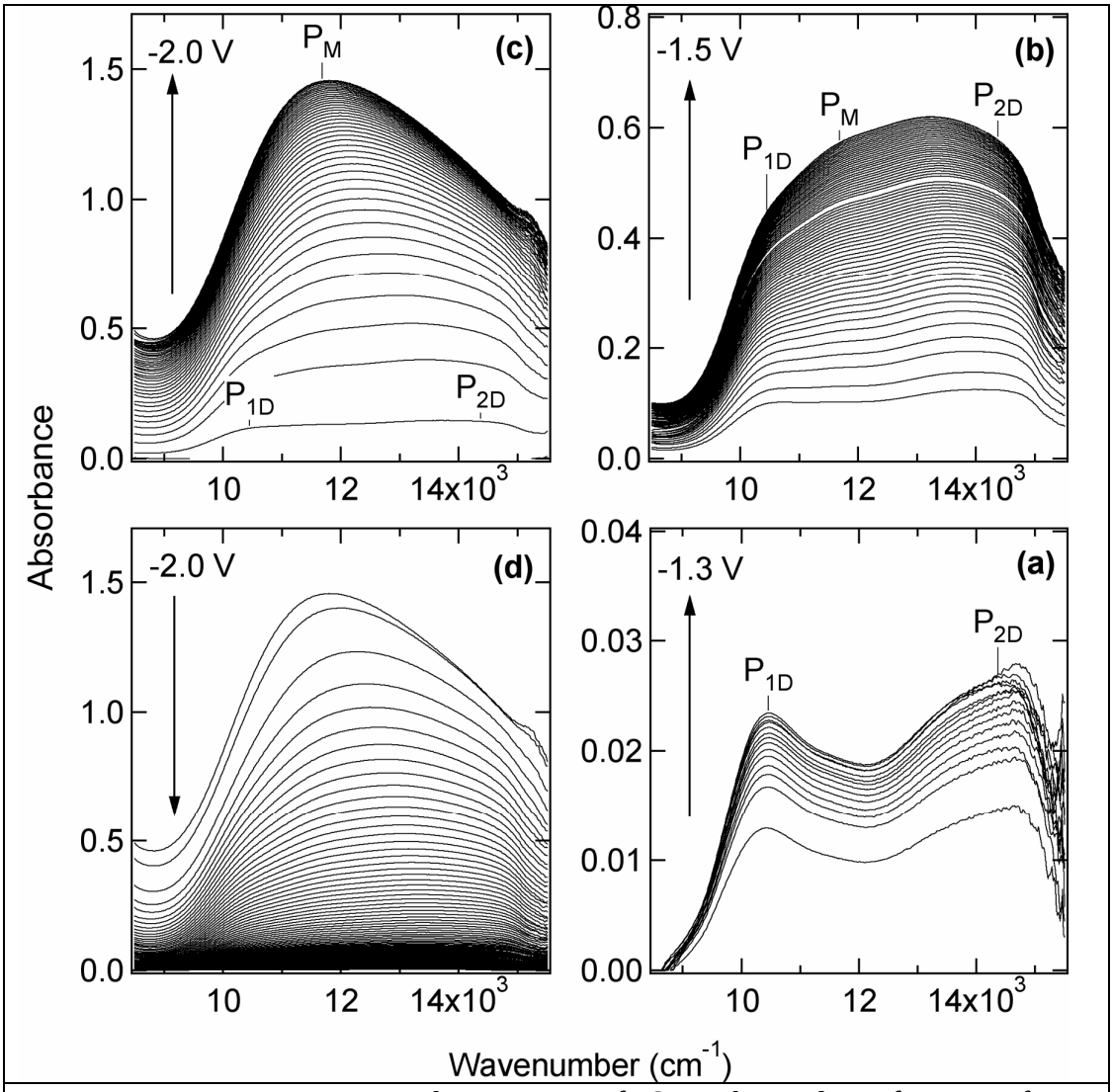

Figure VII-2. FTNIR spectra in the ω_2 region of P3HT obtained as a function of time at the indicated gate bias (V_G = -1.3, -1.5, -2.0 V in panels a, b, and c, respectively). The time interval between consecutive spectra is 100 s. The upward pointing arrows indicate charging, i.e., spectra recorded as a function of time after V_G is switched on at t = 0. The downwards pointing arrow in panel (d) indicates discharging, i.e., spectra recorded after V_G is switched from -2.0 V to 0 V at time zero.

(time) and becomes a clear feature coexisting with the 1D and 2D polarons at saturation. Above the threshold (V_G = -2.0 V), the intermediate peak grows at the expense of the 1D and 2D polarons and becomes a dominating peak at high doping levels. Figure VII-2d shows the reverse process of discharging, i.e., spectra taken at 100s time intervals after the gate bias is switched off to V_G = 0 following the charging experiments at V_G = -2.0 V. In this case, the sharp intermediate polaron peak (P_M) decays back to the broad feature consisting of P_1 and P_2 and, finally, to the baseline at longer times. This establishes the reversibility of the electrochemical doping process.

From the close correlation between the appearance of the intermediate polaron peak (P_M) and the on-state in transistor measurement, we conclude that this peak is a spectroscopic signature for the high-conductance or metallic state in doped P3HT. We now consider the mechanistic implications of this spectroscopic signature.

Thin films of high MW RR-P3HT are known to consist of ~15% crystalline domains in an amorphous matrix, with dimensions of the crystalline domains in the range of a few to a few 10s nm.[5,19] While crystalline domains are expected to be more conductive, it is known that conduction strictly through percolation pathways of crystalline domains is not possible and highly crystalline thin films of low molecular weight P3HT show poor conductivity.[5] Thus, the more conductive thin film from the high molecular weight P3HT sample used here and in previous transistor measurements can be attributed to the connection of crystalline domains by continuous polymer strands. The doublet in the intra-polaron transition shows that ω_2 is blue-shifted by ~0.44 eV going from the 1D amorphous to the 2D crystalline domain. Assuming equal contributions from the upper and lower polaron states to this blue shift, we obtain an

energy difference of ~0.22 eV between the 1D and 2D domains for the singly occupied polaron levels. This energy difference represents a large activation barrier for a hole polaron to hop from the 2D crystalline domain to the 1D amorphous region. The large activation energy is reason for the insulating behavior of P3HT at low doping levels. Thus, the highly conductive or metallic behavior of P3HT at high doping levels must involve the reduction or elimination of this activation energy.

In the conventional picture of the IMT,[12] the metallic state results from the strong screening among singly occupied states, such as dopants in silicon. We believe this traditional picture applies to the metal-like high conductance state in P3HT. At high doping levels, carrier screening decreases the effect of the underlying polymer microstructure, creating a more homogeneous electrostatic landscape. This strong screening removes the energetic barrier impeding the hole polaron from moving freely between the crystalline and amorphous domains. This explains the critical spectroscopic observation, namely that the 1D and 2D polaron states merge into a single intermediate state (P_M in figures VII-1 & VII-2). The merging of these two polaron states indicates that the major energetic barrier for transport, namely, the hopping of polarons from the 2D crystalline to the 1D amorphous regions, has been eliminated. This interpretation is also consistent with the nearly temperature independent conductivity observed for P3HT [10,11] or a related polythiophene [9] at high doping levels in transistors using the PEO-$LiClO_4$ polymer electrolyte dielectrics.

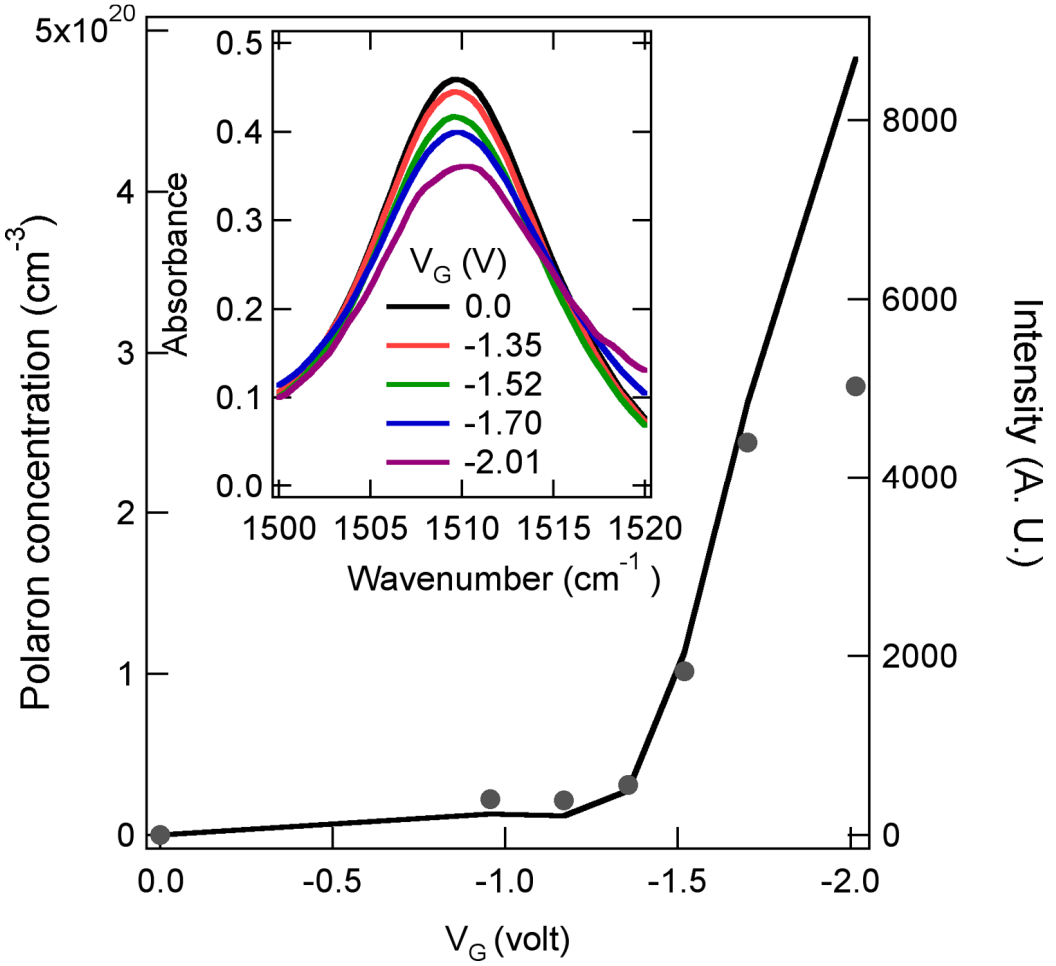

Figure VII-3. Solid circles: polaron concentrations at equilibrium obtained from the intensity loss in the ring-stretch mode (inset) of neutral thiophene as a function of V_G. The solid line is the integrated absorbance (right axis) of the ω_1 polaron peak at equilibrium as a function of V_G. The curve from ω_1 is scaled to match the data points (solid circles) for $V_G \geq -1.5$ V.

In order for screening to play an important part in charge transport and facilitate the insulator-to-metal transition, carrier concentration must increase to a sufficiently high level. Charge carrier concentration can be obtained from absorption spectra via two methods. The first is the low energy polaron transition; the absorbance of this peak (ω_1 in figure VII-1) is proportional to the number of injected holes. This is shown as the solid curve (as a function of V_G) in figure VII-3. The second method is to examine molecular vibrational peaks characteristic of the *neutral* thiophene ring. A positively charged molecule is expected to exhibit vibrational spectra different than that of the neutral molecule. With increasing doping level (increasing gate bias), the intensity of the ring stretch mode (ν_R) of neutral thiophene [20] should decrease, as shown in the inset of VII-3, while that corresponding to the positively charged thiophene should increase. Unfortunately, ν_R of positively charged thiophene is in the spectral region obscured by strong vibrational signal from the PEO dielectric layer. Thus, we rely on the intensity loss of ν_R from neutral thiophene to quantify hole polaron concentration. When we exclude signal contributions from outside the active area of the device, we find that the loss of the neutral thiophene ν_R peak approaches 100% as the gate bias exceeds the critical value (V_G < -1.5 V; gate bias on for ~2 hours to reach equilibrium). This indicates that all thiophene rings in the active channel of the device bear at least a partial charge. The average charge per thiophene ring can be calculated by taking the inverse of the polaron size in monomer units. The size of the polaron is an important parameter in estimating the importance of effects due to correlation between the hole polarons. Based on simultaneous gate-current measurement, we find that the integrated amount of injected hole density of $[h^+] = 2.6 \times 10^{20}/cm^3$ is sufficient to completely remove the C=C ring

stretch mode of neutral thiophene. Using a thiophene monomer concentration of $5.2x10^{21}$/ cm^3 (from the thin film density of 1.33 g/cm^3),[21] we calculate that each injected hole affects 20 thiophene rings, [22] in agreement with the reported size of the hole polaron in P3HT from electron-nuclear double resonance measurements.[23] The solid circles in figure VII-3 show the calculated polaron densities from the decrease in peak intensity of the neutral thiophene ring mode at 1510 cm^{-1}. This calculated density levels off at $[h^+] = 2.6x10^{20}/cm^3$ as no neutral thiophene rings are left and the entire film in the active region are occupied by polarons, each with the size of 20 thiophene rings. Above this doping level, $[h^+]$ can be calculated from the ω_1 polaron peak as shown by the solid curve, which is scaled to match the values obtained from the ring mode at $V_G \geq -1.5$ V.

The charge carrier concentration shown in figure VII-3 increases abruptly at the critical gate bias voltage, which is consistent with the discontinuous change in the number of carriers expected at the insulator-to-metal transition.[12] Given the size (~ 20 thiophene rings) of each hole polaron, the quantitative data in figure VII-3 indicate that these polarons must spatially overlap; resulting in the strong screening of the underlying lattice potential. This screening effectively eliminates the energetic barrier for a hole polaron to move from the 2D crystalline domain to the 1D amorphous matrix, resulting in a highly conductive state.

The IMT does not happen in a spatially homogeneous manner in the device employed here. The slow electrochemical doping process dictates that the critical concentration for IMT is first reached at the P3HT/dielectric interface after the application of necessary V_G, resulting in the on-state in transistor measurement and the

appearance of the metallic state in the intra-polaron transition (figure VII-1 left). The slow diffusion of counter ions then leads to the propagation of the IMT front away from the P3HT/dielectric interface and, eventually, throughout the whole P3HT film, as shown by the time-dependent spectra in figure VII-2. Note that structural changes in P3HT due to the presence of perchlorate dopant ions almost certainly occur on some level. X-ray diffraction experiments on iodine doped P3HT show that at high doping concentrations, the chain packing structure is altered to a degree which might interfere with interchain electronic overlap.[24,25] The relative importance of screening versus that of structural deformations due to dopant intercalation in the insulator-to-metal transition is difficult to estimate from these experiments. However, the overall conclusion that the electronic structure of the metallic phase P3HT is decidedly more homogeneous than P3HT in its insulating phase is not dependent on which interpretation is favored.

D) Conclusion

In conclusion, we show spectroscopic evidence for the insulator-to-metal transition in gate-doped P3HT using a polymer electrolyte dielectric. We find that the two polaronic states in crystalline and amorphous phases of P3HT merge into a single state at high doping levels. At such a high doping level, strong carrier screening and/or structural deformation due to ion penetration removes the energetic barrier for polaron transfer from crystalline to amorphous domains, resulting in the insulator-to-metal transition. This suggests that the activation energy required to move charges from the crystalline to

the amorphous phases of high molecular weight RR-P3HT is an important source of resistance in this material.

E) Acknowledgement

This work was supported by the US Department of Energy under grant number DE-FG02-05ER46252. Partial support from the National Science Foundation under award number CHE-0616427 and the MRSEC Program under award number DMR 0212302 are also acknowledged. We thank Prof. C. D. Frisbie for valuable suggestions and M.J. Panzer and T. Mills for technical assistance.

F) References

[1] Chaing, C.K.; Fincher Jr., C. R.; Park, Y.W.; Heeger, A.J.; Shirakawa, H.; Louis, E.J.; Gau, S.C.; MacDiarmid, A.G. *Phys. Rev. Lett*. **1977**, 39, 1098-1101.

[2] Heeger, A. J.; Kivelson, S.; Schrieffer, J. R.; Su, W.-P. *Rev. Mod. Phys*. **1988**, 60, 781-850.

[3] Takayama, H.; Lin-Liu, Y. R.; Maki, K. *Phys. Rev. B* **1980**, 21, 2388-2393.

[4] Sirringhaus, H.; Brown, P. J.; Friend, R. H.; Nielsen, M. M.; Bechgaard, K.; Langeveld-Voss, B. M. W.; Spiering, A. J. H.; Janssen, R. A. J.; Meijer, E. W. *Synth. Met.* **2000**, 111-112, 129-132.

[5] Kline, R.; McGehee, M. *Polym. Rev*. **2006**, 46, 27-45.

[6] Winokur, M. J.; Chunwachirasiri, W. J. Polym. Sci., Part B: *Polym. Phys*. **2003**, 41, 2630-2648.

[7] Chang, J-F.; Sirringhaus, H.; Giles, M.; Heeney, M.; McCulloch, I. *Phys. Rev. B* **2007**, 76, 205204.

[8] Dhoot, A. S.; Wang, G. M.; Moses, D.; Heeger, A. J. *Phys. Rev. Lett*. **2006**, 96, 246403.

[9] Yuen, J. D.; Dhoot, A. S.; Namdas, E. B.; Coates, N. E.; Heeney, M.; McCulloch, I.; Moses, D.; Heeger, A. J. *J. Am. Chem. Soc.* **2007**,129, 14367-14371.

[10] Panzer, M. J.; Frisbie, C. D. *Adv. Funct. Mater*. **2006**, 16, 1051-1056.

[11] Panzer, M. J.; Frisbie, C. D. *J. Am. Chem. Soc*. **2007**, 129, 6599-6607.

[12] N. F. Mott, Metal-Insulator Transitions; Taylor & Francis, London, 1974, 15-40.

[13] Lee, P. A.; Ramakrishnan, T. V. *Rev. Mod. Phys*. **1985**, 57, 287-337.

[14] Osterbacka, R.; An, C. P.; Jiang, X. M.; Vardeny, Z. V. *Science (Washington D.C)* **2000**, 287, 839-842.

[15] Kaake, L. G.; Zou, Y.; Panzer, M. J.; Frisbie, C. D.; Zhu, X-Y. *J. Am. Chem. Soc.* **2007**, 129, 7824-7830.

[16] Li, Z. Q.; Wang, G.M.; Sai, N.; Moses, D.; Martin, M.C.; Di Ventra, M.; Heeger, A.J.; Basov, D.N. *Nano Lett*. **2006**, 6, 224-228.

[17] Horovitz, B.; Osterbaka, R.; Vardeny, Z.V. *Synth. Met*. **2004**, 141, 179.

[18] Ratner, M. A.; Shriver, D. F. *Chem. Rev*. **1988**, 88, 109-124.

[19] Yang, H.; Shin, T.J.; Yang, L.; Cho, K.; Ryu, C.Y.; Bao, Z. *Adv. Funct. Mater*. **2005**, 15, 671-676.

[20] Brown, P. J.; Sirringhaus, H.; Harrison, M.; Shkunov, M.; Friend, R.H. *Phys. Rev. B* **2001**, 63, 125204.

[21] Erwin, M. M.; McBride, J.; Kadavanich, A. V.; Rosenthal, S. J. *Thin Solid Films* **2002**, 409, 198-205.

[22] Mills, T.; Kaake, L.G.; Zhu, X.-Y. *Appl. Phys. A* **2009**, 95: 291-296.

[23] Kuroda, S.-I.; Marumoto, K.; Sakanaka, T.; Takeuchi, N.; Shimoi, Y.; Abe, S.; Kokubo, H.; Yamamoto, T. *Chem. Phys. Lett*. **2007**, 435, 273-277.

[24] Tashiro K.; Kobayashi M.; Kawai T.; Yoshino K.; *Polymer* **1997**, 38, 2867-2879.

[25] Prosa, T.J.; Winokur, M.J.; Moulton, J.; Smith, P.; Heeger, A.J. *Phys. Rev. B.* **1995**, 51, 159-168.

VIII. Complete Bibliography

I) Introduction: Brief Overview

[1] Sonystyle.com. http://www.sonystyle.com/webapp/wcs/stores/servlet/StoreCatalogDisplay?storeId=10151&catalogId=10551&langId=-1 (Accessed July 28, 2009), Search term OLED returns 7 products.

[2] Samsung United States. http://www.samsung.com/us/index.html (Accessed July 28, 2009), Search term OLED returns 43 results.

[3] Universal Display Corporation. http://www.universaldisplay.com/default.asp?contentID=590 (Accessed July 28, 2009), Page title: OLED lighting.

[4] Konarka Power Plastic. http://www.konarka.com/ (Accessed July 28, 2009).

[5] Patterson, D.A.; Hennessy, J.L. *Computer Organization and Design: The Hardware/Software Interface;* Morgan Kaufmann: San Francisco, CA 2005; pp 11-15.

[6] Vikram, S.C.; Zaumseil, J.; Podzorov, V.; Menard, E.; Willett, R.L.; Takao, S.; Gershenson, M.E.; Rogers, J.A. *Science* **2004**, 303, 1644-1646.

[7] Kittel, C. *Introduction to Solid State Physics*, 8th ed.; John Wiley and Sons: Danvers, MA, 2005; pp 208.

[8] Grahame, D.C. *Chem. Rev.* **1947**, 41, 441-501.

II) Background

[1] Gersten, J.I.; Smith, F.W.; *The Physics and Chemistry of Materials,* John Wiley and Sons: Danvers, MA, 2001.

[2] Kittel, C. *Introduction to Solid State Physics*, 8th ed.; John Wiley and Sons: Danvers, MA, 2005.

[3] Sze, S.M.; Ng, K.K. *Physics of Semiconductor Devices*, 3rd ed.; John Wiley and Sons: Hoboken, NJ, 2007.

[4] Shankar, R. *Principles of Quantum Mechanics*, 2nd ed.; Plenum Press, New York, 1994.

[5] Kittel, C.; Kroemer, H. *Thermal Physics*, 2nd ed.; W.H. Freeman and Company: New York, 2003.

[6] Gersten, J.I.; Smith, F.W. *The Physics and Chemistry of Materials,* John Wiley and Sons: Danvers, MA, 2001; pp 189.

[7] Kittel, C. *Introduction to Solid State Physics*, 8th ed.; John Wiley and Sons: Danvers, MA, 2005; pp 139.

[8] Kittel, C. *Introduction to Solid State Physics*, 8th ed.; John Wiley and Sons: Danvers, MA, 2005; pp 151.

[9] Mott, N.F. *Metal-Insulator Transitions*, 2nd ed.; Taylor and Francis: New York, 1990.

[10] Cheng, Y.C.; Silbey, R.J.; da Silva Filho, D.A; Calbert, J.P.; Cornil, J.; Bredas, J.-L. *J. Chem. Phys.* **2003**, 118, 3764-3774.

[11] Sanchez-Carrera, R.S.; Coropceanu, V.; Kim, E.-G.; Bredas, J.-L. *Chem. Mater.* **2008**, 20, 5832-5838.

[12] Pasveer, W.F.; Cottaar, J.; Tanase, C.; Coehoorn, R.; Bobbert, P.A.; Blom, P.W.M.; de Leeuw, D.M.; Michels, M.A.J.; *Phys. Rev. Lett.* **2005**, 94, 206601.

[13] Shkolvskii, B.I.; Efros, A.L. *Electronic Properties of Doped Semiconductors*, Springer-Verlag: New York, 1984.

[14] Mott, N.F.; Kaveh, M. *Adv. Phys.* **1985**, 34, 329-401.

[15] Bao, Z.; Locklin, J. *Organic Field Effect Transistors*, CRC Press: Boca Raton, FL, 2007 pp 46-48.

[16] Arkhipov, V.I.; Bassler, H. *J. Non-cryst. Solids* **1996**, 198-200, 242-245.

[17] Arkhipov, V.I.; Heremans, P.; Emelianova, E.V.; Adriaenssens, G.J.; Bassler,G. *Phys.Rev. B* **2005**, 72, 235202.

[18] Dhoot, A.S.; Wang, G.M.; Moses, D.; Heeger, A.J. *Phys. Rev. Lett.* **2006**, 96, 246403.

[19] Facchetti, A. *Mater. Today*, **2007**, 10, 28-37.

[20] Campbell, R.B.; Robertson, J.M.; Trotter, *J. Acta Cryst.* **1961**, 14, 705.

[21] Siegrist, T.; Besnard, C.; Haas, S.; Schiltz, M.; Pattison, P.; Chernyshov, D.; Batlogg, B.; Kloc, C. *Adv. Mater.* **2007**, 19, 2079-2082.

[22] Vikram, S.C.; Zaumseil, J.; Podzorov, V.; Menard, E.; Willett, R.L.; Takao, S.; Gershenson, M.E.; Rogers, J.A. *Science* **2004**, 303, 1644-1646.

[23] Li, Z.Q.; Podzorov, V.; Sai, N. Martin, M.C.; Gershenson, M.E.; Di Ventra, M.; Basov, D.N. *Phys. Rev. Lett.* **2007**, 99, 016403.

[24] Podzorov, V.; Menard, E.; Borissov, A.; Kiryukhin, V.; Rogers, J.A.; Gershenson, M.E. *Phys. Rev. Lett*. **2004**, 93, 086602.

[25] Krellner, C.; Haas, S.; Goldmann, C.; Pernstich, K.P.; Gundlach, D.J.; Batlogg, B. *Phys. Rev. B* **2007**, 75, 245115.

[26] Payne, M.M.; Delcamp, J.H.; Parkin, S.R.; Anthony, J.E. *Org. Lett*. **2004**, 6, 1609-1612.

[27] Brown, A.R.; Pomp, A.; de Leeuw, D.M.; Klaassen, D.B.M.; Havinga, E.E.; Herwig, P.; Mullen,K. *J. Appl. Phys*. **1996**, 79, 2136-2138.

[28] Chaing, C.K.; Fincher Jr., C. R.; Park, Y.W.; Heeger, A.J.; Shirakawa, H.; Louis, E.J.; Gau, S.C.; MacDiarmid, A.G. *Phys. Rev. Lett*. **1977,** *39*, 1098-1101.

[29] Heeger, A.J. *J. Phys. Chem. B* **2001**, 105, 8475-8491.

[30] Shirakawa, H. *Angew. Chem. Int. Ed*. **2001**, 40, 2574-2580.

[31] MacDiarmid, A.G. Rev. Mod. Phys. 2001, 73, 701-712.

[32] Pople, J.A.; Walmsley, S.H. *Mol. Phys.* **1962**, 5, 15-20.

[33] Su, W.P.; Schrieffer, J.R.; Heeger, A.J. *Phys. Rev. Lett*. **1979**, 42, 1698-1701.

[34] Fesser, K.; Bishop, A.R.; Campbell, D.K. *Phys. Rev. B* **1983**, 27, 4804-4825.

[35] Campbell, D.K.; Bishop, A.R. *Phys. Rev. B* **1981**, 24, 4859-4862.

[36] Bredas, J.-L.; Street, G.B. *Acc. Chem. Res.* **1985**, 18, 309-315.

[37] Apperloo, J.J.; Groenendaal, L.B.; Verheyen, H.; Jayakannan, M.; Janssen, R.A.J.; Dkhissi, A.; Beljonne, D.; Lazzaroni, R.; Bredas, J.L. *Chem. Eur. J*. **2002**, 8, 2384-2396.

[38] Hotta, S.; Rughooputh, S.D.D.V.; Heeger, A.J.; Wudl, F. Macromolecules **1987**, 20, 212-215.

[39] Newman, C.R.; Frisbie, C.D.; da Silva Filho, D.A.; Bredas, J.-L.; Ewbank, P.C.; Mann, K.R. *Chem. Mater.* **2004**, 16, 4436-4451.

[40] Osterbacka, R.; An, C.P.; Jiang, X.M.; Vardeny, Z.V. *Science* **2000**, 287, 839-842.

[41] Salleo, A. *Mater Today* **2007**, 10, 38-45.

[42] Kline, J.R.; McGhee, M.D.; Kadnikova, E.N.; Liu, J.; Frechet, J.M.J. *Adv. Mater.* **2003**, 15, 1519-1522.

[43] Kline, J.R.; McGhee, M.D.; Kadnikova, E.N.; Liu, J.; Frechet, J.M.J.; Toney, M.F.; *Macromolecules* **2005**, 38, 3312-3319.

[44] Kline, R.; McGehee, M. *Polym. Rev.* **2006**, *46*, 27-45.

[45] Zhang, R.; Iovu, M.C.; Jeffries-EL, M.; Sauve, G.; Cooper, J.; Jia, S.; Tristram-Nagle, S.; Smilgies, D.M.; Lambeth, D.N.; McCullough, R.D.; Kowalewski, T. *J. Am. Chem. Soc.* **2006**, 128, 3480-3481.

[46] Jackson, J.D. *Classical Electrodynamics*, 3rd ed; John Wiley and Sons: New York, 1999.

[47] Tolstoy, V.P; Chernyshova, I.V.; Skryshevsky, V.A. *Handbook of Infrared Spectroscopy of Ultrathin Films*, John Wiley and Sons: Hoboken, NJ, 2003.

[48] Lee, K.; Menon, R.; Yoon, C.O.; Heeger, A.J. *Phys. Rev. B* **1995**, 52, 4779-4787.

[49] Lee, K.; Cho, S.; Park, S.H.; Heeger, A.J.; Lee, C.-W.; Lee, S.-H. Nature 2006, 441, 65-68.

[50] Zhuo, J.-M.; Zhao, L.-H.; Chia, P.-J.; Sim, W.-S.; Friend, R.H.; Ho, P.K.H. *Phys. Rev. Lett.* **2008**, 100, 186601.

[51] Sai, N.; Li, Z.Q.; Martin, M.C.; Basov, D.N.; Di Ventra, M. *Phys. Rev. B* **2007**, 75, 045307.

[52] Brown, P.J.; Sirringhaus, H.; Harrison, M.; Shkunov, M.; Friend, R.H. *Phys. Rev. B* **2001**, 63, 125204.

[53] Beljonne, D. Cornil, J. Sirringhaus, H.; Brown, P.J.; Shkunov, M.; Friend, R.H.; Bredas, J.-L. *Adv. Funct. Mater.* **2001**, 11,229-234.

[54] Sirringhaus, H.; Brown, P.J.; Friend, R.H.; Nielsen, M.M.; Bechgaard, K.; Langeveld-Voss, B.M.W.; Spiering, A.J.H.; Janssen, R.A.J.; Meijer, E.W.; Herwig, P.; de Leeuw, D.M. *Nature*, **1999**, 401, 685-688.

[55] Chang, J.-F.; Sirringhaus, H.; Giles, M.; Heeney, M.; McCulloch, I. Phys Rev. B **2007**, 76, 205204.

[56] Street, R.A.; Salleo, A.; Chabinyc, M.L. *Phys. Rev. B* **2003**, 085316.

[57] Horovitz, B. *Solid State Comm*. **1982**, 41, 729-734.

[58] Carpinelli, J.M.; Weitering, H.H.; Plummer, E.W.; Stumpf, R. *Nautre* **1996**, 381, 398-400.

[59] Brown, S.; Gruner, G. Sci. Amer. 1994, 57, 50-56.

[60] Shimotani, H.; Diguet, G.; Iwasa, Y. *Appl. Phys. Lett*. **2005**, 86, 022104.

[61] Liang, Y.; Frisbie, C.D.; Chang, H.-C.; Ruden, P.R. *J. Appl. Phys.* **2009**, 105, 024514.

[62] Bard, A.J.; Faulkner, L.R. *Electrochemical Methods: Fundamentals and Applications*, 2nd ed.; John Wiley and Sons: Hoboken, NJ, 2001.

[63] Panzer, M.J.; Frisbie, C.D. *Adv. Funct. Mater.* **2006**, 16, 1051-1056.

[64] Panzer, M.J.; Newman, C.R.; Frisbie, C.D. *Appl. Phys. Lett*. **2005**, 86, 103503.

[65] Panzer, M.J.; Frisbie, C.D. *J. Am. Chem. Soc*. **2005**, 127, 6960-6961.

[66] Panzer, M.J.; Frisbie, C.D. *Appl. Phys. Lett*. **2006**, 88, 203504.

[67] Lin, F.; Lonergan, M.C. *Appl. Phys. Lett*. **2006**, 88, 133507.

[68] Dhoot, A.S.; Yuen, J.D.; Heeney, M.; McCulloch, I.; Moses, D.; Heeger, A.J. *Proc. Nat. Acad. Sci.* **2006**, 103, 11834-11837.

[69] Herlogsson, L.; Crispin, X.; Robinson, N.D.; Sandberg, M.; Hagel, O.-J.; Gustafsson, G.; Berggren, M. *Adv. Mater*. **2007**, 19, 97-101.

[70] Inzelt, G. *Conducting Polymers: a New Era in Electrochemistry*, Springer-Verlag, Berlin, Heidelberg, 2008.

III) Experimental

[1] Brugel, W. *An Introduction to Infrared Spectroscopy*, Methuen: London, U.K., 1962.

[2] Kittel, C.; Kroemer, H. *Thermal Physics*, 2nd ed.; W.H. Freeman and Company: New York, 2003.

[3] Griffiths, D.J. *Introduction to Electrodynamics*, Prentice Hall: Upper Saddle River, NJ, 1999.

[4] Rieke, G.H. *Detection of Light: From the Ultraviolet to the Submillimeter*, 2nd ed.; Cambridge University Press, Cambridge, U.K., 2003.

[5] Kauppinen, J.; Partanen, J. *Fourier Transforms in Spectrscopy*, Wiley-VCH, Berlin, 2001.

[6] Tolstoy, V.P; Chernyshova, I.V.; Skryshevsky, V.A. *Handbook of Infrared Spectroscopy of Ultrathin Films*, John Wiley and Sons: Hoboken, NJ, 2003.

[7] Smith, B.C. *Fundamentals of Fourier Transform Infrared Spectroscopy;* CRC Press: Boca Raton, FL, 1996.

[8] Skoog, D.A. *Principles of Instrumental Analysis*, CBS College Publishing: New York, 1985.

[9] Harrick, N.J. *Internal Reflection Spectroscopy*, John Wiley and Sons: New York, 1967.

[10] Klingshirn, C.F. *Semiconductor Optics*, Springer-Verlag: Berlin, Heidelberg, 1995.

[11] Kittel, C. *Introduction to Solid State Physics*, 8th ed.; John Wiley and Sons: Danvers, MA, 2005.

[12] Jackson, J.D. *Classical Electrodynamics*, 3rd ed; John Wiley and Sons: New York, 1999.

[13] *Zinc Selenide*; MSDS No. 96485; Sigma-Aldrich: Saint Louis, MO, Dec 29, 2008.

[14] Panzer, M.J *Polymer Electrolyte-Gated Organic Field-Effect Transistors.* PhD. Thesis, University of Minnesota, Minneapolis, MN, May 2007.

[15] Kline, R.; McGehee, M. *Polym. Rev.* 2006, *46*, 27-45.

[16] Chesterfield, R.J.; McKeen, J.C.; Newman, C.R.; Ewbank, P.C.; da Silva Filho, D.A.; Bredas, J.-L.; Miller, L.L.; Mann, K.R.; Frisbie, C.D. *J. Phys. Chem. B* **2004**, 108, 19281-19292.

[17] Zangwill, A. *Physics at Surfaces;* Cambridge University Press: Cambridge, U.K, 1988.

[18] Choi, K.; Buriak, J.M. *Langmuir* **2000**, 16, 7737-7741.

[19] Gray, F. M.; *Solid Polymer Electrolytes: Fundamentals and Technological Applications*; VCH Publishers: New York, 1991.

[20] Menard, E.; Bilhaut, L.; Zaumseil, J.; Rogers, J.A. *Langmuir* **2004**, 20, 6871-6878.

[21] *Perchloric Acid*; MSDS No. 311421; Sigma-Aldrich: Saint Louis, MO, March 2, 2009.

[22] Cho. J.H.; Lee, J.; He. Y.; Kim, B.-S.; Lodge, T.P.; Frisbie, C.D. *Adv. Mater.* **2008**, 20, 686-690.

[23] Ulman, A. *J. Mater. Educ.* **1989,** 11, 205-280.

IV) Vibrational Spectroscopy Reveals Electrostatic and Electrochemical Doping in Organic Thin Film Transistors Gated with a Polymer Electrolyte Dielectric

[1] Jun, Y.; Zhu, X.-Y. *J. Am. Chem. Soc.* **2004,** 126, 13224-13225.

[2] Chaing, C.K.; Fincher Jr., C. R.; Park, Y.W.; Heeger, A.J.; Shirakawa, H.; Louis, E.J.; Gau, S.C.; MacDiarmid, A.G. *Phys. Rev. Lett.* **1977,** 39, 1098-1101.

[3] Kim, J.-Y.; Kim, E.-R.; Sohn, D.; Sakamoto, A.; Tasumi, M. *Bull. Korean Chem. Soc.* **2001**, *22*, 833-836.

[4] Viehbeck, A.; Goldberg, M.J.; Kovac, C.A *J. Electrochem. Soc.* **1990,** 137, 1460-1466.

[5] Costantini, N.; Lupton, J. M. *Phys. Chem. Chem. Phys.* **2003**, *5*, 749-757.

[6] Chua, L-L.; Zaumseil, J.; Chang, J-F.; Ou, E.C-W.; Ho, P.K-H.; Sirringhaus, H.; Friend, R.H. *Nature* **2005,** 434, 194-199.

[7] Li, Z.Q.; Wang, G.M.; Sai, N.; Moses, M.C.; Martin, M.C.; Di Ventra, M.; Heeger, A.J.; Basov, D.N. Nano Lett. **2006,** 6, 224-228.

[8] Ziemelis, K.E.; Hussian, A.T.; Bradley, D.D.C.; Friend, R.H.; Ruhe,J.; Wegner, G. *Phys. Rev. Lett*. **1991,** 66, 2231-2234.

[9] Deng, Y. Y.; Sirringhaus, H. *Phys. Rev. B* **2005**, *72*, 045207.

[10] Andrews, S. S.; Boxer, S. G. *J. Phys. Chem. A* **2000**, *104*, 11853.

[11] Panzer, M.J.; Newman, C.R.; Frisbie, C.D. *App. Phys. Lett.* **2005,** 86 103503-103503.

[12] Panzer, M.J.; Frisbie, C.D. *Adv. Funct. Mater.* **2006,** 16, 1051-1056.

[13] Dhoot, A.S.; Yuen, J.D.; Heeney, M.; McCulloch, I.; Moses, D.; Heeger, A.J. *P.N.A.S.* **2006,** 103, 11834-11837.

[14] Panzer, M.J.; Frisbie, C.D. *J. Am. Chem. Soc.* **2005,** 127, 6960-6961.

[15] Silinsh, E. A.; Capek, V. *Organic molecular crystals: interaction, localization, and transport phenomena* (**1994**, AIP Press, Woodbury, NY).

[16] Choi, K.; Buriak, J.M.; *Langmuir* **2000,** 16, 7737-7741.

[17] Antunes, P.A.; Constantino, C.J.L.; Aroca, R.; Duff, J. *Appl. Spec.* **2001,** 55, 1341- 1346.

[18] Papke, B. L.; Ratner, M. A.; Shriver, D. F. *J. Electrochem. Soc.* **1982**, *129*, 1434.

[19] Yoshihara, T.; Tadokoro, H.; Murahashi, S. *J. Chem. Phys.* **1964**, 41, 2902.

[20] Chesterfield, R.J.; McKeen, J.C.; Newman, C.R.; Ewbank, P.C.; Demetrio, A. S. F.; Bredas, J-L.; Miller, L. L.; Mann, K.R.; Frisbie, C.D. *J. Phys. Chem. B.* **2004**, 108, 19281-19292.

[21] Hadicke, E.; Graser, F. *Acta Cryst.* **1986,** C42, 189-195.

[22] Wikersheim, K.A. *J. Chem. Phys.* **1959,** 31, 863-869.

[23] Lin, F.; Lonergan, M.C. *Appl. Phys. Lett.* **2006,** 88, 133507-133510.

[24] Ofer, D.; Crooks, R.M.; Wrighton, M.S. *J. Am. Chem. Soc.* **1990,** 112, 7869-7879.

[25] Taniguchi, M.; Kawai, T. *Appl. Phys. Lett.* **2004,** 85, 3298-3300.

V) Time Dependent Operating Mechanisms in Ion Gel Gated Organic Thin Film Transistors

[1] Forrest, S. R. *Nature* **2004**, *428*, 911-918.

[2] Klauk, H.; Zschieschang, U.; Pflaum, J.; Halik, M. *Nature* **2007**, *445*, 745-748.

[3] Gundlach, D. J. *Nat. Mater.* **2007**, 6, 173 – 174.

[4] Someya T.; Kato, Y.; Sekitani, T.; Iba, S.; Noguchi, Y.; Murase, Y.; Kawaguchi, H.; Sakurai, T. *Proc. Natl. Acad. Sci. U S A* **2005**, *102(35)*,12321-5.

[5] Sakamoto, Y.; Suzuki, T.; Kobayashi, M.; Gao, Y.; Fukai, Y.; Inoue, Y.; Sato, F.; Tokito, S. *J. Am. Chem. Soc.* **2004**, *126(26)*, 8138-8140.

[6] Sze, S. M. *Physics of Semiconductor Devices*, Wiley, New York, 1999.

[7] Yoon, M.-H.; Yan, H.; Facchetti, A.; Marks, T. J. *J. Am. Chem. Soc.* **2005**, *127(29)*, 10388-10395.

[8] Kim, S. H.; Yang, S. Y.; Shin, K.; Jeon, H.; Lee, J. W.; Hong, K. P.; Park, C. E. *Appl. Phys. Lett.* **2006**, *89*, 183516.

[9] Kim, C.; Wang, Z.; Choi, H.-J.; Ha, Y.-G.; Facchetti, A.; Marks, T. J. *J. Am. Chem. Soc.* **2008**, *130(21)*, 6867-6878.

[10] Yoon, M.-H.; Facchetti, A.; Marks, T. J. *Proc. Natl. Acad. Sci. U S A* **2005**, *102(13)*, 4678-4682.

[11] Halik, M.; Klauk, H.; Zschieschang, U.; Schmid, G.; Dehm, C.; Schütz, M.; Maisch, S.; Effenberger, F.; Brunnbauer, M; Stellacci, F, *Nature* **2004**, *431*, 963–966.

[12] Hur, S.-H.; Yoon, M.-H.; Gaur, A.; Shim, M.; Facchetti, A.; Marks, T. J.; Rogers, J. A., *J. Am. Chem. Soc.* **2005**, *127(40)*, 13808-13809.

[13] Gray, F. M.; *Solid Polymer Electrolytes: Fundamentals and Technological Applications*; VCH Publishers: New York, 1991.

[14] Bard, A. J.; Faulkner, L. R. *Electrochemical Methods: Fundamentals and Applications*, Wiley, New York, 1980.

[15] Takeya, J.; Yamada, K.; Hara, K.; Shigeto, K.; Tsukagoshi, K.; Ikehata, S.; Aoyagi, Y. *Appl. Phys. Lett.* **2006**, *88*, 112102.

[16] Shimotani, H.; Asanuma, H.; Takeya, J. *Appl. Phys. Lett.* **2006**, *89*, 203501.

[17] Shimotani, H.; Asunuma, H.; Takeya, J.; Iwasa, Y. *Appl. Phys. Lett.* **2006**, *88*, 073104.

[18] Panzer, M. J.; Frisbie, C. D. *Appl. Phys. Lett.* **2006**, *88*, 203504.

[19] Panzer, M. J.; Newman, C. R.; Frisbie, C. D. *Appl. Phys. Lett.* **2005**, *86*, 103503

[20] Panzer, M. J.; Frisbie, C. D. *J. Am. Chem. Soc.* **2005**, *127*, 6960-6961.

[21] Panzer, M. J.; Frisbie, C. D. *Adv. Funct. Mater.* **2006**, *16*, 1051-1056.

[22] Dhoot, A. S.; Yuen, J. D.; Heeney, M.; McCulloch, I.; Moses, D.; Heeger, A. J. *Proc Natl Acad Sci U S A* **2006**, *103*, 11834-11837.

[23] Panzer, M. J.; Frisbie, C. D. *J. Am. Chem. Soc.* **2007**, *129(20)*, 6599-6607.

[24] Herlogsson, L.; Crispin, X.; Robinson, N.D.; Sandberg, M.; Hagel, O.-J.; Gustafsson, G.; Berggren, M. *Adv. Mater*. **2007**, *19*, 97.

[25] Rosenblatt, S.; Yaish, Y.; Park, J.; Gore, J.; Sazanova, V.; McEuen, P. L. *Nano Lett.* **2002**, *2*, 869.

[26] Siddons, G. P.; Merchin, D.; Back, J. H.; Jeong, J. K.; Shim, M. *Nano Lett.* **2004**, *4*, 927-931.

[27] Ozel, T.; Gaur, A.; Rogers, J. A.; Shim, M. *Nano Lett.* **2005**, *5*, 905-911.

[28] Shimotani, H.; Kanbara, T.; Iwasa, Y.; Tsukagoshi, K.; Aoyagi, Y.; Kataura, H. *Appl. Phys. Lett*. **2006**, *88*, 073104.

[29] Lee, J.; Panzer, M. J.; He, Y.; Lodge, T. P.; Frisbie, C. D. *J. Am. Chem. Soc.* **2007**, *129(15)*, 4532-4533.

[30] Cho, J. H.; Lee, J.; He, Y.; Kim, B.S.; Lodge, T.P.; Frisbie, C.D. *Adv. Mater*. **2008**, *20*, 686.

[31] Lee, J.; Kaake, L.G.; Cho, J.H.; Zhu, X.-Y.; Lodge, T.P.; Frisbie, C.D. *J. Phys. Chem. C* **2009**, 113, 8972-8981.

[32] Kaake, L. G.; Zou, Y.; Panzer, M. J.; Frisbie, C. D.; Zhu, X-Y. J. *Am. Chem. Soc.* **2007**, *129*, 7824-7830.

[33] Heeger, A. J.; Kivelson, S.; Schrieffer, J. R.; Su, W.-P. *Rev. Mod. Phys.* **1988**, *60*, 781-850.

[34] Yuen, J. D.; Dhoot, A. S.; Namdas, E. B.; Coates, N. E.; Heeney, M.; McCulloch, I.; Moses, D.; Heeger, A. J. *J. Am. Chem. Soc.* **2007**,*129*, 14367-14371.

[35] Mills, T.; Kaake, L.G; Zhu, X.-Y. *Appl. Phys. A*, **2009**, 95, 291-296.

[36] Powers, D.L. *Boundary Value Problems, Third Edition;* Harcourt Brace Jovanovich: Orlando, FL, 1987; pp 136-139.

[37] Tashiro K.; Kobayashi M.; Kawai T.; Yoshino K.; *Polymer* **1997**, *38*, 2867-2879.

[38] Prosa, T.J.; Winokur, M.J.; Moulton, J.; Smith, P.; Heeger, A.J.; *Phys. Rev. B.* **1995**, *51*, 159-168.

[39] Kaneto, K.; Agawa, H.; Yoshino, K. *J. Appl. Phys.* **1987**, *61*, 1197.

[40] Geankoplis, C.J. *Mass Transport Phenomena, Sixth Printing;* Edwards Brothers: 1995; pp 182-184.

[41] Joshi, S.; Grigorian, S.; Pietsch, U. *Phys. Status. Solidi A* **2008**, *205*, 488-496.

VI) The Polyelectrolyte Dielectric/Polymer Semiconductor Interface: Electrostatics and Electrically Driven Mixing

[1] Gundlach, D. J. *Nat. Mater.* 2007, 6, 173 – 174.

[2] Yoon, M.-H.; Yan, H.; Facchetti, A.; Marks, T. J. *J. Am. Chem. Soc.* 2005, *127(29)*, 10388-10395.

[3] Kim, S. H.; Yang, S. Y.; Shin, K.; Jeon, H.; Lee, J. W.; Hong, K. P.; Park, C. E. *Appl. Phys. Lett.* 2006, *89*, 183516.

[4] Kim, C.; Wang, Z.; Choi, H.-J.; Ha, Y.-G.; Facchetti, A.; Marks, T. J. *J. Am. Chem. Soc.* 2008, *130(21)*, 6867-6878.

[5] Yoon, M.-H.; Facchetti, A.; Marks, T. J. *Proc. Natl. Acad. Sci. U S A* 2005, *102(13),* 4678-4682.

[6] Halik, M.; Klauk, H.; Zschieschang, U.; Schmid, G.; Dehm, C.; Schütz, M.; Maisch, S.; Effenberger, F.; Brunnbauer, M; Stellacci, F, *Nature* 2004, *431*, 963–966.

[7] Hur, S.-H.; Yoon, M.-H.; Gaur, A.; Shim, M.; Facchetti, A.; Marks, T. J.; Rogers, J. A., *J. Am. Chem. Soc.* 2005, *127(40),* 13808-13809.

[8] Panzer, M. J.; Newman, C. R.; Frisbie, C. D. *Appl. Phys. Lett.* 2005, *86*, 103503.

[9] Panzer, M. J.; Frisbie, C. D. *J. Am. Chem. Soc.* 2005, *127*, 6960-6961.

[10] Panzer, M. J.; Frisbie, C. D. *Adv. Funct. Mater.* 2006, *16*, 1051-1056.

[11] Herlogsson, L.; Crispin, X.; Robinson, N.D.; Sandberg, M.; Hagel, O.-J.; Gustafsson, G.; Berggren, M. *Adv. Mater*. 2007, *19*, 97.

[12] Said, E.; Crispin, X.; Herlogsson, L.; Elhag, S.; Robinson, N.D.; Berggren, M. *Appl. Phys. Lett.* 2006, 89, 143507.

[13] Lee, J.; Panzer, M. J.; He, Y.; Lodge, T. P.; Frisbie, C. D. *J. Am. Chem. Soc.* 2007, *129(15)*, 4532-4533.

[14] Cho, J. H.; Lee, J.; He, Y.; Kim, B.S.; Lodge, T.P.; Frisbie, C.D. *Adv. Mater*. 2008, *20*, 686.

[15] Ahn, C.H.; Bhattacharya, A.; Di Ventra, M.; Eckstein, J.N.; Frisbie, C.D.; Gershenson, M.E.; Goldman, A.M.; Inoue, I.H.; Mannhart, J.; Millis, A.J.; Morpurgo, A.F.; Natelson, D.; Triscone, Rev. Mod. Phys. 2006, 78, 1185-1212.

[16] Gray, F. M.; *Solid Polymer Electrolytes: Fundamentals and Technological Applications*; VCH Publishers: New York, 1991.

[17] Bard, A. J.; Faulkner, L. R. *Electrochemical Methods: Fundamentals and Applications*, Wiley, New York, 1980.

[18] L.G. Kaake, Y. Zou, M.J. Panzer, C.D. Frisbie, X.-Y. Zhu, *J. Am Chem. Soc.* 2007, 129, 7824.

[19] J. D. Yuen, A.S. Dhoot, E.B. Namdas, N.E. Coates, M. Heeney, I. McCulloch, D. Moses, A.J. Heeger, J. Am. Chem. Soc. 2007, 129, 14368.

[20] J. Lee, L.G. Kaake, J.H. Cho, X.-Y. Zhu, T.P. Lodge, C. D. Frisbie, J. Phys. Chem. C 2009, 113, 8972.

[21] M. Taniguchi, T. Kawai, *Appl. Phys. Lett.* 2004, 85, 3298.

[22] H. Shimotani, G. Diguet, Y. Iwasa, *Appl. Phys. Lett.* 2005, 86, 022104.

[23] Tashiro K.; Kobayashi M.; Kawai T.; Yoshino K.; *Polymer* 1997, *38*, 2867-2879.

[24] Prosa, T.J.; Winokur, M.J.; Moulton, J.; Smith, P.; Heeger, A.J.; *Phys. Rev. B.* 1995, *51*, 159-168.

[25] Shimotani, H.; Digut, G.; Iwasa, Y. *Appl. Phys. Lett*. 2005, 86, 022104.

[26] Arkhipov, V.I.; Emelianova, E.V.; Heremans, P.; Bassler, H. *Phys. Rev. B* 2005, 72, 235202.

[27] Mills, T.; Kaake, L.G.; Zhu, X.-Y. *Appl. Phys. A* 2009, 95, 291-296.

[28] Li, Z.Q.; Wang, G.M.; Sai, N.; Moses, D.; Martin, M.C.; Di Ventra, M.; Heeger, A.J.; Basov, D.N. *Nano Lett*. 2006, 6, 224-228.

[29] Chua, L.-L.; Zaumseil, J.; Chang, J.-F.; Ou, E. C.-W.; Ho, P.K.-H.; Sirringhaus, H.; Friend, R.H. *Nature (London)* 2005, 434, 194-199.

[30] Boudouris, B. W.; Molins, F.; Blank, D. A.; Frisbie, C. D.;

Hillmyer, M. A. *Macromolecules* **2009**, 42, 4118-4126.

[31] Loewe, R. S.; Khersonsky, S. M.; McCullough, R. D. *Adv. Mater*. **1999**, 11, 250-253.

[32] Fesser, K.; Bishop, A.R.; Campbell, D.K. *Phys. Rev. B* 1983.

[33] Kaake, L.G.; Zhu, X.-Y. *J. Phys. Chem. C* **2008**, 2008, 112, 16174-16177.

[34] H. Sirringhaus, P.J. Brown, R.H. Friend, M.M. Nielsen, K. Bechgaard, B.M.W. Langeveld-Voss, A.J.H. Spiering, R.A.J. Janssen, E.W. Meijer, P. Herwig, D.M. de Leeuw, *Nature* 1999, 401, 685.

[35] J.-F. Chang, H. Sirringhaus, M. Giles, M. Heeney, I. McCulloch, *Phys. Rev. B* 2007, 76, 205204.

[36] R. Osterbacka, C.P. An, X. M. Jiang, Z. V. Vardeny, *Science* 2000, 287, 839.

[37] D. Beljonne, J. Cornil, H. Sirringhaus, P. J. Brown, M. Skunov, R.H. Friend, J.-L. Bredas, *Adv. Funct. Mater.* 2001, 11, 229.

VII) Charge Transport, Nanostructure and the Mott Insulator-to-Metal Transition in Poly (3-hexylthiophene)

[1] Chaing, C.K.; Fincher Jr., C. R.; Park, Y.W.; Heeger, A.J.; Shirakawa, H.; Louis, E.J.; Gau, S.C.; MacDiarmid, A.G. *Phys. Rev. Lett*. **1977**, 39, 1098-1101.

[2] Heeger, A. J.; Kivelson, S.; Schrieffer, J. R.; Su, W.-P. *Rev. Mod. Phys*. **1988**, 60, 781-850.

[3] Takayama, H.; Lin-Liu, Y. R.; Maki, K. *Phys. Rev. B* **1980**, 21, 2388-2393.

[4] Sirringhaus, H.; Brown, P. J.; Friend, R. H.; Nielsen, M. M.; Bechgaard, K.; Langeveld-Voss, B. M. W.; Spiering, A. J. H.; Janssen, R. A. J.; Meijer, E. W. *Synth. Met.* **2000**, 111-112, 129-132.

[5] Kline, R.; McGehee, M. *Polym. Rev*. **2006**, 46, 27-45.

[6] Winokur, M. J.; Chunwachirasiri, W. J. Polym. Sci., Part B: *Polym. Phys*. **2003**, 41, 2630-2648.

[7] Chang, J-F.; Sirringhaus, H.; Giles, M.; Heeney, M.; McCulloch, I. *Phys. Rev. B* **2007**, 76, 205204.

[8] Dhoot, A. S.; Wang, G. M.; Moses, D.; Heeger, A. J. *Phys. Rev. Lett*. **2006**, 96, 246403.

[9] Yuen, J. D.; Dhoot, A. S.; Namdas, E. B.; Coates, N. E.; Heeney, M.; McCulloch, I.; Moses, D.; Heeger, A. J. *J. Am. Chem. Soc.* **2007**,129, 14367-14371.

[10] Panzer, M. J.; Frisbie, C. D. *Adv. Funct. Mater*. **2006**, 16, 1051-1056.

[11] Panzer, M. J.; Frisbie, C. D. *J. Am. Chem. Soc*. **2007**, 129, 6599-6607.

[12] N. F. Mott, Metal-Insulator Transitions; Taylor & Francis, London, 1974, 15-40.

[13] Lee, P. A.; Ramakrishnan, T. V. *Rev. Mod. Phys*. **1985**, 57, 287-337.

[14] Osterbacka, R.; An, C. P.; Jiang, X. M.; Vardeny, Z. V. *Science (Washington D.C)* **2000**, 287, 839-842.

[15] Kaake, L. G.; Zou, Y.; Panzer, M. J.; Frisbie, C. D.; Zhu, X-Y. *J. Am. Chem. Soc.* **2007**, 129, 7824-7830.

[16] Li, Z. Q.; Wang, G.M.; Sai, N.; Moses, D.; Martin, M.C.; Di Ventra, M.; Heeger, A.J.; Basov, D.N. *Nano Lett*. **2006**, 6, 224-228.

[17] Horovitz, B.; Osterbaka, R.; Vardeny, Z.V. *Synth. Met*. **2004**, 141, 179.

[18] Ratner, M. A.; Shriver, D. F. *Chem. Rev*. **1988**, 88, 109-124.

[19] Yang, H.; Shin, T.J.; Yang, L.; Cho, K.; Ryu, C.Y.; Bao, Z. *Adv. Funct. Mater*. **2005**, 15, 671-676.

[20] Brown, P. J.; Sirringhaus, H.; Harrison, M.; Shkunov, M.; Friend, R.H. *Phys. Rev. B* **2001**, 63, 125204.

[21] Erwin, M. M.; McBride, J.; Kadavanich, A. V.; Rosenthal, S. J. *Thin Solid Films* **2002**, 409, 198-205.

[22] Mills, T.; Kaake, L.G.; Zhu, X.-Y. *Appl. Phys. A* **2009**, 95: 291-296.

[23] Kuroda, S.-I.; Marumoto, K.; Sakanaka, T.; Takeuchi, N.; Shimoi, Y.; Abe, S.; Kokubo, H.; Yamamoto, T. *Chem. Phys. Lett*. **2007**, 435, 273-277.

[24] Tashiro K.; Kobayashi M.; Kawai T.; Yoshino K.; *Polymer* **1997**, 38, 2867-2879.

[25] Prosa, T.J.; Winokur, M.J.; Moulton, J.; Smith, P.; Heeger, A.J. *Phys. Rev. B.* **1995**, 51, 159-168.

IX. Letters of Permission

At the time of submission, three of the chapters included in this thesis contain previously published material. License agreements for published materials are therefore included in accordance with copyright law. Three such documents are followed by the terms of the license agreement, which are identical for all three license agreements.

AMERICAN CHEMICAL SOCIETY LICENSE TERMS AND CONDITIONS

Aug 03, 2009

This is a License Agreement between Loren G Kaake ("You") and American Chemical Society ("American Chemical Society") provided by Copyright Clearance Center ("CCC"). The license consists of your order details, the terms and conditions provided by American Chemical Society, and the payment terms and conditions.

All payments must be made in full to CCC. For payment instructions, please see information listed at the bottom of this form.

License Number	2241580711421
License Date	Aug 03, 2009
Licensed content publisher	American Chemical Society
Licensed content publication	Journal of the American Chemical Society
Licensed content title	Vibrational Spectroscopy Reveals Electrostatic and Electrochemical Doping in Organic Thin Film Transistors Gated with a Polymer Electrolyte Dielectric
Licensed content author	L. G. Kaake et al.
Licensed content date	Jun 1, 2007
Volume number	129
Issue number	25
Type of Use	Thesis/Dissertation
Requestor type	Not specified
Format	Print
Portion	Full article
Author of this ACS article	Yes
Order reference number	003
Title of the thesis / dissertation	In situ optical spectroscopy of the organic semiconductor/electrolyte dielectric interface
Expected completion date	Aug 2009
Estimated size(pages)	225
Billing Type	Invoice
Billing Address	Apt 102 1108 8th st SE Minneapolis, MN 55414 United States
Customer reference info	
Total	0.00 USD
Terms and Conditions	

AMERICAN CHEMICAL SOCIETY LICENSE TERMS AND CONDITIONS

Aug 03, 2009

This is a License Agreement between Loren G Kaake ("You") and American Chemical Society ("American Chemical Society") provided by Copyright Clearance Center ("CCC"). The license consists of your order details, the terms and conditions provided by American Chemical Society, and the payment terms and conditions.

All payments must be made in full to CCC. For payment instructions, please see information listed at the bottom of this form.

License Number	2241580592343
License Date	Aug 03, 2009
Licensed content publisher	American Chemical Society
Licensed content publication	The Journal of Physical Chemistry C
Licensed content title	Ion Gel-Gated Polymer Thin-Film Transistors: Operating Mechanism and Characterization of Gate Dielectric Capacitance, Switching Speed, and Stability
Licensed content author	Jiyoul Lee et al.
Licensed content date	May 1, 2009
Volume number	113
Issue number	20
Type of Use	Thesis/Dissertation
Requestor type	Not specified
Format	Print
Portion	Full article
Author of this ACS article	Yes
Order reference number	002
Title of the thesis / dissertation	In situ optical spectroscopy of the organic semiconductor/electrolyte dielectric interface
Expected completion date	Aug 2009
Estimated size(pages)	225
Billing Type	Invoice
Billing Address	Apt 102 1108 8th st SE Minneapolis, MN 55414 United States
Customer reference info	
Total	0.00 USD
Terms and Conditions	

AMERICAN CHEMICAL SOCIETY LICENSE TERMS AND CONDITIONS

Aug 03, 2009

This is a License Agreement between Loren G Kaake ("You") and American Chemical Society ("American Chemical Society") provided by Copyright Clearance Center ("CCC"). The license consists of your order details, the terms and conditions provided by American Chemical Society, and the payment terms and conditions.

All payments must be made in full to CCC. For payment instructions, please see information listed at the bottom of this form.

License Number	2241580198077
License Date	Aug 03, 2009
Licensed content publisher	American Chemical Society
Licensed content publication	The Journal of Physical Chemistry C
Licensed content title	Charge Transport, Nanostructure, and the Mott Insulator-to-Metal Transition in Poly(3-hexylthiophene)
Licensed content author	L. G. Kaake et al.
Licensed content date	Oct 1, 2008
Volume number	112
Issue number	42
Type of Use	Thesis/Dissertation
Requestor type	Not specified
Format	Print
Portion	Full article
Author of this ACS article	Yes
Order reference number	001
Title of the thesis / dissertation	In situ optical spectroscopy of the organic semiconductor/electrolyte dielectric interface
Expected completion date	Aug 2009
Estimated size(pages)	225
Billing Type	Invoice
Billing Address	Apt 102 1108 8th st SE Minneapolis, MN 55414 United States
Customer reference info	
Total	0.00 USD
Terms and Conditions	

Thesis/Dissertation

ACS / RIGHTSLINK TERMS & CONDITIONS
THESIS/DISSERTATION

INTRODUCTION
The publisher for this copyrighted material is the American Chemical Society. By clicking "accept" in connection with completing this licensing transaction, you agree that the following terms and conditions apply to this transaction (along with the Billing and Payment terms and conditions established by Copyright Clearance Center, Inc. ("CCC"), at the time that you opened your Rightslink account and that are available at any time at <http://myaccount.copyright.com>).

LIMITED LICENSE
Publisher hereby grants to you a non-exclusive license to use this material. Licenses are for one-time use only with a maximum distribution equal to the number that you identified in the licensing process; any form of republication must be completed within 60 days from the date hereof (although copies prepared before then may be distributed thereafter).

GEOGRAPHIC RIGHTS: SCOPE
Licenses may be exercised anywhere in the world.

RESERVATION OF RIGHTS
Publisher reserves all rights not specifically granted in the combination of (i) the license details provided by you and accepted in the course of this licensing transaction, (ii) these terms and conditions and (iii) CCC's Billing and Payment terms and conditions.

PORTION RIGHTS STATEMENT: DISCLAIMER
If you seek to reuse a portion from an ACS publication, it is your responsibility to examine each portion as published to determine whether a credit to, or copyright notice of, a third party owner was published adjacent to the item. You may only obtain permission via Rightslink to use material owned by ACS. Permission to use any material published in an ACS publication, journal, or article which is reprinted with permission of a third party must be obtained from the third party owner. ACS disclaims any responsibility for any use you make of items owned by third parties without their permission.

REVOCATION
The American Chemical Society reserves the right to revoke a license for any reason, including but not limited to advertising and promotional uses of ACS content, third party usage, and incorrect figure source attribution.

LICENSE CONTINGENT ON PAYMENT
While you may exercise the rights licensed immediately upon issuance of the license at the end of the licensing process for the transaction, provided that you have disclosed complete and accurate details of your proposed use, no license is finally effective unless and until full payment is received from you (by CCC) as provided in CCC's Billing and Payment terms and conditions. If full payment is not received on a timely basis, then any license preliminarily granted shall be deemed automatically revoked and shall be void as if never granted. Further, in the event that you breach any of these terms and conditions or any of CCC's Billing and Payment terms and conditions, the license is automatically revoked and shall be void as if never granted. Use of materials as described in a revoked license, as well as any use of the materials beyond the scope of an unrevoked license, may constitute copyright infringement and publisher reserves the right to take any and all action to protect

its copyright in the materials.

COPYRIGHT NOTICE: DISCLAIMER
You must include the following copyright and permission notice in connection with any reproduction of the licensed material: "Reprinted (“Adapted” or “in part”) with permission from REFERENCE CITATION. Copyright YEAR American Chemical Society."

WARRANTIES: NONE
Publisher makes no representations or warranties with respect to the licensed material.

INDEMNITY
You hereby indemnify and agree to hold harmless publisher and CCC, and their respective officers, directors, employees and agents, from and against any and all claims arising out of your use of the licensed material other than as specifically authorized pursuant to this license.

NO TRANSFER OF LICENSE
This license is personal to you or your publisher and may not be sublicensed, assigned, or transferred by you to any other person without publisher's written permission.

NO AMENDMENT EXCEPT IN WRITING
This license may not be amended except in a writing signed by both parties (or, in the case of publisher, by CCC on publisher's behalf).

OBJECTION TO CONTRARY TERMS
Publisher hereby objects to any terms contained in any purchase order, acknowledgment, check endorsement or other writing prepared by you, which terms are inconsistent with these terms and conditions or CCC's Billing and Payment terms and conditions. These terms and conditions, together with CCC's Billing and Payment terms and conditions (which are incorporated herein), comprise the entire agreement between you and publisher (and CCC) concerning this licensing transaction. In the event of any conflict between your obligations established by these terms and conditions and those established by CCC's Billing and Payment terms and conditions, these terms and conditions shall control.

JURISDICTION
This license transaction shall be governed by and construed in accordance with the laws of the District of Columbia. You hereby agree to submit to the jurisdiction of the courts located in the District of Columbia for purposes of resolving any disputes that may arise in connection with this licensing transaction.

THESES/DISSERTATION TERMS
Publishing implications of electronic publication of theses and dissertation material
Students and their mentors should be aware that posting of theses and dissertation material on the Web prior to submission of material from that thesis or dissertation to an ACS journal may affect publication in that journal. Whether Web posting is considered prior publication may be evaluated on a case-by-case basis by the journal’s editor. If an ACS journal editor considers Web posting to be “prior publication”, the paper will not be accepted for publication in that journal. If you intend to submit your unpublished paper to ACS for publication, check with the appropriate editor prior to posting your manuscript electronically.

If your paper has already been published by ACS and you want to include the text or portions of the text in your thesis/dissertation in **print or microfilm formats**, please print the

ACS copyright credit line on the first page of your article: "Reproduced (or 'Reproduced in part') with permission from [FULL REFERENCE CITATION.] Copyright [YEAR] American Chemical Society." Include appropriate information.

Submission to a Dissertation Distributor: If you plan to submit your thesis to UMI or to another dissertation distributor, you should not include the unpublished ACS paper in your thesis if the thesis will be disseminated electronically, until ACS has published your paper. After publication of the paper by ACS, you may release the entire thesis (**not the individual ACS article by itself**) for electronic dissemination through the distributor; ACS's copyright credit line should be printed on the first page of the ACS paper.

Use on an Intranet: The inclusion of your ACS unpublished or published manuscript is permitted in your thesis in print and microfilm formats. If ACS has published your paper you may include the manuscript in your thesis on an intranet that is not publicly available. Your ACS article cannot be posted electronically on a publicly available medium (i.e. one that is not password protected), such as but not limited to, electronic archives, Internet, library server, etc. The only material from your paper that can be posted on a public electronic medium is the article abstract, figures, and tables, and you may link to the article's DOI or post the article's author-directed URL link provided by ACS. This paragraph does not pertain to the dissertation distributor paragraph above.

Other conditions:

v1.1

Gratis licenses (referencing $0 in the Total field) are free. Please retain this printable license for your reference. No payment is required.

If you would like to pay for this license now, please remit this license along with your payment made payable to "COPYRIGHT CLEARANCE CENTER" otherwise you will be invoiced within 30 days of the license date. Payment should be in the form of a check or money order referencing your account number and this license number 2241580198077.
If you would prefer to pay for this license by credit card, please go to http://www.copyright.com/creditcard to download our credit card payment authorization form.

Make Payment To:
Copyright Clearance Center
Dept 001
P.O. Box 843006
Boston, MA 02284-3006

If you find copyrighted material related to this license will not be used and wish to cancel, please contact us referencing this license number 2241580198077 and noting the reason for cancellation.

Questions? customercare@copyright.com or +1-877-622-5543 (toll free in the US) or +1-978-646-2777.